National Library
of Canada

Acquisitions and
Bibliographic Services Branch

395 Wellington Street
Ottawa, Ontario
K1A 0N4

Bibliothèque nationale
du Canada

Direction des acquisitions et
des services bibliographiques

395, rue Wellington
Ottawa (Ontario)
K1A 0N4

Your file Votre référence

Our file Notre référence

NOTICE

The quality of this microform is heavily dependent upon the quality of the original thesis submitted for microfilming. Every effort has been made to ensure the highest quality of reproduction possible.

If pages are missing, contact the university which granted the degree.

Some pages may have indistinct print especially if the original pages were typed with a poor typewriter ribbon or if the university sent us an inferior photocopy.

AVIS

La qualité de cette microforme dépend grandement de la qualité de la thèse soumise au microfilmage. Nous avons tout fait pour assurer une qualité supérieure de reproduction.

S'il manque des pages, veuillez communiquer avec l'université qui a conféré le grade.

La qualité d'impression de certaines pages peut laisser à désirer, surtout si les pages originales ont été dactylographiées à l'aide d'un ruban usé ou si l'université nous a fait parvenir une photocopie de qualité inférieure.

Canada

FAST NMDA TRANSMISSION AND NON-LINEAR SYNAPTIC INTERACTIONS IN A SENSORY FEEDBACK PATHWAY

by

JAMES R. PLANT, B.A., M.Sc.

A thesis submitted to the School of

Graduate Studies and Research

In partial fulfilment

of the requirements for the degree of

Doctor of Philosophy

Department of Anatomy and Neurobiology

University of Ottawa

Ottawa, Ontario

April, 1994

ISBN 0-612-00550-X

UNIVERSITÉ D'OTTAWA
UNIVERSITY OF OTTAWA

ABSTRACT

Excitatory amino acid (EAA) neurotransmitters are extensively utilized at excitatory synapses throughout the vertebrate nervous system, with functional diversity being conferred by multiple forms of EAA receptors. Non-NMDA ionotropic EAA receptors (Kainate and AMPA) have typically been ascribed roles as mediators of fast neural transmission, with NMDA receptors hypothesized to contribute to slower processes such as temporal integration and synaptic plasticity. Employing extracellular field potentials, current source density analysis, and intrasomatic and dendritic recordings, the present studies demonstrated the relative contribution of non-NMDA and NMDA receptors to sensory feedback synapses within a highly stratified *in vitro* slice preparation of the electrosensory lateral line lobe (ELL) of the weakly electric fish *Apteronotus leptorhynchus*. Results confirmed a significant contribution of both a non-NMDA, and a fast NMDA component to EPSPs evoked by stimulation of the *tractus stratum fibrosum* (tSF) pathway. A voltage-dependent synaptically-mediated persistent Na^+ (slow) component of the tSF-evoked EPSP interacts with both fast NMDA and non-NMDA components, producing highly non-linear "thresholding" behaviour at the tSF synapses within the ventral molecular layer (VML) of the ELL. When viewed within the context of the *in vivo* physiology of this sensory feedback pathway, the complex response properties of the VML synapse suggests a rich diversity in EAA receptor/channel characteristics giving rise to dynamic functional properties which are consistent with its previously hypothesized role as a mediator of attentional processes within the electrosensory system.

DEDICATION

To my daughter Jennifer,
who has always shown me that
in the simplest things lie
the greatest adventures.

ACKNOWLEDGMENTS

The work presented here could not have been undertaken without the generous moral, financial, and academic support granted to me since undertaking my Ph.D. studies in the Department of Anatomy and Neurobiology at the University of Ottawa. In this light I would like to acknowledge my supervisor Dr. Len Maler for his never failing, revitalizing, and contagious enthusiasm for the pursuit of understanding. To the many individuals whom I, with freshly plotted data, cornered in the hallways....your patient and good natured indulgence was greatly appreciated. I would also like to thank Bill Ellis, and many others for their on-going technical assistance during my studies here. To the few who were allocated the task of reading earlier drafts of this thesis (such as Elizabeth Ring or Dr. Neil Berman), or like Dr. Ray Turner who both allowed me the unrestricted use of his laboratory, and endured my countless questions....my sincere sympathy.

In all such endeavours there are always countless personal sacrifices, it is my greatest gift that I did not have to bear them alone. To my parents, John and Mildred Plant, my deepest and growing appreciation of a job well done. To Gerry and Junine Houlden whom looked after my family in my absence, and to my dear friends Bryan Rooney, and Peter and Francine Ely, whom during the final months took me in like family, my deepest and heart-felt thanks. Finally, to my wife Patti and my little daughter Jennifer, whom have both endured and sacrificed so much....."*da da will be home soon*".

TABLE OF CONTENTS

Page

Page

LIST OF TABLES

LIST OF FIGURES AND ILLUSTRATIONS

"...for the pleasures arising from thinking and learning will make us think and learn all the more."

Aristotle
Nicomachean Ethics,
Book VII, chapter 12

INTRODUCTION

I. Excitatory Amino Acid Receptors

Excitatory amino acids (EAA's) such as glutamate (Glu) or aspartate (Asp) constitute the most abundant and widespread class of excitatory neurotransmitters within the vertebrate central nervous system (95), and have been demonstrated to mediate excitatory synaptic transmission within structures such as the hippocampus (21,33,36,41,60,83,85,96), as well as in both sensory (3,9,35,39,43,52,65,78,86) and motor pathways (27,30). Traditionally, EAA receptor/channel complexes have been grouped into two broad families according to their mechanism of signal transduction. Metabotropic EAA receptors regulate channel conductance indirectly through a modulation of second messenger systems, often resulting in prolonged alterations in neuronal excitability via a reduction of K^+ (19) or Ca^{2+} (103) ion conductance(s). In contrast to metabotropic receptors, ionotropic EAA receptors produce changes in neuronal excitability through directly interacting with and gating an increase in their associated ion channel's conductance (51,61). While the majority of ionotropic EAA receptors are gated by the binding of glutamate, the time scale over which they modulate neuronal excitability varies greatly, determined in part by diversity in the channel's subunit composition.

Ionotropic EAA receptor diversity:

Non-NMDA receptor subtypes

Using selective agonists and antagonists, ionotropic EAA receptors have been traditionally divided into two major classes, the N-methyl-d-aspartate (NMDA) and non-NMDA EAA receptor subtypes. Non-NMDA receptors are further classified as either

kainate (KA) or AMPA receptor subtypes (31,77) on the basis of differential binding, and their selective activation by specific glutamate analogues (ie KA or AMPA). With the development of highly selective and potent non-NMDA receptor antagonists, such as 6-Cyano-7-nitroquinoxaline-2,3-dione (CNQX) (46), a comprehensive characterization of the biophysical properties of these EAA receptor subtypes has been undertaken in an attempt to determine the functional contributions which they make to synaptic transmission within the nervous system.

Activation of non-NMDA ionotropic EAA receptors typically produces excitatory post-synaptic potentials (EPSPs) having a rapid onset and peak (ie <10 msec), which are mediated by a voltage-independent increase in channel conductance to both Na^+ and K^+ ions (61). Since these receptor/channel complexes require only the binding of two molecules of their agonists to be directly gated (98), they have been often found to contribute to fast neurotransmission at central excitatory synapses. Although it has been suggested that the rapid time course of non-NMDA receptors (such as AMPA) might be mediated by a low affinity of glutamate for this receptor (98), intrinsic processes such as rapid receptor desensitization (49,122) have been demonstrated to significantly contribute to this channel's fast kinetics.

Recently, attempts have been made to correlate the distinct pharmacological and physiological properties exhibited by non-NMDA ionotropic EAA receptor subtypes with the molecular diversity seen in their subunit composition (31,45). Through the application of expression cloning techniques, a clearer picture is now beginning to emerge of the common characteristics shared between non-NMDA receptor subtypes, and a variety of

other ligand-gated ion channels. Typical of the majority of ligand-gated channels, non-NMDA receptor/channel complexes are comprised of a pentameric arrangement of subunits, with pharmacological and kinetic specificity being conferred by the channel's subunit composition (87). A common structural feature of all non-NMDA channel subunits is the existence of four putative membrane-spanning domains (M1-M4), with domain M2 having been demonstrated to contribute to the formation of the ion conducting channel pore (38,45).

High-affinity AMPA receptor/channel complexes can be formed through co-expressing differential combinations from four recently cloned non-NMDA EAA receptor subunits (GluR-1 to GluR-4, also known as GluR-A to GluR-D) (45). While functional homomeric glutamate or AMPA-gated channels can be constructed by the expression of either the GluR-1, GluR-3, or GluR-4 subunits in isolation, their resultant electrophysiological and ion permeation properties significantly differ from those of native AMPA receptors. Channels formed by the expression of any one of these subunits in isolation exhibit an abnormally high permeability to Ca^{2+} ions, and a significant rectification of both depolarizing or hyperpolarizing injected currents. In contrast to these homomeric channels, when heteromeric channels are constructed by the co-expression of any combination of the above subunits with the GluR-2 subunit, channels are formed whose electrophysiological and ion permeation characteristics closely resembling those of native AMPA channels (16).

In light of the above results, it has been suggested that the GluR-2 subunit plays a crucial role in determining the specific ion conductance properties of heteromeric non-

NMDA channels. Supporting this interpretation are experimental results demonstrating that point mutations of a specific amino acid residue within the GluR-2 subunit's M2 region alters the selective permeation properties which this subunit confers upon heteromeric AMPA channels. While GluR-1, GluR-3, and GluR-4 subunits all posses a glutamine residue at this crucial position (known as the Q/R site), GluR-2 subunits contain an arginine residue which is introduced as a result of post-translational mRNA editing (17). Experimental deletion, or substitution of other amino acids at the Q/R site in the M2 region of GluR-1, GluR-3, or GluR-4 subunits results in the formation of heteromeric AMPA channels exhibiting an unusually high Ca^{2+} permeability.

Further molecular studies have resulted in the isolation and characterization of several additional non-NMDA receptor/channel subunits (GluR-5 to GluR-7, and KA-1 and KA-2) which, when combined in expression cloning systems, produce high-affinity kainate receptors (40). While either GluR-5 or GluR-6 subunits can be expressed in isolation to form rapidly desensitizing homomeric kainate receptor/channels, neither GluR-7, KA-1 or KA-2 subunits can form functional homomeric complexes in isolation. However, when either KA subunits are co-expressed with GluR-5 or GluR-6 subunits, the result is a significant alteration in both the heteromeric channel's kinetics as well as its agonist specificity.

Convergent results from molecular, pharmacological, and electrophysiological studies have contributed to a growing appreciation of both the commonalities and diversity encompassed by the non-NMDA receptor family. All non-NMDA subunits appear to be extensively regulated by post-translational mRNA modifications (such as

alternate splicing), creating subunit diversity which demonstrates both significant tissue specificity as well as differential developmental regulation (79). The resultant high degree of diversity in the composition and molecular structure of non-NMDA receptor/channel complexes is ultimately reflected in the broad functional repertoire recently being described for this class of EAA receptors.

NMDA receptor subtypes

In contrast to non-NMDA receptors, EPSPs mediated by NMDA receptors are typically described as having a slow onset (ie 20-30 msec to peak), as well as a prolonged time course (ie >100 msec) (59,61). NMDA channels also exhibit an unique voltage-dependent magnesium blockade of ionic conductance at membrane potentials more hyperpolarized than -80 mV (73,77,94), resulting in channel conductances which are typically evoked only following membrane depolarization caused by either temporal summation of high frequency synaptic input (41), or by heterosynaptic summation of EPSPs (53). In addition to their unique voltage-dependence, activation of NMDA channels also requires the concurrent binding of two molecules of its agonist, and two molecules of glycine (13a). The kinetics of NMDA channel gating can be further modulated by the specific binding of zinc (20), as well as a number of polyamines (34), properties which might contribute to this receptor's rich functional variability.

Expression cloning (and subsequent homology-based PCR screening) studies have recently resulted in the isolation and characterization of a number of specific NMDA receptor/channel subunits. The first such subunit to be isolated, the NMDA-R1 subunit, has subsequently been shown by in situ hybridization to be widely expressed throughout

the vertebrate brain (84). When expressed in isolation, this subunit can form a functional homomeric NMDA-gated channel exhibiting a reduced peak conductance, but with the complete range of the voltage and modulatory features evident in native NMDA channels. In contrast to the broadly distributed expression pattern of the NMDA-R1 subunit, multiple forms of a second type of NMDA receptor subunit (NMDA-R2A through D) exhibit a marked tissue specificity within the brain (48,50). Co-expression of these various NMDA-R2 subunits with the NMDA-R1 subunit both significantly enhances the resultant channel's peak conductance, as well as changing the sensitivity of the heteromeric channel to modulators such as Mg^{2+} or glycine (54).

Unlike the non-selective ionic conductance properties exhibited by non-NMDA AMPA or KA receptors, NMDA receptors permit permeation of their channels by Ca^{2+} ions. This Ca^{2+} selectivity has been shown to result from the presence of an asparagine residue at a site within the NMDA-R1 subunit's M2 region homologues to the Q/R site of the non-NMDA receptor subunits (84). While NMDA-R2 subunits also posses an asparagine residue at an equivalent position, its presence within these subunits appears to contribute more to the process of voltage-dependent Mg^{2+} blockade than to a direct regulation of channel permeability (82). Ca^{2+} influx through NMDA channels has been implicated in many diverse processes such as long-term potentiation (LTP) (4,5,22) and long-term depression (LTD) (5,33), as well as in the process of glutamate induced neurotoxicity (75).

As with the non-NMDA receptor family, the functional characteristics of NMDA receptor subunits have been demonstrated to be under significant control by alternate

splicing and post-translational mRNA editing. Within the NMDA-R1 family alone, alternate splicing results in the production of seven distinct splice variants with different physiological profiles (118). Differentially expressed combinations of NMDA subunit forms, or a modulation of the Q/R site within the M2 region of the NMDA-R1 or NMDA-R2 receptor subunits, can therefore result in heteromeric NMDA receptor/channel complexes exhibiting diverse structural and biophysical characteristics. What *functional role* these diverse forms of ionotropic EAA receptor channels might play in neuronal processing remains as an intriguing and challenging question at the interface of molecular and systems neuroscience.

Role of ionotropic EAA receptors in sensory processing:

An understanding of the precise functional roles performed by NMDA or non-NMDA receptors in the vertebrate nervous system is often concealed by the complex interactions of the respective channel's intrinsic biophysical properties, with the unique characteristics of the specific neural circuitry within which they are embedded. To further complicate matters, some central excitatory synapses which use EAAs as neurotransmitters appear to utilize both NMDA and non-NMDA EAA receptors for transmission at the same synapse (3,55,93,104,105,112), thereby obscuring their individual contributions.

Sensory physiology has been a very productive context in which to study the functional consequence of EAA receptor diversity (91). For example, using extracellular single unit recordings *in vivo* (104), it has been demonstrated that somatosensory-evoked increases in the firing rates of ventrobasal (vb) thalamic neurons can be blocked by the

non-selective EAA receptor antagonist kynurenate (kyn). Responses evoked with short duration stimulation (ie 10-20 msec duration puffs of air to the vb neuron's receptive field) were primarily composed of an "early" component which could be selectively reduced with antagonists of non-NMDA receptors, while application of NMDA receptor antagonists had no discernable effect. In contrast, prolonged sensory stimulation (ie 2000 msec) evoked a "late" component of the responses which could be selectively abolished by application of NMDA receptor antagonists. Intracellular recordings subsequently confirmed the underlying bi-phasic nature of these sensory-evoked EPSPs, and highlighted the relative contribution (and differential functional roles) of both non-NMDA and NMDA receptors to sensory encoding in the vb thalamus (105).

In the visual system (ie the lateral geniculate nucleus;LGN), it has also been suggested that NMDA receptors mediate delayed responses to visual input (lagged cells;36). The above results suggest that the rapid kinetic properties of non-NMDA receptors might allow them to preferentially respond to short-duration sensory input, therefore making them uniquely suited to the functional role of mediators of fast sensory transmission. In contrast, the voltage-dependent and prolonged temporal response characteristics typically ascribed to NMDA-mediated synaptic events appears to suggest that this EAA receptor's *functional role* is to integrate on-going sensory transmission. However, a recent number of reports have drawn into question this arbitrary segregation of NMDA and non-NMDA receptor's functional roles based purely on descriptions of their "characteristic" response kinetics.

Within the lateral geniculate nucleus (35), visual (93,112) and somatosensory cortex (119), and on cerebellar granule cells (26), it has been demonstrated that a significant proportion of synaptic currents occurring at (or less than) latencies of 10 msec are actually mediated by "fast" NMDA receptors. In addition, the duration of NMDA-mediated currents in the developing visual system appears to undergo a reduction in the mean duration of their channel openings (18,42), significantly altering their channel's kinetics. The exact mechanism underlying this developmental change in NMDA receptor/channel kinetics is unknown, and the role of relatively fast NMDA transmission in sensory systems has not been adequately addressed.

While immunohistochemical, electrophysiological, and pharmacological studies have all suggested important roles for EAA transmission within numerous sensory systems, the inherent complexity of most experimental preparations has significantly hampered attempts to clearly define the respective contribution of the various forms of ionotropic EAA receptors to sensory processing. For example, both synaptic terminals of intracortical (24,32), as well as commissural (6) fibers, have been demonstrated to utilize EAA as neurotransmitters. As such, even though pharmacological experiments might clearly demonstrate physiological effects of EAA antagonists, it is extremely difficult to determine what proportion of this effect is due to blockade of synaptic input from each of the multiple and functionally diverse sources. To overcome this limitation, one must undertake to study the respective contributions of ionotropic EAA receptors to sensory processing within the context of a clearly defined and constrained neural system. One such system is an *in vitro* slice preparation of the electrosensory system of the

weakly electric fish *Apteronotus leptorhynchus* (71).

II. The Electrosensory System

Significant advances in the understanding of neural mechanisms mediating sensory processing are only possible when clearly defined questions can be addressed using constrained experimental preparations. Many insights have been gained into the varied neural mechanisms utilized for signal transduction within various experimental preparations. However, an understanding of how these mechanisms might interact to generate sensory processing is a difficult, if not an intractable task in many sensory systems, due to their high degree of structural complexity. One sensory system where cellular properties have been directly implicated in processes at both a neural systems level, and at the level of the on-going behaviour of the organism, is the electrosensory system of the weakly electric fish (10,11,12,15,76,115,123).

Electrosensory lateral line lobe (ELL)

Weakly electric fish actively generate electric fields (electric organ discharges; EODs) which are subsequently use for both communication (128), as well as for the detection of objects in their surrounding environment (10,15). Distortions in the fish's electric field caused by objects with conductive properties differing from that of the surrounding water are detected by specialized receptive organs which are distributed across the body of the fish. Electrosensory information is then conveyed centrally through the electrosensory primary afferents to the electrosensory lateral line lobe (ELL) where their projections are sorted to form central representations of the fish's electrosensory periphery.

Structurally, the ELL of gymnotidform electric fish is highly laminar, and is divided into four anatomically and functionally defined segments which extract and process different features of the electrosensory input. The medial segment (MS) of the ELL is distinct in that it receives and processes input from specialized ampullary (low frequency) electroreceptors which are specifically tuned to detect passively generated low-frequency electric fields generated by other organisms. The remaining three segments of the ELL, the centromedial (CMS), centrolateral (CLS), and lateral (LS) segments, all receive identical input from tuberous electroreceptors tuned to the frequency of the fish's own electric organ discharge. As these tuberous afferents project to the ELL they trifurcate, and then terminate in a manner which produces three somatotopic maps of the fish's body's surface within the tuberous segments (CMS, CLS, LS) of the ELL (57).

Each ELL segment has both anatomical (114) and physiological (113) specializations which appear to contribute to their unique functional roles. Since the ELL possesses relatively few neuronal cell types, which are distributed in a highly organized and laminar manner (63,70), it has been possible to gain unique insights into some of the direct functional consequences of the various cellular and segmental specializations observed within the ELL. Pyramidal cells, the principle output neurons of the ELL which project to higher centres involved in the processing of electrosensory information (69), are classified as being either "E" (excited) or "I" (inhibited) types on the basis of their electrophysiological responses to increases in primary afferent input. While "E" type pyramidal cells increase their firing frequency in response to increased primary afferent input, "I" type pyramidal cells decrease their firing rate to the same stimulus (10,108).

The segregation of ELL pyramidal cells into two distinct functional classes on the basis of their response to primary afferent input can be accounted for on the basis of their distinctive morphological characteristics. "E" type pyramidal cells (also described as Basilar Pyramidal cells; BP) possess prominent basal dendrites which extend ventrally to receive direct synaptic input from the primary afferents in the deep neuropil layer of the ELL (63,70). In contrast, "I" type pyramidal cells lack a basal dendrite (and are described as non-Basilar Pyramidal cells; NBP), and therefore only receive primary afferent input indirectly through inhibitory interneurons. As a result, while increases in primary afferent firing excites BP "E"-type cells, it also actively inhibits NBP "I"-type cells. Therefore, a clear relationship can be drawn between ELL pyramidal cell morphological diversity and their resultant distinctive functional specializations.

Anatomical specializations are also seen at the neuronal circuit level within the various tuberous segments of the ELL, and have been suggested as contributing to segmental functional specialization. Within the CMS, primary afferent fibers terminate on the basilar dendrites of basilar pyramidal cells, granule cells, and various other interneurons with very little overlap of their terminal bushes (57,114). As a result, the centromedial segment possess the highest spatial resolution for electrosensory input. In contrast, the extensive overlap of primary afferent fiber terminations within the smaller lateral segment of the ELL results in a low spatial resolution, and the highest temporal resolution for electrosensory input (114). Variations in ELL neuronal morphology, circuitry, and response characteristics might therefore be directly related to the functional properties of differential spatial and temporal tuning within the ELL segments, thus

highlighting the utility of such a simplified sensory system as an experimental preparation.

Sensory feedback pathways to the ELL

The vast majority of synaptic connections made within the ELL originate not from primary afferent input, but from massive feedback projections (66) which synapse on the apical dendrites of "E" and "I" pyramidal cells, (as well as on to a number of interneurons), as they extend dorsally into the molecular layer of the ELL (106). The molecular layer is further subdivided into the dorsal (DML) and ventral (VML) subdivisions, each receiving their own distinct and spatially segregated feedback projections. Therefore, in contrast to many other sensory systems, the relatively simple structure and neuronal composition of the electrosensory system of weakly electric fish offers an unique opportunity for an initial investigation of the roles of feedback projections in on-going sensory processing.

The nucleus praeminentialis pars dorsalis (Pd) is an isthmic structure receiving prominent ascending projections from the ELL, as well as descending input from the *torus semicircularis dorsalis* (TSd), a higher order (midbrain) electrosensory processing region. Pyramidal cells of the ELL project to the Pd, which then contributes to the formation of both the direct (Pd-ELL) and indirect (Pd-EGp-ELL) sensory feedback pathways. Ascending projections from "E" and "I"-type ELL pyramidal cells terminate in the central Pd in such a way as to maintain multiple representations of the various electrosensory segments or maps found in the ELL (106). Further input to the Pd comes from the TSd, whose projections terminate in the lateral Pd, interdigitating with those arising directly from the ELL pyramidal cells (15). Output from the Pd is then sent back to the ELL

through both a topographical (direct), and a diffuse (indirect) projection pathway, each presumably making specific contributions to electrosensory processing at this first level of the electrosensory system.

Indirect electrosensory feedback pathway

The indirect feedback system begins in the Pd with several cell classes; multipolar cells, tufted cells and fusiform cells (106,107). Of these cells, the response of multipolar cells to electrosensory input has been extensively analyzed by Bastian and Bratton (11). Multipolar cells receive synaptic input directly from ELL pyramidal cells, and respond tonically (with a short latency) to changes in the amplitude of the surrounding EOD electric field (12). Functionally, multipolar neurons of the Pd exhibit large receptive fields, a low sensitivity to spatially restricted modulations in the electric field, and a high spontaneous firing rate which is tonically modulated by changes in ELL pyramidal cell input. These neurons then project, via the *tractus praeminentialis-cerebellaris* (tP-Cb), to the caudal cerebellum overlying the ELL (the *eminentia granularis pars posterior*; EGp) where they make spatially diffuse synaptic connections with granule cells (11). The granule cell axons in turn project back as parallel fibers to terminate in the dorsal molecular layer (DML) of the ELL. Similar to the tP-Cb projections, the EGp-ELL projection system appears to be organized in a spatially diffuse manner (63).

The relative accessability of the tP-Cb and EGp has allowed for direct experimental manipulations of the indirect sensory feedback pathway *in vivo*, and therefore has made possible an initial characterization of its functional contributions to electrosensory processing. Consistent with the multipolar's demonstrated sensitivity to

small modulations in the strength of the fish's on-going electric field, many properties of the indirect Pd-EGp-ELL feedback system have suggested a role in the high resolution encoding of changes in electric field strength (11). Discrete injections of local anaesthetics into, or focal electrolytic lesions of the tP-Cb tract, or surgical ablation of the EGp itself all result in a significant increase in the excitatory response of both "E" and "I"-type pyramidal cells to their respective optimal stimuli (7,8).

While pyramidal cells typically exhibit a rapidly adapting response to EOD amplitude modulations, following blockade or removal of the indirect feedback system (7,8), pyramidal cells respond in a tonic manner more closely resembling the response properties of the primary afferents. In addition, functional removal (115) of the indirect feedback pathway results in an increase in the spatial extent of the inhibitory surround portion of the pyramidal cell's receptive fields. Taken together, these data support the hypothesis that the principle functional role of the indirect Pd-ELL feedback pathway is that of a modulator of spatial and temporal inhibitory processes contributing to the control of electrosensory gain and spatial/temporal filtering (7,8,11,64,115).

Direct electrosensory feedback pathway

Both "E" and "I"-type ELL pyramidal cells project topographically to the Pd, and synapse upon Pd stellate cells in a manner which maintains their functional segregation (15,106). Unlike the large receptive fields and tonic firing properties of Pd multipolar cells, "E" and "I" forms of Pd stellate cells have small receptive fields, and are typically silent in the absence of modulations of their electrosensory input. Functionally appropriate stimulation of the Pd stellate neuron's receptive field results in a phasic

increase in the cell's firing rate. These cells therefore are (both spatially and temporally) functionally well suited to detect spatially restricted distortions in the surrounding EOD field caused by the movement of objects across their receptive fields (15).

Stellate cells of the Pd project directly back to the ELL through a myelinated pathway, the *tractus stratum fibrosum* (tSF), whose fibers enter the ELL rostro-medially giving off fine unmyelinated collateral branches which ascend to synapse on the proximal apical dendrites of pyramidal cells and interneurons within the VML (63). Unlike the relatively easy experimental accessability of the indirect feedback system, the direct Pd-ELL (tSF) feedback system is positioned in such a way as to make extensive *in vivo* manipulations difficult. As a result, a clear understanding of the functional role this pathway might play in on-going electrosensory behaviour is still being sought, and is at present based on limited data.

Functionally, the Pd-ELL direct sensory feedback pathway has been assumed to be excitatory in nature on the basis of synaptic morphology (70), the biochemical distribution of amino acids within the lamina of the ELL (86), the immunohistochemical localization of glutamate in the tSF terminals within the VML (126), and binding of both non-NMDA and NMDA EAA ligands within the VML and DML (65). Direct evidence for EAA-mediated excitation of ELL pyramidal cell apical dendrites has recently been reported, demonstrating that ejection of EAA agonists (AMPA, Glu, NMDA) in the DML can result in a dramatic increase in pyramidal cell excitability (9). In addition, ejection of non-NMDA receptor antagonists into the DML significantly altered the characteristic response properties of pyramidal cells to electrosensory input, (while NMDA antagonists

had no discernable effect). These results suggest that EAA receptors play an important role within the indirect sensory feedback pathway. Although the direct Pd-ELL feedback pathway has begun to be characterized *in vivo* (15), no direct tests concerning the role of EAAs within this feedback pathway have been carried out.

A clear understanding of the functional contribution that the direct Pd-ELL feedback pathway might make to on-going electrosensory processing is impossible without first characterizing its functional attributes through direct experimental manipulations of this pathway in isolation. While exceedingly difficult to accomplish with *in vivo* experimental preparations, a transverse *in vitro* slice preparation of the ELL has been developed (71) which allows for the precise activation and selective pharmacological manipulation of the tSF pathway. As a result, the present studies were undertaken using this *in vitro* slice preparation to attempt to physiologically and pharmacologically characterize the VML synapses of the direct Pd-ELL pathway with the aim of determining the functional roles which might be attributed to this direct sensory feedback pathway.

MATERIALS and METHODS

I. Experimental animals and surgical procedure

A total of 65 weakly electric fish of the species *Apteronotus leptoryhchus* (Brown Ghost Knife Fish) were used in the following studies. Fish of either sex, weighing between 2.1 and 9.6 grams, were immobilized by a subcutaneous injection of Flaxedil (1%), transferred to a foam-rubber lined holder, and were maintained with a 11-14 ml/min flow of oxygenated water containing approximately 0.7g/1000ml of the anaesthetic 3-aminobenzoic acid ethyl ester (MS-222), or 2-phenoxy-ethanol (1ml/1000ml) via a pipette inserted in their mouths. All subsequent surgical procedures were carried out under a Zeiss stereo microscope.

Multiple intramuscular injections of 2% lidocaine were made into the dorsal neck muscles of the fish, as well as a series of subcutaneous ejections along the dorsal extent of the head. After a few minutes the skin overlying the skull was cut and retracted, and the dorsal portion of the skull was carefully cut away using iris scissors. The exposed brain was then kept continuously moist by superfusion with artificial cerebral spinal fluid (ACSF) which was bubbled with 95% O_2-5% CO_2 (see table 1. for compositions of ACSFs). An initial assessment of the general viability of the fish could be made at this point by observing the integrity of blood circulation through the vasculature overlying and adjacent to the ELL.

Using a micro-scalpel, a coronal cut was first made caudal to the ELL transecting the brain stem of the fish. A second incision was made, at an angle of approximately 45 degrees relative to the true coronal plane, transecting the brain rostral to the ELL. This

TABLE 1. **Composition of ACSF's* (in mM)**

ACSF's	NaCl	$NaHCO_4$	D-Glucose	KH_2PO_4	KCL	$MgSO_4$	$CaCl_2$
Control	124.0	24.0	10.0	1.25	2.0	2.0	2.0
0-Mg^{2+}	124.0	24.0	10.0	1.25	2.0	----	2.0
Mn^{2+}	129.0	-----	10.0	----	3.25	----	0.2

Mn^{2+}= 4.0 TRIS= 11.4 HEPES= 20.0

* **Note:** All solutions are continuously bubbled with 95% O_2 - 5% CO_2

(Adapted from 71)

angle proved critical for maintaining the continuity of the tSF fibers and their synaptic terminations in the vML, and determined whether robust field potentials could be evoked within the slice. Lastly, the scalpel was passed inside the cranial cavity along the lateral aspects of the brain just rostral to the ELL to sever the primary afferents of the anterior lateral line nerve ganglion (ALLNg) prior to their entering the ELL. The fish was then immediately transferred to a petri dish containing ice cold ACSF, and the brain anterior to the 45 degree cut was removed with a spatula. The remaining posterior portion of the brain containing the ELL was then carefully removed from the cranial cavity.

II. *In vitro* slice preparation and maintenance

Once removed from the cranial cavity, the tissue block containing the ELL was removed from the chilled ACSF, firmly affixed by its anterior surface to a Vibratome cutting block with cyanoacrylate glue, and warmed gelatin (18-20% in saline), or agar (2% in ACSF) was applied with a syringe around the tissue block for mechanical support. Between two and four 500 µm thick true transverse ELL sections were then cut (while immersed in oxygenated ice cold ACSF) on a Vibratome. The above thickness and orientation of the ELL slices was found to be optimal for maintaining the integrity of the descending tSF projections, as well as the apical dendrites of the ELL neurons upon which they synapse (71).

Since the tSF fibers run rostro-caudally within the ELL (63), slices were positioned rostral side up in an interface slice chamber (Fine Science Tools), allowing for stimulation of the fibers as they course laterally through the ELL segments and descend into the slice. To allow for stabilization, slices were maintained at room temperature in

oxygenated control ACSF for a minimum of 1 hour before recordings were begun. For a more extensive description of this *in vitro* slice preparation, see (71).

III. Stimulation and Recording configurations

Extracellular, and intracellular (70 - 200 MΩ) recording pipettes were pulled from 1.5 mm diameter glass capillary tubing (A-M Systems) on a model P-87 Flaming-Brown, or Frederick Haer micropipette puller, and back filled with 3 M potassium acetate (KAc). Tips of the extracellular pipettes were broken back to approximately 2 µm outside diameter under a microscope, allowing for a high spatial resolution and the isolation of tSF-evoked single unit spikes. For intracellular recordings, pipette tips were dipped in a silicone solution (SIGMACOTE) to enhance membrane sealing after penetration.

Slices were illuminated, either from above by a fiberoptic lighting system or below by light reflected through the base of the recording chamber, and were visualized with a stereo dissecting microscope containing a calibrated graticule for precise positioning of the recording, pressure ejection, and stimulating electrodes. Under these conditions the laminar organization and segmental boundaries of the ELL could clearly be distinguished, and served as references for the placement of stimulating and recording electrodes. Extracellular recording pipettes were positioned in the slice at a minimum depth of 50 µm using a Narishigi hydraulic manipulator, while intracellular pipettes were positioned with a NRC manual manipulator and advanced into the tissue using a Burleigh 6000 controller and microdrive system. Stable intracellular impalements with orthodromic tSF-evoked EPSPs were typically obtained at depths of greater than 75 µm, but rarely exceeding 250 µm into the slice preparations.

Since (a) within the ELL molecular layers the apical dendrites of cells in the more lateral segments tend to curve medially and caudally relative to the position of their somas in the cell body layers (Maler, unpublished observation), and (b) the probability of maintaining continuity of the tSF fibers and their synaptic connections in the VML decreases with distance, both extracellular and intracellular recordings were exclusively carried out within the confines of the Centromedial Segment (CMS). In addition, unless otherwise stated, stimulation was delivered to the tSF fibers as they coursed laterally through the adjacent Medial Segment (MS) of the ELL (as in figure 1.).

For extracellular field recordings, stimulation (180 µsec, 0.2-0.5 Hz) was delivered just dorsal to the tSF pathway via a bipolar electrode, (made from two twisted epoxide strands of 65 µm diameter nichrome wire), connected to a constant-voltage isolated stimulator (Digitimer Ltd.). In a limited number of experiments, paired-pulse stimulation of the tSF pathway was used to assess the possible existence and magnitude of short-term facilitation at the VML synapse. In these cases, the peak amplitude of a control VML response (PK1) was compared to that of a second response (PK2) evoked at an inter-stimulus interval (ISI) ranging from 10 to 130 msec. The relative magnitude of PK2 was then expressed and plotted as a percentage of the peak amplitude of PK1.

In each experiment, the position of the stimulating electrode and stimulus intensity were adjusted to maximize the size of the tSF-evoked field potentials, while minimizing the probability of evoking (a) inhibitory responses by activation of the direct inhibitory feedback pathway just ventral to the tSF (67), and (b) antidromic activation of pyramidal cells via their axons within the plexiform layer (ventral to the tSF). Any contamination

Figure 1. True transverse *in vitro* ELL slice preparation showing position of stimulating (**S**) electrode used in a typical experiment, as well as the segmental organization of the ELL. The dashed vertical line within the CMS (**Rec**) represents a series of recording sites along the dendro-somatic axis of ELL pyramidal cells. **EGp=** *eminentia granularis pars posterior*; **LS=** *lateral segment*; **CLS=** *centrolateral segment*; **CMS=** *centromedial segment*; **MS=** *medial segment*. Asterisk denotes the direct sensory feedback pathway into the ELL, the *tractus stratum fibrosum* (**tSF**).

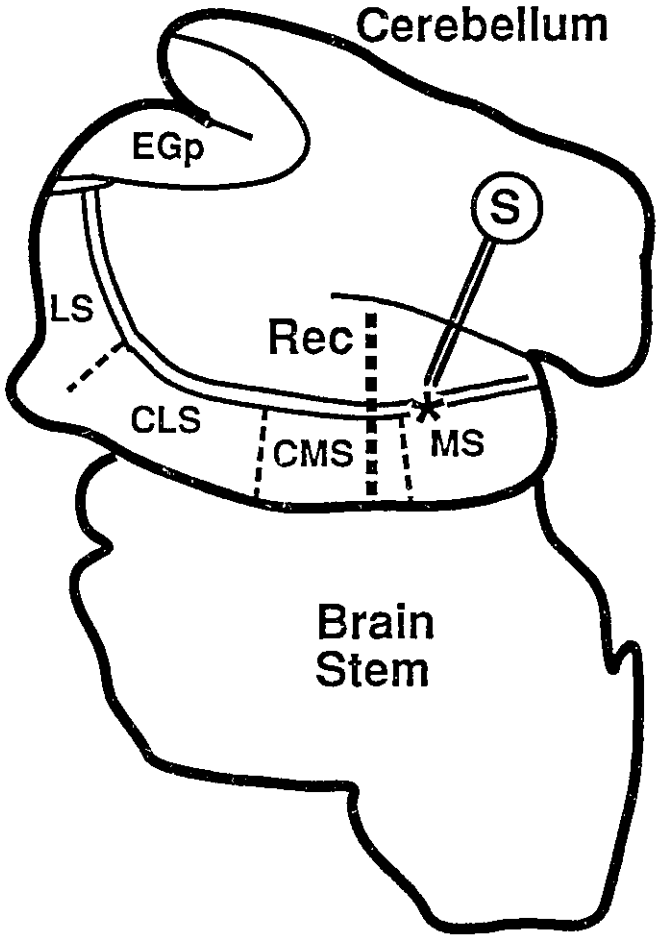
Cerebellum
EGp
S
LS
Rec
CLS
CMS
MS
Brain
Stem

of tSF-evoked responses by antidromic activation could clearly be distinguished (arrows in figure 2, B & C) by a short latency negative-going population spike (pop-spike) in the field recordings at the level of the pyramidal cell layer (123). The mean latency of antidromic pop-spikes was 0.96 msec (±SD=0.42 msec), significantly less ($t=17.698$; $df=15$; $p<0.001$) than the mean latency of 4.30 msec (±SD=0.36 msec) for orthodromic pop-spikes, and therefore their presence was easily detected. In a subset of recordings (N=16), stimulus intensity was incremented over a range of voltages to create stimulus-intensity profiles for the tSF-evoked responses, while in the remaining experiments a maximal stimulus intensity was chosen as above.

Control of timing parameters for stimulation, focal pressure ejection of drugs, and intracellular current injections was carried out using a Master-8 programable controller (A.M.P.I., Israel) triggered by an IBM compatible 386 computer utilizing an Axon Instruments TL-1 interface unit and data acquisition software (PCLAMP Ver. 5.5). The amplitude, duration, polarity, and number of incrementing intracellular current injections collected during each experiment were controlled by PCLAMP data acquisition parameter files.

Extracellular and intracellular recordings of tSF-evoked responses were made using Axon Instruments model HS-2 headstages (gain= X1L and X0.1L respectively) connected to an Axoclamp-2A amplifier. Evoked responses were displayed in real time on a storage oscilloscope (and occasionally a chart recorder), and pre-filtered with a Tektronix AM 502 Differential Amplifier (DC-10 kHz). These analog signal were then digitized with the TL1 interface unit at a 0.04 msec sampling resolution, and stored for further analysis

Figure 2. Averaged extracellular field potentials from the pyramidal cell layer (**PCL**) showing various degrees of antidromic contamination due to excessive stimulus intensity or improper stimulation electrode placement. **A:** Somatic field potential (PCL) uncontaminated by antidromic activation. Arrows in **B** and **C** indicate short latency antidromic population spikes (pop-spikes) at the level of the PCL, while asterisks in **A** & **B** indicate orthodromic pop-spikes superimposed on the underlying PCL field potentials. Note that the antidromic pop-spike precedes (and can be easily distinguished from) the orthodromic pop-spike by a mean of 3.35 msec: ▲= stimulus artifact: ■ = blanked calibration pulse. Calibration bars; (**A** & **B**:1mV/10msec), (C:0.5mV/10msec).

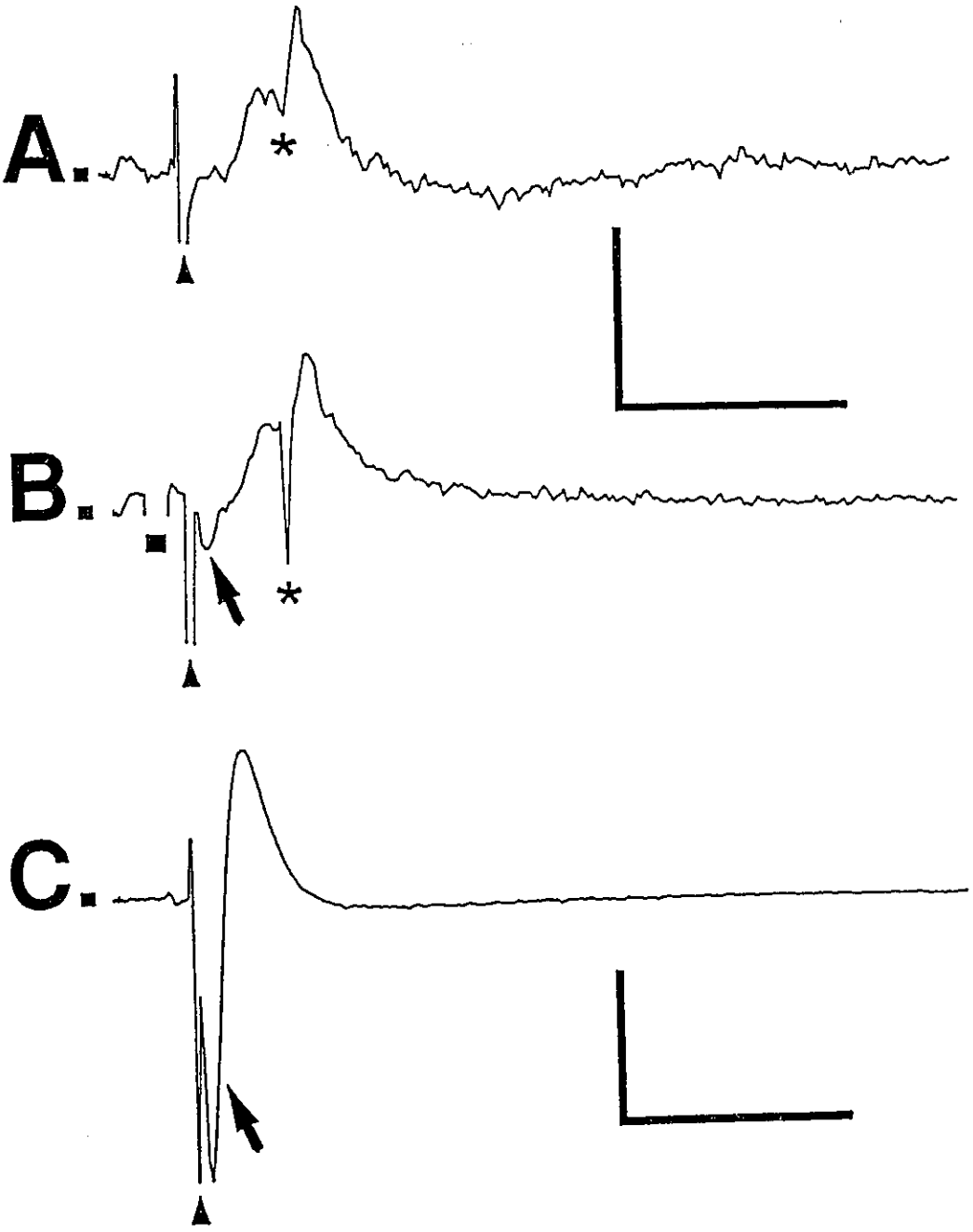
A.
B.
C.

using Axon Instruments data analysis program CLAMPAN. This high sampling rate was chosen for maximal resolution of early tSF-evoked events (ie <50 msec), at the expense of clearly establishing the time course of longer events. Therefore, in a limited number of experiments the sampling rate was reduced to allow for recording of stimulus-evoked events over a time course of several hundred milliseconds.

IV. Application of Pharmacological Agents

Pharmacological manipulations of the ELL slice preparations were carried out by three different methods. In two groups of experiments, VML field potentials evoked under control ACSF conditions were contrasted with those evoked after a minimum of 1 hour bath application of either (a) Mn^{2+} containing ACSF solution to block Ca^{2+}-mediated synaptic transmission, or (b) Mg^{2+}-free (0-Mg^{2+}) ACSF to assess the presence and possible contribution of NMDA receptors to the tSF-evoked responses (see table 1 for ACSF compositions).

The second form of drug application used in these studies was focal pressure ejection, or "micro-drop" application of drugs to the surface of the slice. Ejections were delivered using a PPM-2 Pneumatic pump controlled by a NeuroPhore BH-2 ejection system (Medical Systems Corp.). Pressure ejection pipettes were pulled on the Flaming-Brown puller, broken back to a tip diameter of between 3 and 7 μm, and backfilled with various drugs (see below). Ejection pressures typically were under 10 psi, (to avoid possible mechanical movement of the pipette tip during the ejection), with gated durations of between 80 and 190 msec.

Drugs applied by focal pressure ejection were kynurenic acid (Kyn; 2 mM:Sigma), 3-((RS)-2-Carboxypiperazin-4-yl)-propyl-1-phosphonic acid (CPP; 1 mM:Tocris), 6-Cyano-7-nitroquinoxaline-2,3-dione (CNQX; 1 mM:Tocris), N-Methly-D-aspartic acid (NMDA; 250 µM:Tocris), and (S)-α-Amino-3-hydroxy-5-methyl-4-isoxazolepropionic acid (L-AMPA; 12.5 µM:Tocris). Drugs were mixed in ACSF or PBS, with the exception of CNQX which was first pre-dissolved in 100 µl of DMSO before diluting to its final concentration in control ACSF. Where possible, drug concentrations were chosen which could be directly compared to those previously used *in vivo* (9) or *in vitro* (71;Turner, personal communication). The effects of focal pressure ejections of control solutions (ACSF containing DMSO, PBS and control ACSF) on tSF-evoked VML responses were also tested.

All focal pressure ejections of drugs were into the region of synaptic termination of the tSF fibers in the VML. When slices were back-lit and viewed through a stereo dissecting microscope, the approximate spatial extent of drug pressure ejection could be estimated by the initial change in the refractive index of the tissue at the tip of the pipette. Using this technique, the observable extent of the pressure ejection within the VML was estimated to be typically less than 200 µm in diameter. In contrast, "micro-drop" application typically resulted in a dispersion of the drugs over a significant portion of the slice surface, and therefore was only utilized in experiments for the applications of EAA receptor antagonists (ie CNQX and CPP).

A third method of pharmacological manipulation was used during a limited number of intracellular experiments. Due to the previous immunocytochemical and

electrophysiological (123) localization of Na^+ channels on the soma and proximal apical dendrites of ELL pyramidal cells, recording pipettes filled with the intracellular Na^+ channel blocker (23,90) QX-314 (100 mM in 3 M KAc) were used to assess the possible contribution of voltage-dependent Na^+ conductances to the magnitude and time course of post-synaptic EPSPs evoked by tSF stimulation. For optimal delivery and effectiveness of QX-314 application (23), series of hyperpolarizing to depolarizing current pulses (immediately preceded by hyperpolarizing conditioning pulses) were passed through the recording pipette.

V. Acquisition of Extracellular Field Potentials

Under each stimulus or recording condition, ten to fifteen consecutive tSF-evoked field potentials were collected and averaged using CLAMPAN, and unless otherwise stated, all further analysis was carried out on these averaged waveforms. Field potentials were mapped along the dendro-somatic axis of the ELL pyramidal cells (as in Figure 1.) by two methods. First, tSF-evoked field potentials were recorded from positions corresponding to visually identifiable anatomical structures within the ELL slice preparation (see figure 3.), allowing for the construction of low spatial resolution maps of the extracellular field potentials evoked by tSF stimulation.

In three experiments, a microscope graticule was positioned orthogonal to the orientation of the ELL lamina, and was used as a reference tract for the placement of the extracellular recording electrodes. Multiple recordings (at a constant depth of 50 μm relative to the surface of the slice) were then made at 25 μm steps throughout the total dorsal to ventral extent of the ELL pyramidal cell axis (as in figure 1.). The resulting

Figure 3. Relative positions of the various ELL lamina, as well as the typical stimulation electrode placement just dorsal to the tSF fibers to avoid stimulation of the direct inhibitory feedback pathway ventral to the tSF (not shown), and antidromic activation of pyramidal cell axons within the *plexiform layer* (**PL**). Also depicted are the unmyelinated collaterals of the tSF which climb dorsally to synapse on the proximal apical dendrites of the pyramidal cells forming the *ventral molecular layer* (**VML**). Other abbreviations used: **DFL**= *deep fiber layer*; **GCL**= *granule cell layer*; **PCL**= *pyramidal cell layer*; **DML**= *dorsal molecular layer*. Recording sites in the DML are shown at 100 μm steps relative to the VML recording site.

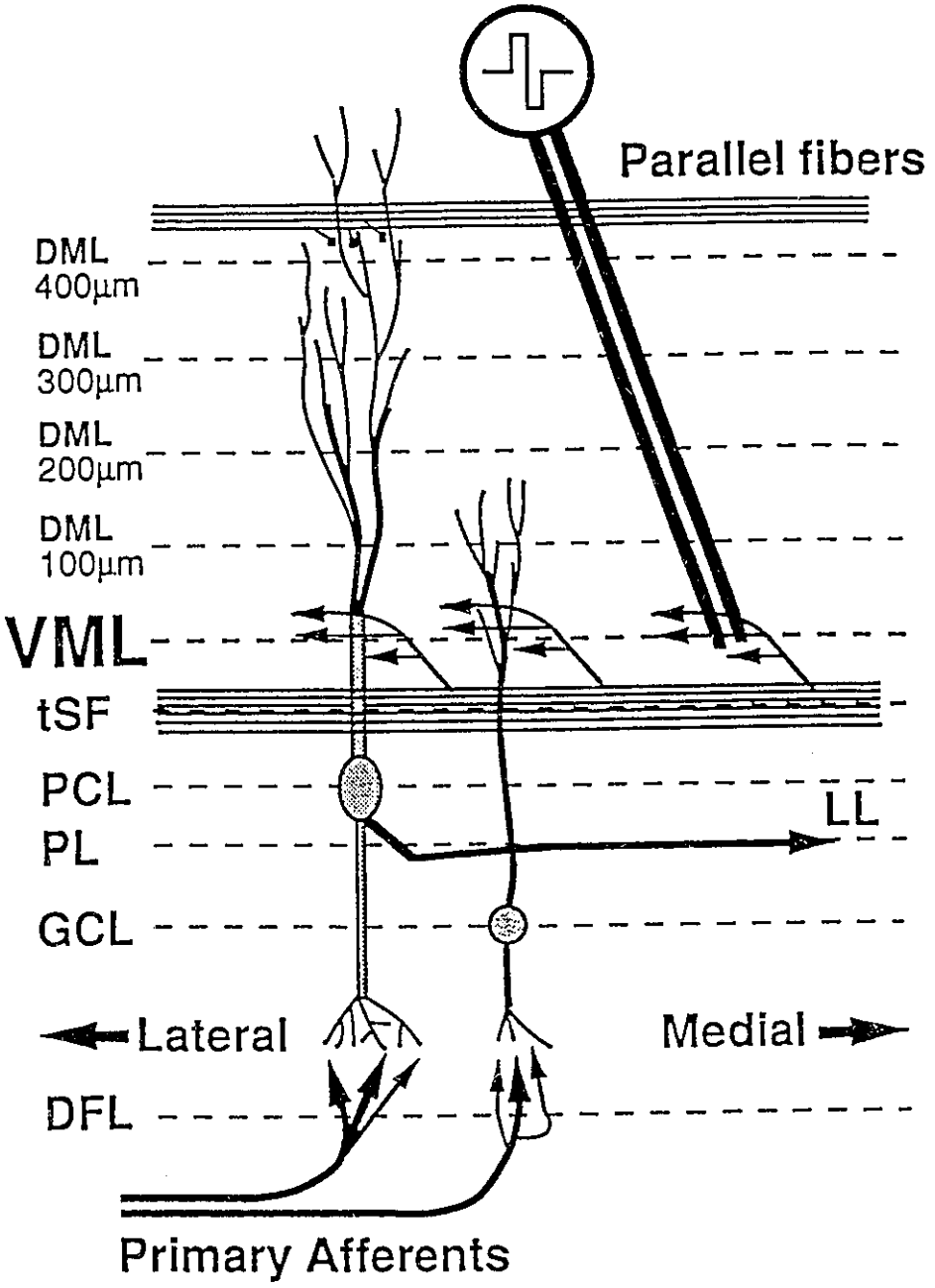
Parallel fibers
DML
400µm
DML
300µm
DML
200µm
DML
100µm
VML
tSF
PCL
PL
LL
GCL
Lateral
Medial
DFL
Primary Afferents

high spatial resolution maps of averaged tSF-evoked field potentials were comprised of either 33 (1 case) or 50 (2 cases) recording sites, and were subsequently used for one-dimensional current source density (CSD) calculations to assist in the interpretation of the field potentials.

VI. Analysis of Extracellular Field Potentials

Preliminary quantification

Averaged extracellular field potentials (10-15) were initially analyzed using Axon Instruments analysis software, CLAMPAN. Other than those collected from the VML, all field potentials recorded during the low spatial resolution mapping of tSF-evoked responses were used for qualitative comparisons only. Measurements were made of the post-stimulus latency to peak and amplitude of the peak of the VML responses under control conditions, and all subsequent effects of various pharmacological manipulations were assessed by measuring the amplitude of the VML response under experimental conditions at the latency of the peak of their matched control responses (see figure 4, A 1 & 2). The resultant raw data values were presented (as in figure 4), and for the sake of clarity, as percentage of their appropriate matched control responses; however analysis was carried out on the raw data using Student's T-test for paired samples. Results were considered significant with computed P values equal or less than 0.05.

Further estimates of the magnitude of VML responses evoked under control and experimental conditions were carried out using a program written to numerically integrate the field potential over time. Assuming the total resistance at the recording site does not change appreciably, the resultant values (total mV x msec) can be viewed as being

Figure 4. Three methods used in the initial quantification of tSF-evoked VML field potentials under control and experimental conditions. **A:** (1) measurements of the post-stimulus latency to the peak of the VML response (**L**), and its amplitude from baseline (**a**) are collected under control conditions, then compared to (2) the amplitude of the VML responses recorded at the control latency (**L**) under experimental conditions.
B: comparison of the integrated voltage over time of the VML response under control (1) and experimental (2) conditions. **C:** VML potentials evoked under conditions of synaptic blockade (ie Mn^{2+}) are digitally subtracted from their matched control responses, and measurements of post-stimulus latency (**L**), amplitude at peak (**a**), and 50% rise (**Rt**) and fall times (**Ft**) of the resultant waveforms are used to estimate the post-synaptic component of the tSF-evoked VML field responses.

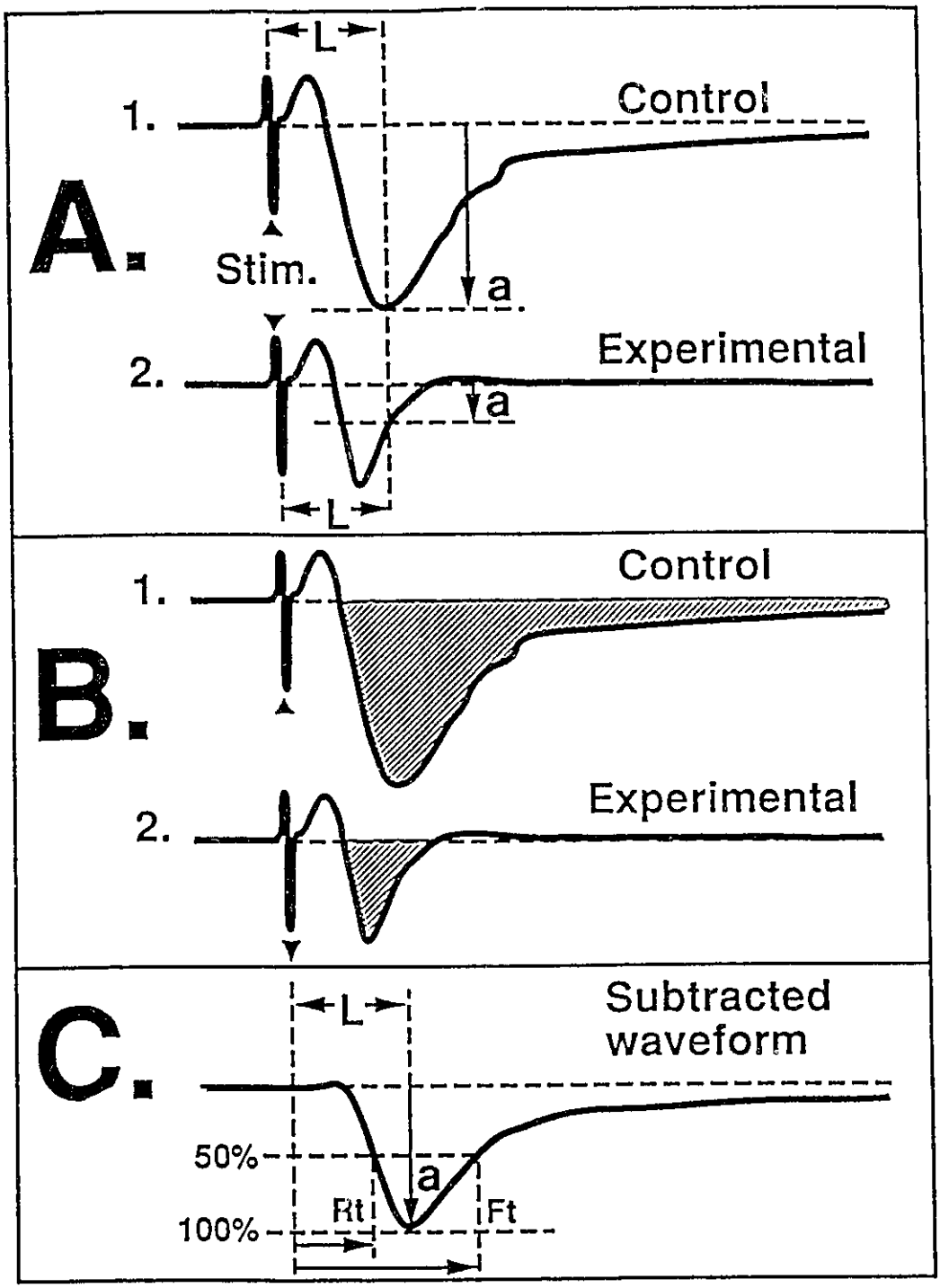
A.
L
1.
Control
Stim.
a
2.
Experimental
a
L
B.
1.
Control
2.
Experimental
C.
L
Subtracted
waveform
50%
a
Rt
Ft
100%

proportional to the total VML currents (synaptic plus voltage gated) evoked by stimulation of the tSF feedback pathway. Comparison of control responses and those evoked under different pharmacological conditions could therefore be made over the entire duration of the recorded response, thus giving a more sensitive (and temporally independent) assessment of the various pharmacological effects on the tSF-evoked VML potentials (see figure 4, B 1 & 2). As above, the effects of pharmacological manipulations on the integrated voltages were expressed as a percentage of that under their matched control responses.

Since extracellular field potentials recorded at the level of the VML reflect the summed contribution of depolarizing pre and post-synaptic membranes, VML responses evoked after 1 hour of blockade of Ca^{2+}-mediated synaptic transmission (4 mM Mn^{2+}/0.2 mM Ca^{2+}; see table 1.) were digitally subtracted from their matched control responses. The latency to peak, peak amplitude, and half-height rise and fall times of these resultant subtracted waveforms were then measured using CLAMPAN and used to approximate the magnitude and temporal characteristics of the post-synaptic component of the tSF-evoked VML field potentials recorded at this synapse (see figure 4, B 3).

In three experiments carried out under Mn^{2+} ACSF perfusion, the delay to the peaks of tSF field potentials recorded at varying distances along the tSF pathway were measured. After recording the post-stimulus latency to the peak of a reference tSF response, the recording pipette was advanced in 100 μm steps along the tSF fiber tract, and the latencies to the peaks of responses recorded at these new positions were used to calculate a mean conduction velocity for this pathway. In addition, a comparison of the

post-stimulus latency to the peak of reference tSF responses, and matched field potentials recorded 100 μm dorsal in the VML, were used to estimate the conduction delay introduced by the unmyelinated tSF collaterals which ascend and synapse in the VML.

One-dimensional Current Source Density Analysis

Extracellular recorded field potentials represent the algebraic sum of all current sinks (inward currents) and sources (outward currents) generated by neural structures spatially distributed within the slice preparation. As such, even though an evoked field potential is recorded at a spatial location corresponding to a specific neural structure within the slice (ie. the VML or PCL), it is impossible, without specialized analytical techniques, to interpret any component of these evoked responses as being *generated* at the location of the recording electrode. One such analytical technique, which has been applied successfully *in vitro* (14,102,120), is one-dimensional Current Source Density analysis (CSD).

Application of CSD analysis to extracellular recorded evoked field potentials allows for a detailed analysis of the spatio-temporal nature of synaptic activity in laminar neural structures. However, before a CSD analysis can be carried out, a number of assumptions regarding the physical characteristics of the extracellular medium are made. These are (a) that the extracellular space behaves like an Ohmic conductor, (b) that the majority of current flow in the laminar structure is along the dendro-somatic axis, and is invariant parallel to the layers, and (c) that the magnitude and form of the evoked field responses are constant over time (92). While important to allow for a *quantitative* analysis of the various localized current sinks or sources, these assumptions can be

violated to a great extent with little effect on the *qualitative* nature (ie. being a sink or source), or the temporal nature of the CSD results. Since no direct testing of these assumptions were carried out for the present studies, all subsequent CSD data was used exclusively for determining the temporal and spatial localization of the various tSF-evoked currents within the ELL slice preparations, and was only used as an aid for the interpretation of field potential data.

A subroutine was written within the data analysis program to perform one-dimensional CSD analysis on averaged tSF-evoked field potentials collected during the three high spatial resolution mappings of the ELL slice preparation. At the core of this subroutine is an algorithm which iteratively applies an equation to carry out the one-dimensional CSD analysis (see equation 1. below), while taking into account both the spatial sampling interval used in the recording of the evoked responses (ΔZ= 25 µm), as well as allowing for the interactive control and optimization of the size of the CSD integration grid ($n^*\Delta Z$) used in the computation (see 14). The CSD results from each recording position were then plotted as waveforms across time, or were plotted as a waveform comprised of CSD values taken at a set time and plotted across space. The latter technique allowed for a spatial localization of the various tSF-evoked current sinks and sources within the ELL slice preparation.

Equation 1.(adapted from 14)

$$\frac{\partial^2 \Phi}{\partial z^2} = \frac{\Phi(z+n^*\Delta z)-2\Phi(z)+\Phi(z-n^*\Delta z)}{(n^*\Delta z)^2}$$

∂= first derivative: ∂^2=second derivative: Φ=evoked potential: z=spatial location: Δz=sampling interval: $n^*\Delta z$=CSD integration grid

VII. Acquisition of Intracellular Data

Classification of recording position

Intracellular impalements were obtained by slowly advancing the recording pipette through the tissue (at the level of the PCL, or just ventral or dorsal to the tSF) while constantly monitoring for any fluctuations in the recorded potential at the tip of the electrode. Repetitive hyperpolarizing current pulses (-0.7 nA, 100 msec, 1Hz) were continuously passed through the recording pipette, and the subsequent voltage deflections were used both to monitor any changes in the input resistance of the pipettes, and as a reference to maintain the balance of the amplifier "bridge" circuitry. Slow changes in recorded extracellular potential were monitored and cancelled using the amplifier DC offset.

An increase in recorded noise, small negative deflections in the recorded potential, "injury potentials", or an increase in the input impedance of the pipette, frequently preceded the impalement of neurons. At this point, impalements could often be achieved by a brief "buzzing" or saturation the capacitive compensation circuitry of the Axoclamp-2A amplifier. Various amounts of constant hyperpolarizing current injection were often used immediately after penetration to assist in the stabilization and sealing of the impaled neurons, and then was gradually reduced or stopped prior to data collection.

Previous studies (71) have suggested that recordings from cells in the ELL slice preparation can be tentatively classify as having either "pyramidal" or "polymorphic-like" characteristics on the basis of their response to intracellular depolarizing current ejection. "Polymorphic-like" responses are identified as having extremely fast and narrow action

potentials with very prominent and sharp after-hyperpolarizations (AHPs) (Turner, unpublished observation). These responses are typically recorded only from positions in the deeper PCL and superficial plexiform layer, the location where most polymorphic cells are located (63). As the recording positions in the present studies where typically more dorsal in the PCL, "polymorphic cell-like" responses where rarely encountered (N=2). As such, since within the PCL pyramidal cells are far more numerous and significantly larger in diameter (ie. 18 µm vs 12 µm) than polymorphic cells (63), it is assumed that the majority of stable intracellular recordings were obtained from either basilar or non-basilar pyramidal cells. Although recent studies have suggested that there might be functionally distinct classes of ELL pyramidal cells (12), no attempt was made to distinguish these cells in the present studies.

While intracellular recordings were acquired from morphologically unidentified neurons, on the basis of (a) the visual placement of the recording electrode within the lamina of the ELL, and (b) the characteristic form of action potentials and their AHPs evoked by depolarizing current ejection or antidromic activation (123), the location of the intracellular impalements were classified as being either "somatic" or "dendritic".

Stimulation protocol

For intracellular recordings, stimulation was delivered through a sharp monopolar tungsten electrode which could be positioned adjacent to or in the tSF fiber bundle, thereby optimising for stimulation intensity and placement. In each experiment, stimulus intensity was increased to determine the orthodromic action potential threshold, then gradually reduced to an intensity which consistently evoked EPSPs (at the resting

membrane potential) which were sub-threshold for the initiation of action potentials. To assess the effects of various pharmacological agents on tSF-evoked EPSPs, between 5 to 15 consecutive control responses were evoked and recorded at the resting membrane potential of the cell, averaged, and then contrasted (as described below) with the form and magnitude of their matched averaged EPSPs evoked under the drug conditions.

In a limited number of experiments, paired-pulse stimulations were delivered (with a set ISI of 40 msec), while the cell's membrane potential was held at various hyperpolarizing to depolarizing potentials. In this way the relative contribution of both voltage-dependent post-synaptic processes, and presynaptic processes such as facilitation of transmitter release, to paired-pulse potentiation could be assessed. Short trains of tetanic stimulation (10 stimulations @ 100 Hz) were also used to investigate the magnitude of frequency facilitation at this synapse.

VIII. Analysis of Intracellular Data

Immediately after the slices had stabilized, the occurrence and form of any spontaneous neural activity was noted. The mean basal membrane potential (Vm) of cells (relative to the potential recorded in the extracellular space) were computed off line by measuring the digitally averaged basal membrane potential (across all trials) recorded immediately preceding current ejection. Input resistance (Ri) of the impaled soma or dendrite was calculated by measuring the steady-state membrane potential achieved by various magnitudes of subthreshold hyperpolarizing to depolarizing current ejection (-1 nA to +1 nA; 0.15 nA increments). When the magnitude (in mV) of the stabilized membrane potential shift was plotted as a function of current ejection intensity (in nA),

and fit with a linear regression, the slope of the regression line could be used as an approximation of the neuron's input resistance. In addition to the above measurements, the mean current-evoked action potential halfwidths from somatic and dendritic impalements were also collected, and the above data from somatic and dendritic impalements were compared using Student's T-test for independent samples.

The time course and form of tSF-evoked EPSPs were further characterized in a limited number of cases by exponential fitting of the decay phase of the EPSPs. The decay phase of the EPSP was first fit with an exponential function, and a measure of the "goodness of fit" was calculated (Chi^2) and compared to that obtained by attempting to fit the decay phase of the EPSP with double exponential curves. The resultant values served to both characterize the general form, and approximate time course of tSF-evoked post-synaptic events.

Analysis of EPSP voltage-dependence

To determine the possible voltage-dependence of tSF synaptic input, EPSPs were recorded at the basal membrane resting potential, and with the cell's membrane potential clamped at various levels with hyperpolarizing or depolarizing current ejections. The magnitude, form, and time course of intracellular recorded tSF-evoked EPSPs were then measured at various membrane potentials. Measurements of the stabilized basal membrane potential of the cell at the time of the evoked EPSP, latencies to 10% and the peak amplitude of the EPSP, the 10-to-90% rise time, the EPSP peak amplitude, EPSP half width, and the amplitude of the EPSP at a post-stimulus interval of 40 msec were all computed (see figure 5, 2 & 3). The above quantitative measures could then be plotted

Figure 5. Parameters used in the quantification of intracellular recorded EPSPs.
1: Effects of hyperpolarizing to depolarizing current ejection, both alone and combined with synaptic activation (as depicted), are first collected. **2:** After the awmbrane potential has stabilized during current ejection, a series of 34 consecutive data points are averaged to calculate the pre-stimulus mean baseline potential. At stimulation (▲), the stimulus artifact is automatically blanked (**B**), and used as a time reference for th+wcalculation of post-stimulus latencies of the EPSP peak amplitude (**C**), as well as its amplitude at 40 msec (**D**). **3:** Measurements of EPSP peak amplitude (from subtracted baseline), latency to 10% of the EPSP peak amplitude (**A**), 10%-90% rise time (**B**), as well as the EPSP half-width (**C**) are also collected.

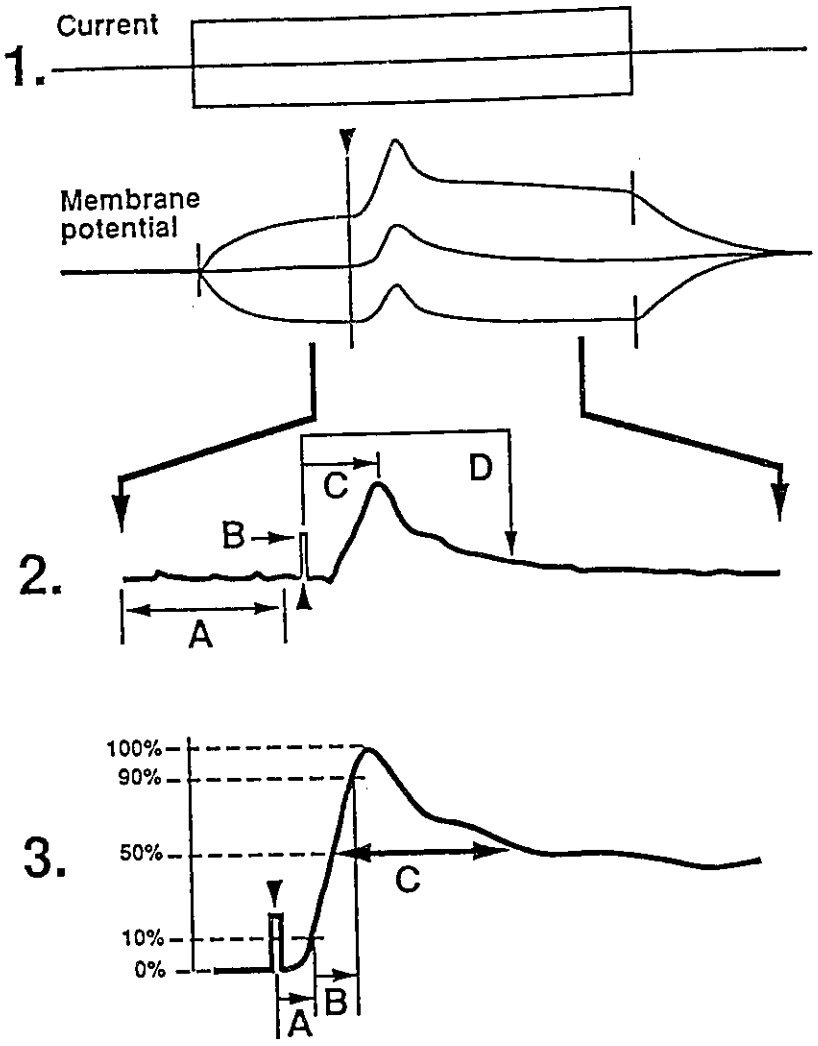
1.
Current
Membrane potential
2.
A
B
C
D
3.
100%
90%
50%
10%
0%
A
B
C

as a function of the membrane potential at stimulation to determine the presence of any voltage-dependent components of the tSF-evoked EPSPs.

Quantification of Pharmacological effects

Averaged tSF-evoked EPSPs (comprised of between 8 to 15 consecutive responses) were first collected under control ACSF conditions. Approximately one minute following pressure ejection of a pharmacological agent into the region of the VML, a second set of EPSPs were collected and averaged. Pre and post drug averaged EPSPs were then plotted for direct comparison, and EPSPs evoked under the various drug conditions were digitally subtracted from their matched control responses to estimate the form and magnitude of the pharmacological effects. In the case of QX-314 application, since the onset of this drug's effects are rapid, and in the present studies the exact time course of onset is not known, the relative effects of QX-314 on tSF-evoked EPSPs were only assessed by comparison to EPSPs recorded from equivalent control impalements.

RESULTS

EXTRACELLULAR STUDIES

I. Mapping of tSF-evoked responses

Qualitative Characterization

Extracellular field potentials evoked by stimulation of the tSF feedback pathway were collected from 44 slices, and in 8 experiments extracellular field potentials were mapped at multiple locations along the dendro-somatic axis of the ELL pyramidal cells. Extracellular recording positions were verified visually using a stereo dissecting microscope, and correlated with the position of identifiable anatomical structures within the ELL slice preparation (as in figure 3).

Field potentials recorded at the level of the pyramidal cell layer (PCL) were characterized by a positive-going potential, upon which stimulus-evoked single unit spikes were often seen (figure 6, PCL). Ventral to the PCL, this potential rapidly decayed (ie figure 6, PL), and was absent in recordings from the deeper layers of the ELL (ie GCL or DFL). Recordings from within the tSF fiber tract consisted of a short latency (ie 1.73 msec;±SD=0.30 msec) negative-going potential (figure 6, tSF) whose latency to peak (1, figure 6) preceded those in the VML (2, figure 6) and PCL (3, figure 6). These results suggest the existence of both synaptic delay (~1.06 msec) at the VML synapse (1-2), as well as a delay (~1.93 msec) introduced by passive dendro-somatic current spread (2-3). By far the largest tSF-evoked extracellular field potentials (figure 6, VML) were recorded at a spatial location corresponding to the zone of synaptic termination of the tSF fibres in the VML (63). At a position 100 μm dorsal to this recording site (figure 6, DML(1)),

Figure 6. Low spatial resolution map of tSF-evoked field potentials recorded at positions and structures corresponding to those depicted in Figure 3. The latency (1.06 msec) between the peak of tSF fiber volley (1), and peak of the VML response (2), suggest synaptic delay followed by a further delay (1.93 msec) due to current spread to the PCL (3): **DFL**= *deep fiber layer*; **GCL**= *granule cell layer*; **PL**= *plexiform layer*; **PCL**= *pyramidal cell layer*; **tSF**= *tractus stratum fibrosum*; **VML**= *ventral molecular layer*; **DML(1)-DML(4)**= successive 100 µm advancements of the recording pipette (relative to the VML recording site) into the overlaying *dorsal molecular layer* of the ELL. Calibration bars; 1mV/5msec: ▲= stimulus artifact.

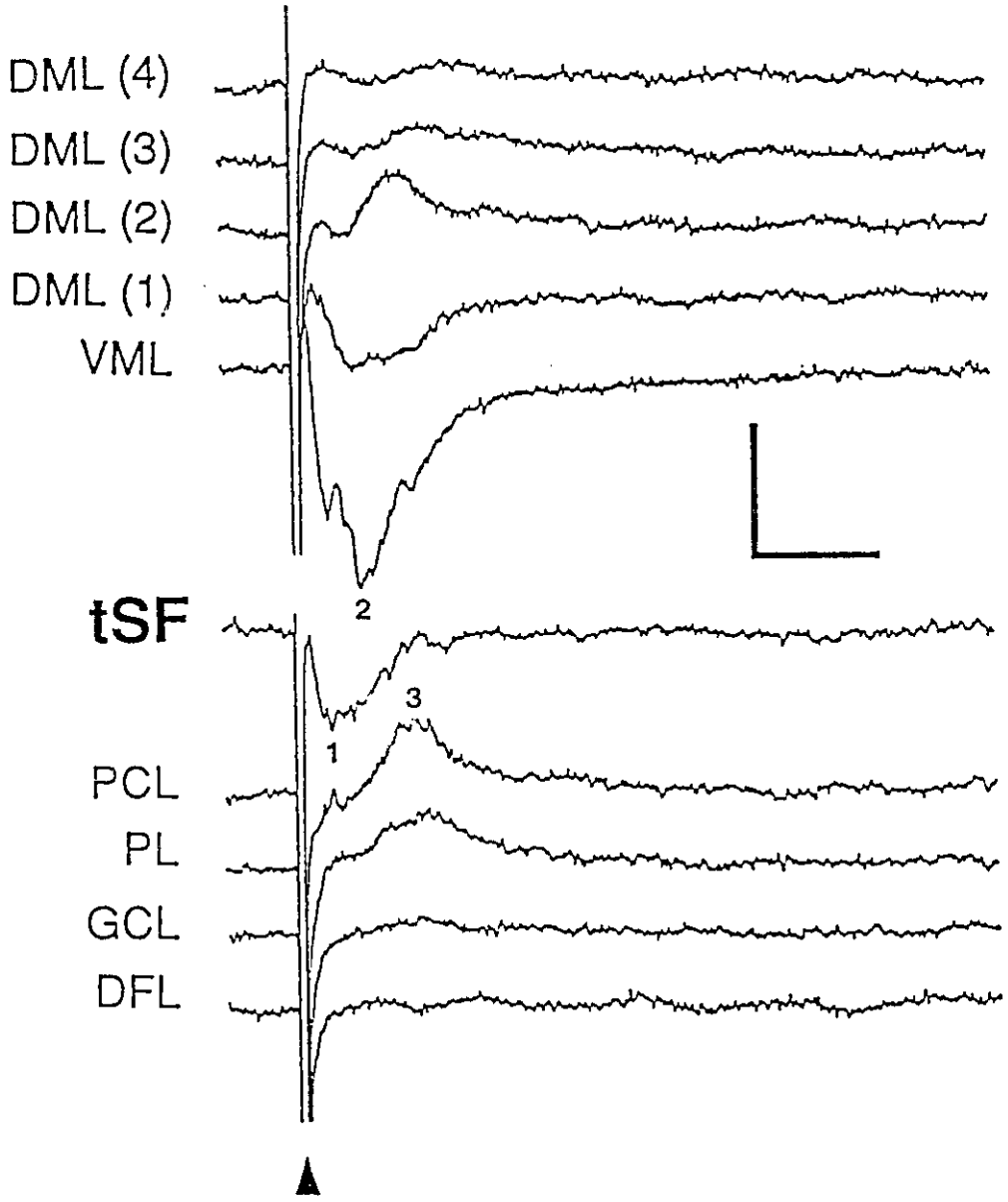
DML (4)
DML (3)
DML (2)
DML (1)
VML
tSF
PCL
PL
GCL
DFL
1
2
3

the magnitude of the evoked response was significantly diminished, and with successive 100 μm advances of the recording electrode into the DML, the response reversed polarity (DML 2) and decayed (DML 3 & 4) in a manner consistent with passive current spread. The spatially restricted nature of the tSF-evoked VML response strongly suggested the existence of a highly localized current sink at this position. This interpretation was subsequently tested utilizing one-dimensional current source density analysis.

Current Source Density (CSD) Analysis

One-dimensional current source density analysis confirmed the spatially restricted nature of the tSF input in the VML. Using a differentiation grid of 3, a prominent current sink was localized in the VML which was spatially and temporally coincident with the large extracellular field potential also recorded at the VML site (see figure 7, A & B). When all current values recorded at the time of this maximal current sink (see arrow in figure 7 B) were plotted against their relative spatial locations along the dendro-somatic axis of the ELL (see inset, figure 7), the prominence and spatially restricted nature of the VML current sink could clearly be seen. These results therefore electrophysiologically confirm the previously morphologically characterized spatially restricted nature of the tSF pathway's termination pattern in the VML (63). In addition, the high degree of spatial and temporal correspondence between the computed VML CSDs and their extracellular field potentials further supports the interpretation that the generation of these VML field potentials are primarily local in nature, and validates the use of the recorded VML field potentials as a proportional approximation of tSF-evoked VML currents.

Figure 7. Comparison of a superimposed high spatial resolution map of tSF-evoked field potentials (**A**) with the corresponding results of a one-dimensional current source density analysis (**B**). Inset depicts the various lamina of the ELL scaled to the spatial location of the current densities recorded at the latency of the maximal current sink (2.6 msec) in the CSD (arrow in **B**). When graphed this way, the CSD results clearly show the spatially restricted nature of the tSF-evoked VML currents: n= size of CSD differentiation grid: Δz= spatial sampling interval.

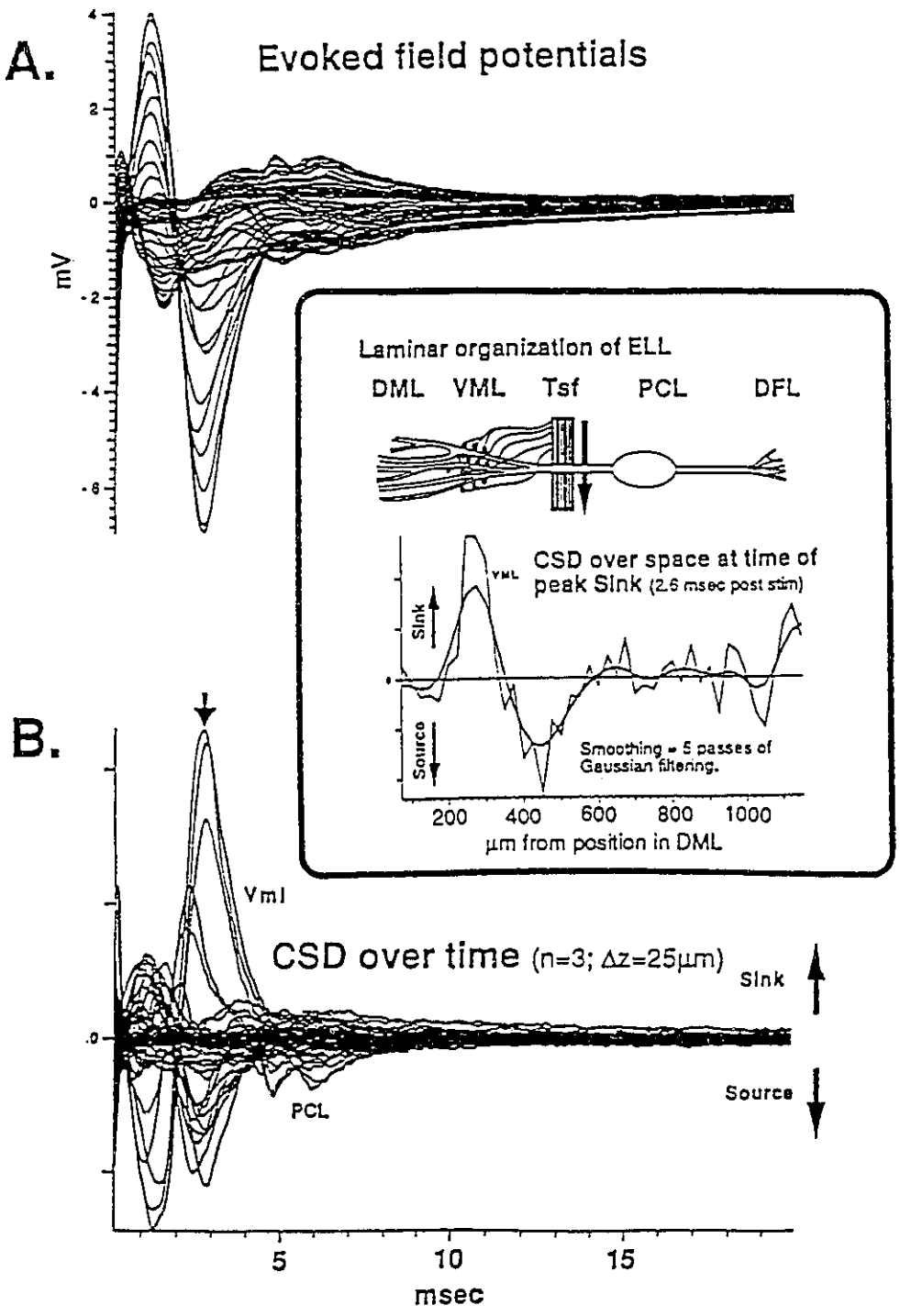
A.
Evoked field potentials
mV
Laminar organization of ELL
DML VML Tsf PCL DFL
CSD over space at time of peak Sink (2.6 msec post stim)
Sink
Source
VML
Smoothing = 5 passes of Gaussian filtering.
200 400 600 800 1000
µm from position in DML
B.
Vml
CSD over time (n=3; Δz=25µm)
Sink
Source
PCL
5 10 15
msec

II. Characterization of VML Responses

Control VML field potentials

Averages of 10 to 15 consecutive tSF-evoked VML potentials, recorded from 35 cases under control ACSF conditions, were used to calculate the magnitude and time course of the components consistently seen in all VML responses. All VML field potentials were consistently comprised of at least two distinct components or phases, and a third variable early component which was occasionally observed. In a number of cases, activation of the tSF pathway with bipolar stimulation (mean intensity of 66.32 volts; ±SD=14.52) resulted in an early positively-going component which (a) varied in occurrence or magnitude between slices, and (b) whose amplitude was dependent on the recording electrode's position along a plane orthogonal to, and transecting that of the VML (see asterisk in figure 8, 1). This earliest component of the VML response was most prominent in slices whose orientation of cut deviated from being truly transverse, and where the magnitude of the two later invariant components of the VML response were often significantly diminished. In these cases, in contrast to a sharply delineated pathway, the tSF was often seen as a dispersed band of white matter extending dorsally into the region of the VML.

In light of (a) the rapid onset of this earliest component of the VML response, (b) its polarity, and (c) the fact that it was variably effected by subsequent pharmacological manipulations (see figure 11, A & B), it was concluded that this initial positivity in the VML field might represent distal current sinks being generated in the tSF fibers or the VML medial to the recording site. As such, following stimulation of the tSF pathway both

Figure 8. Common components seen in all tSF-evoked VML field potentials under control ACSF conditions. **1:** Control response, (and response evoked after ejection of control PBS vehicle into the VML), showing, (**A**) fast negative-going component of the VML response, (**B**) initial fast decay phase, and (**C**) slow decay phase back to baseline. Asterisk in **1** indicates the highly variable positive component of the VML response. **2:** tSF-evoked VML response shown with a longer time base illustrating the typical duration and decay of the late phase (asterisk); note that the early positive-going component (arrow) is very small in this case. Calibration bars; (**1**:1mV/5msec), (**2**:1mV/25msec): ▲=stimulus artifact.

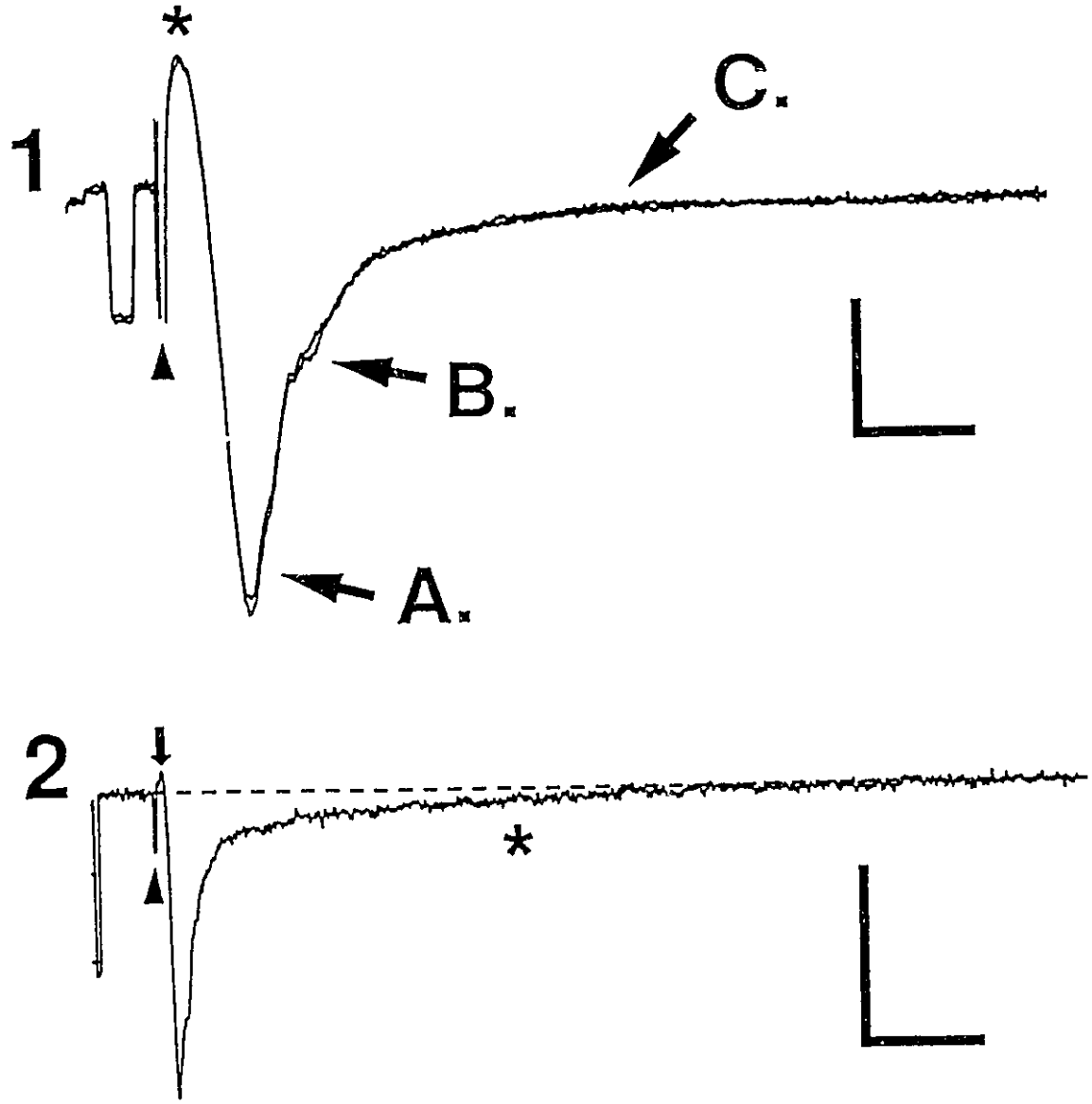
1
*
C.
B.
A.
2
*

conduction and synaptic delays would result in a spread of excitation laterally towards the VML recording site, which would initially be detected as a brief current source temporally preceding the activation and local generation of a current sink. Due to its highly variable nature, and ambiguous mode of generation, this early positive-going component was not included in any subsequent estimates of the magnitude of tSF-evoked VML responses under control or pharmacological conditions.

The two invariant components of all tSF-evoked VML field potentials were a rapid negativity (A, figure 8,1), reaching a mean peak amplitude of -3.02 mV (±SD= 1.50 mV), and occurring at a mean post-stimulus latency of 3.16 msec (±SD=0.56 msec). This negativity was then immediately followed by an initial fast decay phase (B, figure 8,1), and a subsequent slow decay back to baseline which occasionally lasted up to 200 msec (see C in figure 8 (1), & asterisk in 2). This slow decay phase was only observed in recordings made at the level of the VML, and was absent in the field potentials and CSDs taken at positions in the tSF or the DML (see figure 6).

Effects of Mn^{2+} blockade on tSF-evoked VML fields

In six experiments, bath application of Mn^{2+} (and low Ca^{2+}) containing ACSF resulted in a significant suppression of the tSF-evoked VML responses (see figure 9(1), A vs B). The mean peak amplitude of VML responses evoked under Mn^{2+} was reduced to only 29.90% (±SD=15.59%) of the peak amplitude of their matched control responses (t=3.57; df=5; p=0.016). Likewise, the mean integrated voltage of VML responses evoked under Mn^{2+} were reduced to 18.97% (±SD= 11.14%) of their matched control responses (t=2.695; df=5; p=0.043).

Figure 9. Effect of Mn^{2+} blockade of calcium mediated synaptic transmission on the tSF-evoked VML field potential. **1:** Averaged control VML field potential (**B**) contrasted with an averaged potential recorded after 1 hour exposure to Mn^{2+} containing ACSF (**A**). **2:** Digital subtraction of wave **A** from **B** (above) showing the magnitude and time course of the synaptically mediated component of the tSF-evoked VML response. Asterisk in **2.** indicates the prolonged late decay phase of the EPSP. Calibration bars; 1mV/5msec: ▲=stimulus artifact.

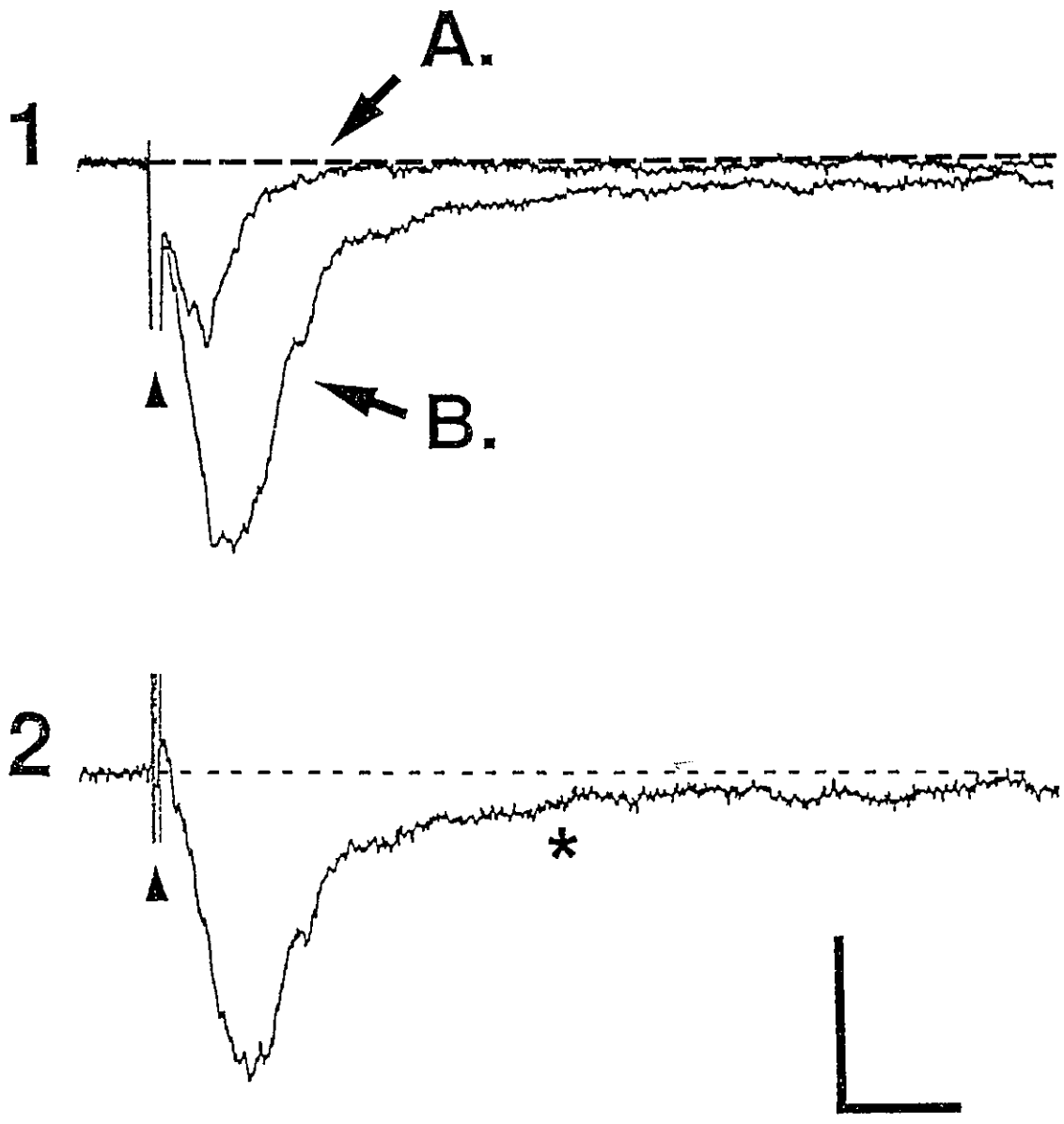
A.
1
B.
2
*

Using CLAMPAN, field potentials evoked under Mn^{2+} ACSF conditions were digitally subtracted from their matched control responses. The resultant subtracted responses (ie figure 9, 2) represent the Ca^{2+}-dependent synaptically-mediated component of the tSF-evoked VML response, having a mean peak amplitude of -1.73 mV (±SD= 0.99 mV) at a mean post-stimulus latency of 4.30 msec (±SD= 1.29 msec), and having mean half-height rise and fall times of 2.57 msec (±SD= 0.57 msec) and 6.54 msec (±SD= 1.17 msec) respectively. The time course of this Mn^{2+}-sensitive component of the VML field potential suggests a biphasic post-synaptic response comprised of a rapid depolarization and decay followed by a prolonged late decay phase (asterisk in figure 9, 2).

The mean peak latency of VML responses evoked under Mn^{2+} perfusion (2.55 msec; ±SD=0.73 msec) was significantly ($t=2.856$; $df=5$; $p=0.036$) less than that of their matched control or subtracted waveforms, consistent with the interpretation that this residual component of the tSF-evoked VML field potential seen under Mn^{2+} represents presynaptic fiber volley in the tSF fibers and their collaterals. While interpretation of extracellular field potentials must be constrained by the spatially diffuse nature of their generation, in the case of tSF-evoked VML responses the (a) prominence of this spatially restricted field potential, as well as (b) its temporal and spatial correspondence with the large spatially restricted VML CSD current sink, both suggest that these subtracted field potentials truly reflect the relative contribution of *local* post-synaptic mechanisms to the generation of these responses. As such, recordings made under Mn^{2+} suppression of Ca^{2+}-mediated synaptic transmission allows for an approximation of the time course and

magnitude of the post-synaptic components underlying the extracellular recorded VML field potentials.

In figure 10, VML responses evoked over a wide range of stimulation intensities (5-50 V) under control (A) and Mn^{2+} ACSF conditions (B) are shown, as well as their respective subtracted waveforms (C). When stimulus intensity was gradually increased, a progressive enhancement of the early negative-going component of the response was seen, some of which could be accounted for by an increased contribution of non-synaptic (ie fiber volley or antidromic) contamination (as seen in Figure 10 B.). At increasing stimulus intensities (ie 20-25 volts), a Mn^{2+}-sensitive enhancement of the late component of the VML response was seen (see asterisk in Figure 10, A & C.), suggesting an intensity-dependent tSF-mediated recruitment of the post-synaptic response.

Blockade of Ca^{2+}-mediated synaptic transmission by Mn^{2+} ACSF perfusion also permitted the recording of isolated fiber volley within the tSF pathway itself, (and its collaterals in the VML), thereby allowing for an estimation of conduction velocities and presynaptic transmission delays within this pathway. Data from three experiments conducted under Mn^{2+} perfusion was collected to estimate the mean conduction velocity along the tSF pathway. Based on a comparison of the post-stimulus latency to the peak of a reference tSF field potential (figure 11, 1 A & dashed line), and the peak of responses recorded 100 μm (figure 11, 1 B) and 200 μm (figure 11, 1 C) lateral along the tSF, a mean conduction velocity of 0.31 m/sec was calculated for the tSF pathway within this slice preparation.

Figure 10. Stimulus intensity profiles (5 to 50 volts) comprised of 10 averaged evoked VML responses under control (**A**) and Mn^{2+} containing ACSF conditions (**B**), as well as their resultant subtracted waveforms (**C**). Asterisk in **A** and **C** show the Mn^{2+} sensitive (and therefore presumably post-synaptic) voltage-dependent later components of the VML response observed at higher stimulus intensities. Calibration bars; 1mV/5msec: ▲=stimulus artifact.

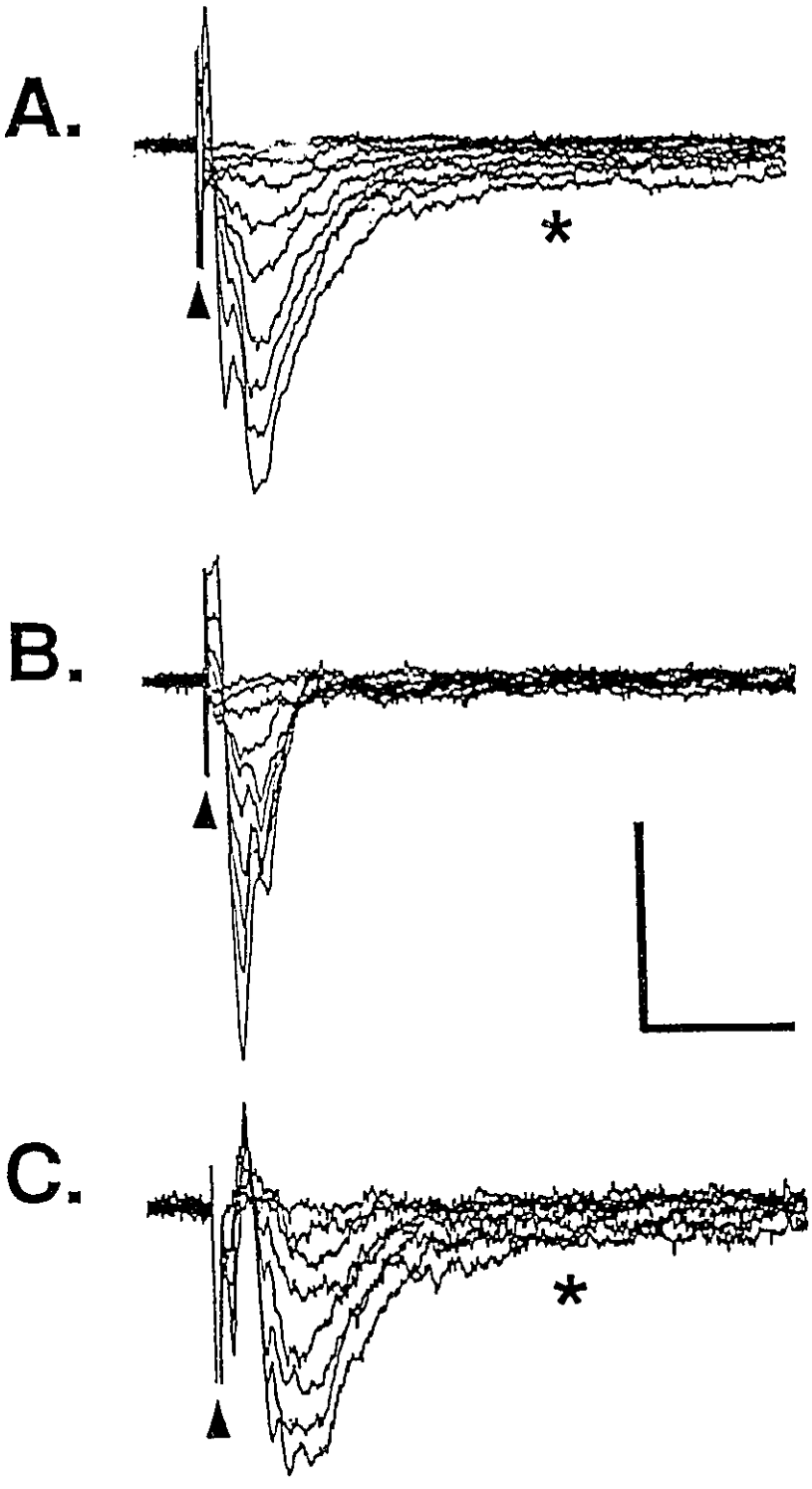
A.
B.
C.

Figure 11. Estimation of mean conduction velocity for tSF, and collateral fibers within the VML, under Mn^{2+} blockade of Ca^{2+}-mediated synaptic transmission. 1.(**A**) Reference recording from tSF (dashed vertical line in 1 & 2 denotes latency of the peak of reference response), and responses recorded (**B**) 100 µm and (**C**) 200 µm lateral in the tSF fiber tract. **2.** Comparison of mean post-stimulus latencies of tSF (**B**), and field potentials recorded 100 µm immediately dorsal in the VML (**A**). Note conduction delay of 0.28 msec likely introduced by the unmyelinated collaterals of the tSF fibers in the VML. Calibration bars; (1: 1mV/5msec), (2: 2mV/5msec): ▲=stimulus artifact.

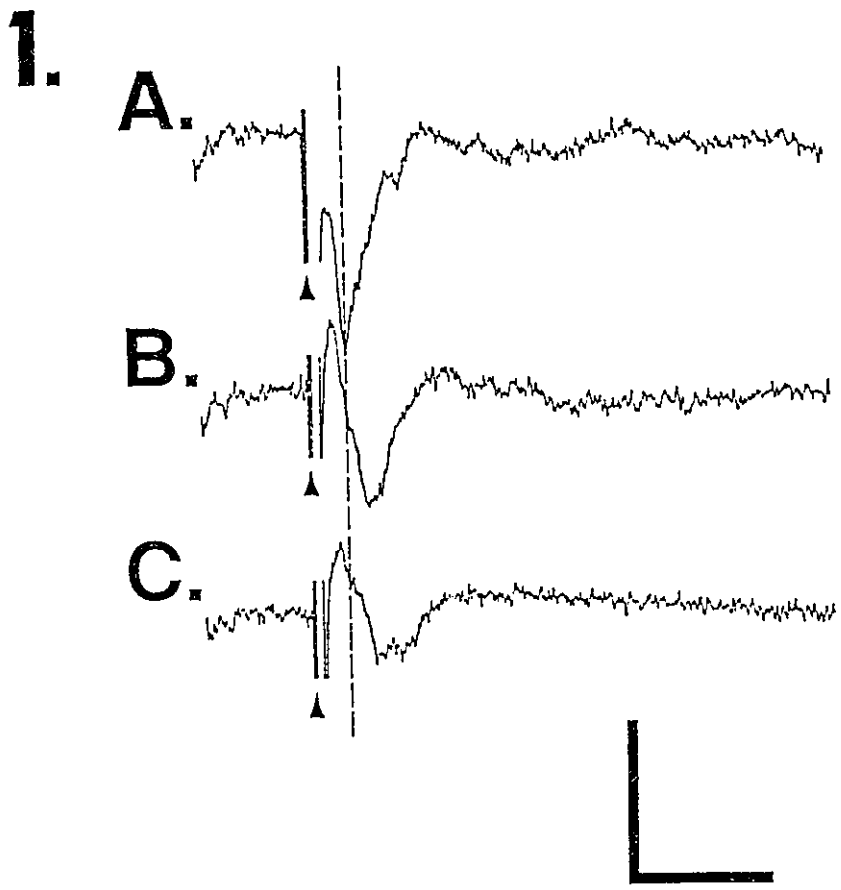
1.
A.
B.
C.

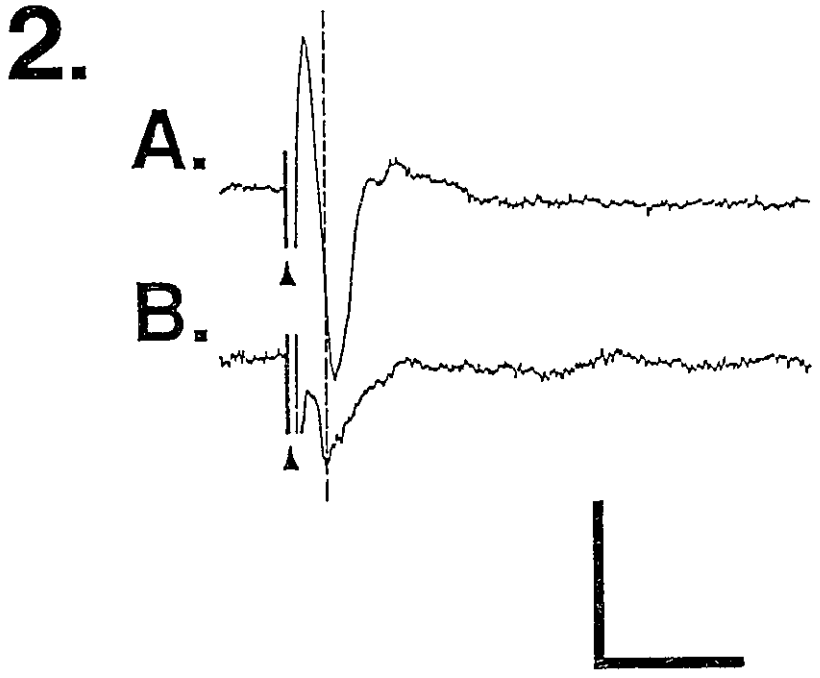
2.
A.
B.

In eight recordings, the mean post-stimulus latency to the peak of tSF field potentials recorded under Mn^{2+} (figure 11, 2 B & dashed line) were compared to those of responses recorded 100 µm immediately dorsal in the VML (see figure 11, 2 A). The mean latency to the peak of reference tSF potentials was 1.84 msec (±SD= 0.43 msec), significantly (t=3.869; df=7; p=0.006) less than the mean post-stimulus latency of 2.12 msec (±SD= 0.42 msec) to the peak of the fiber volley in their matched VML recordings. These results suggest a mean conduction delay of approximately 0.28 msec (±SD= 0.20 msec) introduced by the unmyelinated collateral of the tSF fibers which ascend and synapse in the VML.

III. Role of Excitatory Amino Acid (EAA) Transmission at the VML Synapse

Biochemical assays (86), receptor binding (65), immunohistochemistry (126), and pharmacological studies (9) have all implicated EAAs, specifically glutamate (126), as important neurotransmitters of the tSF of *Apteronotus leptorhynchus.* In an attempt to assess the possible contribution of EAA receptors to synaptic transmission at the VML synapse, various EAA receptor agonists and antagonists were applied by pressure ejection, and their effects on unit activity and tSF-evoked VML field potentials were assessed.

Activation by EAA receptor agonists

Utilizing both intracellular recordings, and extracellular single unit recordings with cumulative spike histograms, it was demonstrated that cells within the PCL respond to pressure application of both AMPA and NMDA within the VML by an increase in their firing rate, suggesting a post-synaptic localization of these EAA receptor subtypes. In addition, local inhibitory interneurons within the VML, as well as inhibitory interneurons

whose apical dendrites ascend through the VML (67), also appear to respond to the application of EAAs in the VML. Pressure ejection of AMPA (10 μM) into the VML directly dorsal to the recorded neuron within the PCL resulted in a bi-phasic effect on the spontaneous firing rate of the cell. This response consisted of a short latency increase in the neuron's spontaneous firing rate which was subsequently followed by a period of inhibition (see figure 12, A). When the pressure ejection pipette was initially positioned lateral to the recorded cell, the form of this bi-phasic response was reversed in that a long-latency (ie approx. 8-10 sec) inhibition now preceded an increase in the spontaneous firing rate of the cell (see figure 12, B).

These results suggest that pressure ejection of AMPA directly into the dendritic arborization of the recorded cell results in the immediate excitatory component of the response, which is subsequently followed by a diffusion of the drug thereby activating nearby inhibitory interneurons. In contrast, pressure ejection of AMPA more lateral to the recorded cell initially activates inhibitory interneurons, which is followed by a diffusion to and activation of the recorded cell's apical dendrites. Similar results were also obtained subsequent to pressure ejection of NMDA in the VML (data not shown).

Specificity of EAA receptor antagonists

The use of "specific" EAA receptor antagonists assumes a constancy of receptor structure across species, an assumption which may not be valid. As such, we attempted to establish the limits of selectivity for EAA receptor antagonists within the experimental preparation used in these studies. Utilizing extracellular single unit recordings and cumulative spike histograms (with 10 second bin widths), results demonstrated that

Figure 12. Bi-phasic responses evoked by application of AMPA in the VML.
A: Pressure ejection of AMPA in the VML dorsal to the recorded cell results in a short latency increase, followed by a transient inhibition (black arrow) of the cell's spontaneous firing rate. **B:** Ejection of AMPA lateral in the VML to the recorded cell results in an initial inhibition of the cell (black arrow), followed by a transient increase in the cells firing rate. Each point represents the cumulative number of spikes in consecutive one second bin widths. Mean and standard deviations are given for the periods preceding drug application, and the maximum of the responses are also noted. Horizontal bars in **A & B** represents time of AMPA application.

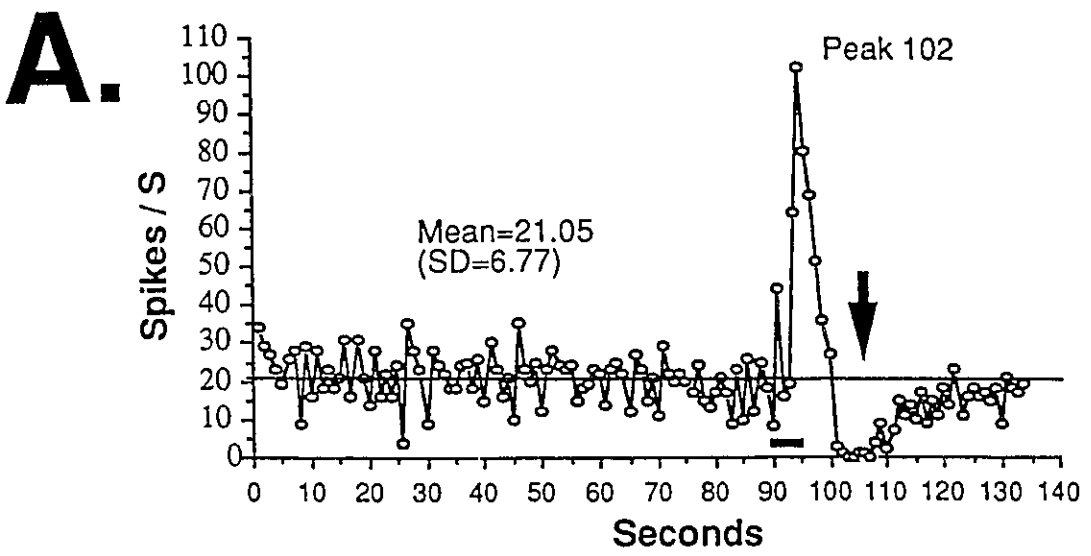
A.
Peak 102
Mean=21.05
(SD=6.77)
Spikes / S
Seconds
0 10 20 30 40 50 60 70 80 90 100 110 120 130 140
0 10 20 30 40 50 60 70 80 90 100 110

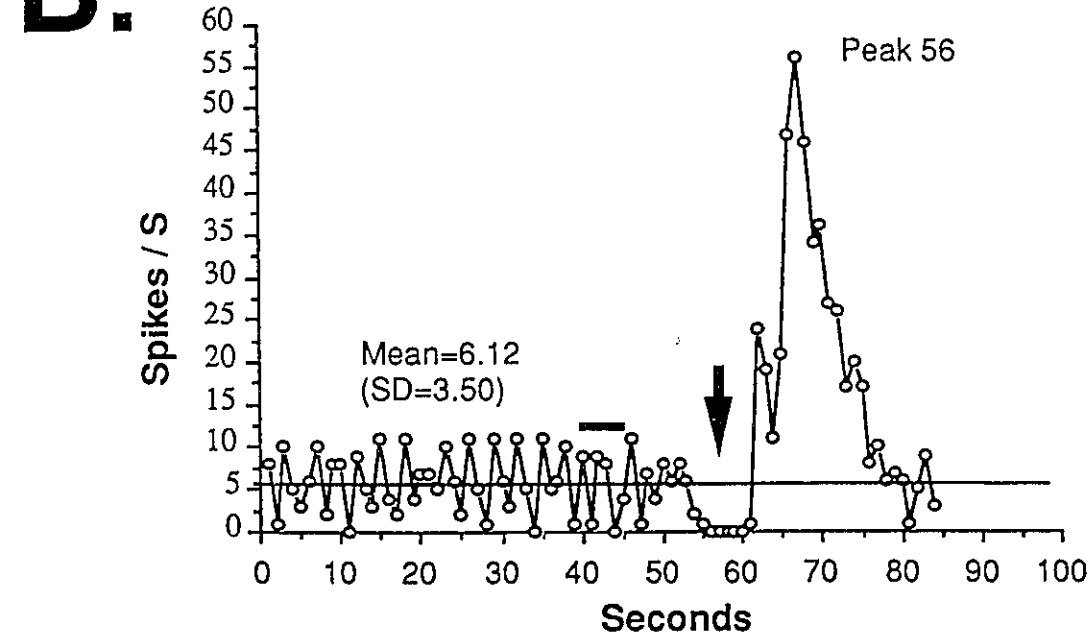
B.
Peak 56
Mean=6.12
(SD=3.50)
Spikes / S
Seconds
0 10 20 30 40 50 60 70 80 90 100
0 5 10 15 20 25 30 35 40 45 50 55 60

application of both AMPA (figure 13,1) and NMDA (figure 13,4) in the VML, resulted in an approximate doubling of the spontaneous firing rate of the recorded pyramidal cell. Pre-application of CNQX (150 μM) resulted in a selective antagonism of AMPA-induced increases in neuronal firing (see figure 13,3) while having minimal effects on excitation induced by application of NMDA (figure 13,5). Conversely, pre-application of CPP (1 mM) completely antagonised the excitation induced by application of NMDA (figure 13,6) with little effect on the response induced by AMPA application (figure 13,2). These results confirm in this experimental preparation the previously reported (46,97) selectivity of these EAA receptor antagonists, thereby allowing for their use in establishing the relative contribution and functional role of NMDA and non-NMDA receptors to synaptic transmission within the VML feedback pathway.

Kynurenic acid

In seven experiments, the effects of a non-specific EAA receptor antagonist, Kynurenic acid (Kyn; 2 mM), was tested on the tSF-evoked VML response. Pressure ejection of Kyn into the region of the VML resulted in a significant ($t=7.981$; $df=6$; $p< 0.001$) and reversible (after 1 hour) reduction in the tSF-evoked VML responses to a mean peak amplitude of only 34.79% (±SD=21.10%) of their matched control responses (see figure 14, A). Similarly, the mean integrated voltage of the VML response evoked under Kyn was reduced in magnitude to a mean of only 25.91% (±SD=14.11%) of their matched control responses ($t=4.129$; $df=6$; $p=0.006$). Note (in figure 14, A) that after Kyn that there is still a small residual late component of the VML response. This late component was completely eliminated under Mn^{2+} ACSF perfusion (figure 14, B).

Figure 13. Test of ionotropic EAA receptor agonist and antagonist specificity in the ELL slice preparation. **1:** Example of the excitatory effect of AMPA ejection in the VML (peak response=260 spikes/10s). **2:** Under CPP, AMPA still evokes an excitatory response (peak=604 spikes/10s). **3:** After pre-application of CNQX, application of AMPA in the VML has little effect on the spontaneous firing rate of the recorded cell. **4:** Example of the excitatory effect of NMDA application in the VML (peak=527 spikes/10s). **5:** Under CNQX, NMDA still evokes an excitatory response (peak=637 spikes/10s). **6:** Pre-application of CPP blocked NMDA induced excitation. The above results demonstrates the previously reported specificity of theses EAA receptor antagonists, and validates their use in this experimental preparation. Each bar represents the cumulative number of spikes recorded in consecutive 10 second bin widths. Integration over 10 seconds helped controlled for the bi-phasic temporal nature of EAA-evoked responses as illustrated in Figure 12: ▲=time of agonist application.

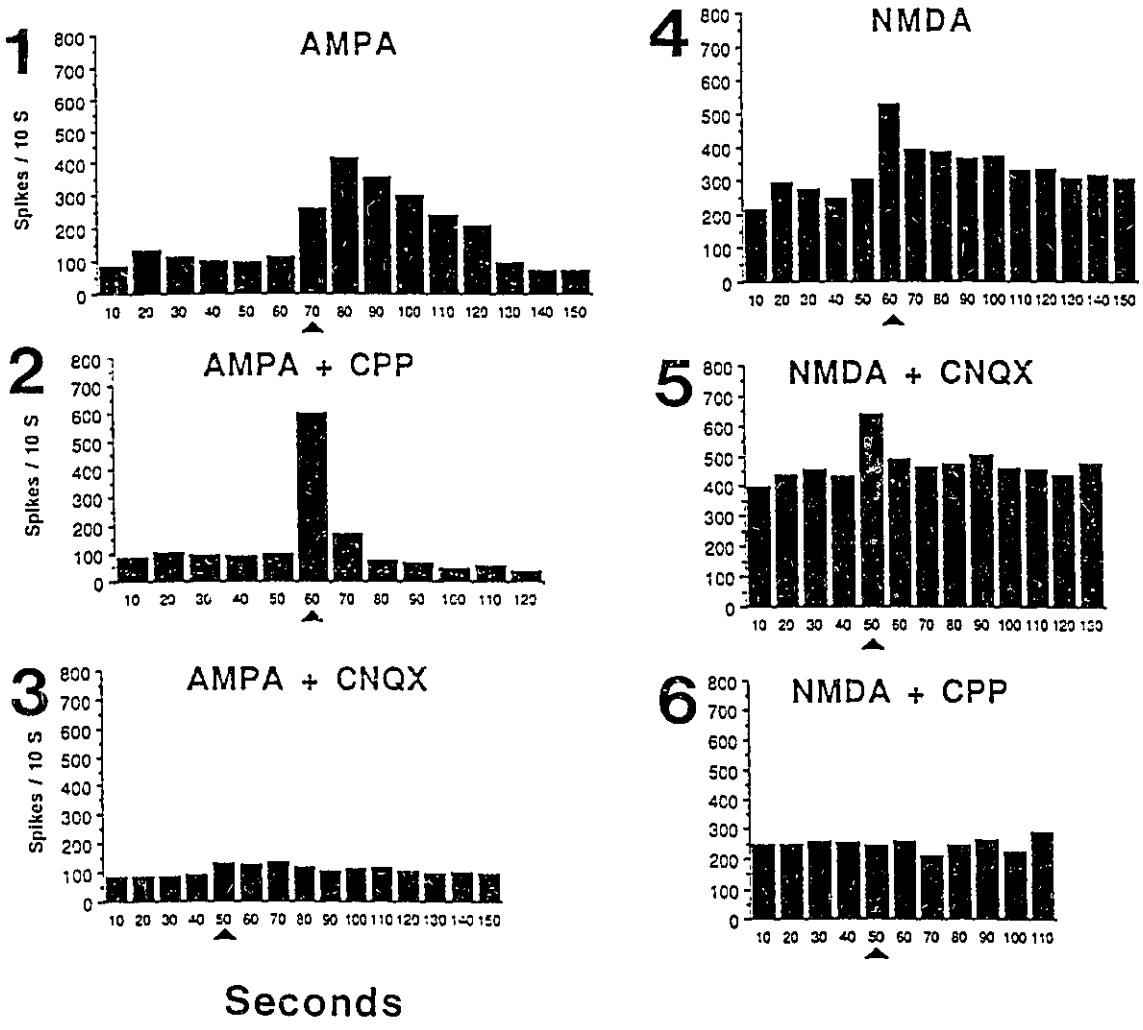
1
AMPA
2
AMPA + CPP
3
AMPA + CNQX
4
NMDA
5
NMDA + CNQX
6
NMDA + CPP
Spikes / 10 S
Seconds

Figure 14. Blockade of tSF-evoked VML potentials with the non-specific EAA receptor antagonist Kynurenic acid. **A:** Reversible blockade of the VML field potential (**2mM Kyn**) compared to a control response, and a response evoked after 1 hour recovery. Note that there is a small portion of the late phase which appears resistant to Kyn. **B:** For the purpose of comparison, the magnitude of the blockade of the VML response seen after 1 hour Mn^{2+} perfusion is shown. The almost equivalent antagonism by Kyn suggests an important role for EAA receptors in transmission at this synapse. Calibration bars; 1mV/5msec: ▲=stimulus artifact.

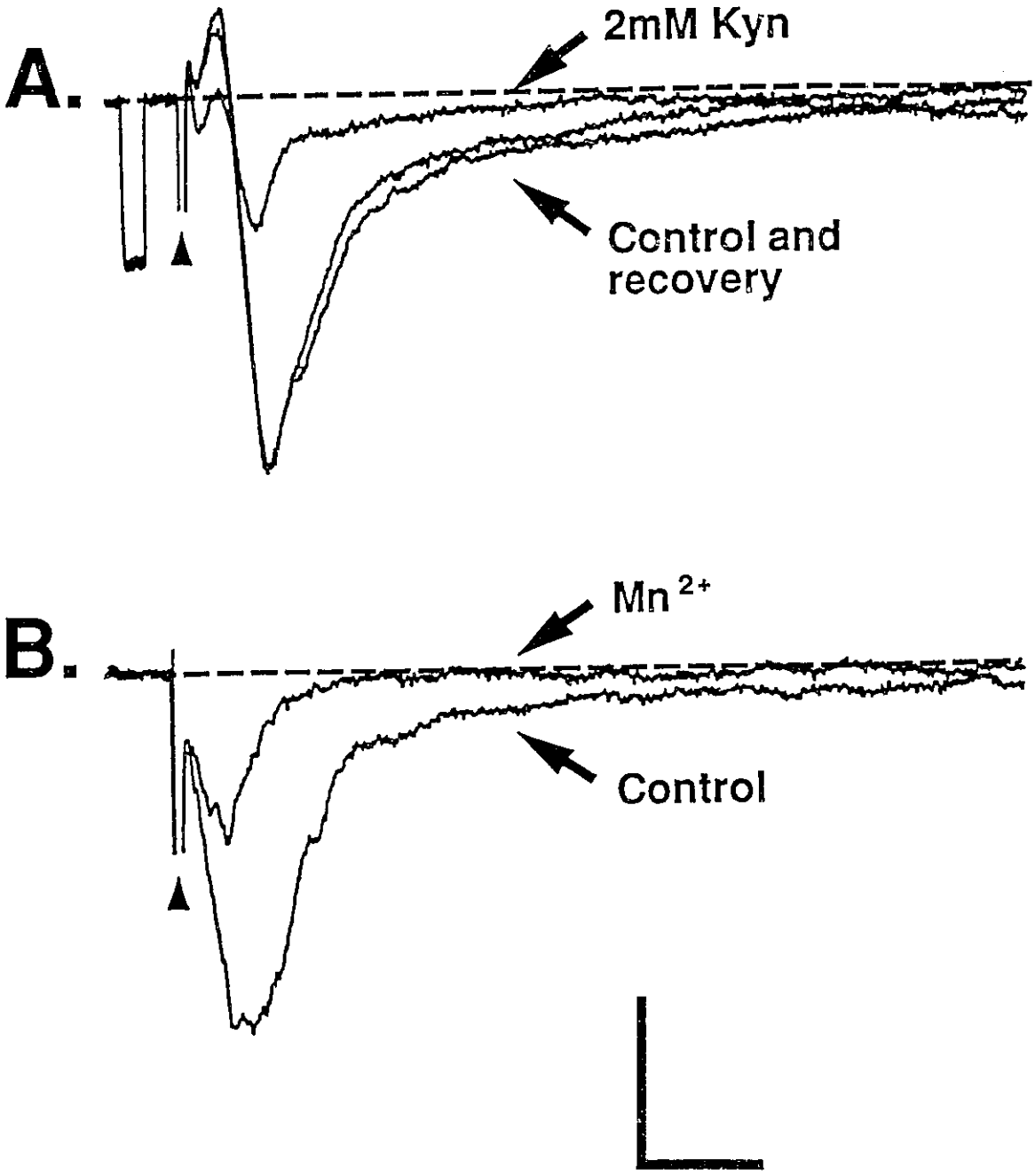
A.
2mM Kyn
Control and
recovery
B.
Mn 2+
Control

Since (a) focal pressure ejection of EAA receptor agonists into the VML results in pronounced excitatory responses, and (b) the relative reduction in magnitude of the VML responses evoked under 2 mM Kyn closely resembled that seen under Mn^{2+} blockade (ie see figure 14, B), it can be concluded that EAAs likely play a significant role in transmission at the VML synapse. Further experiments were therefore carried out to assess the possible contribution of both NMDA and non-NMDA ionotropic EAA receptor subtypes to tSF-evoked VML field potentials.

Role of NMDA receptors:

Antagonism with CPP

Pressure ejection of the highly potent and selective (97) NMDA receptor antagonist CPP (1 mM) to the region of the VML was carried out in 12 experiments. Application of CPP was found to significantly ($t=7.724$; $df=11$; $p<0.001$) reduce both the mean peak amplitude of the tSF-evoked VML responses, as well as the integrated voltage under the VML responses ($t=10.158$; $df=11$; $p<0.001$). CPP reversibly reduced the peak amplitude of the VML responses to a mean of 52.15% (±SD=17.07%) of the amplitude of their matched control response. Similarly, there was a reduction in the magnitude of the late decay phase of the evoked responses, reflected in a subsequent reduction in the integrated voltage under the VML response to a mean of 41.88% (±SD=16.18%) of their matched control value (see figure 15, VML). CPP also diminished the magnitude of tSF-evoked field potentials recorded at the level of the PCL, often reducing them to a level sub-threshold for the initiation of orthodromic pop-spikes (see figure 15, PCL).

Figure 15. Effects of the selective NMDA receptor antagonist CPP (1mM) on tSF-evoked VML responses. **VML:** Reversible suppression of the tSF-evoked VML potential (**1mM CPP**) compared to its matched control response, and a response evoked after 1 hour recovery. Note the significant suppression of boh the short latency negative-going and late component of the VML response by CPP (asterisk); the late slowly decaying phase of the response, while still present, is clearly reduced under CPP. **PCL:** CPP ejected into the VML also dramatically reduced the magnitude of tSF-evoked PCL field potentials (**control vs 1mM CPP**), selectively blocking orthodromic pop-spikes (asterisk) while having no effect on antidromic pop-spikes (arrows). Calibration bars; 1mV/5msec: ▲=stimulus artifact:■= blanked calibration pulse.

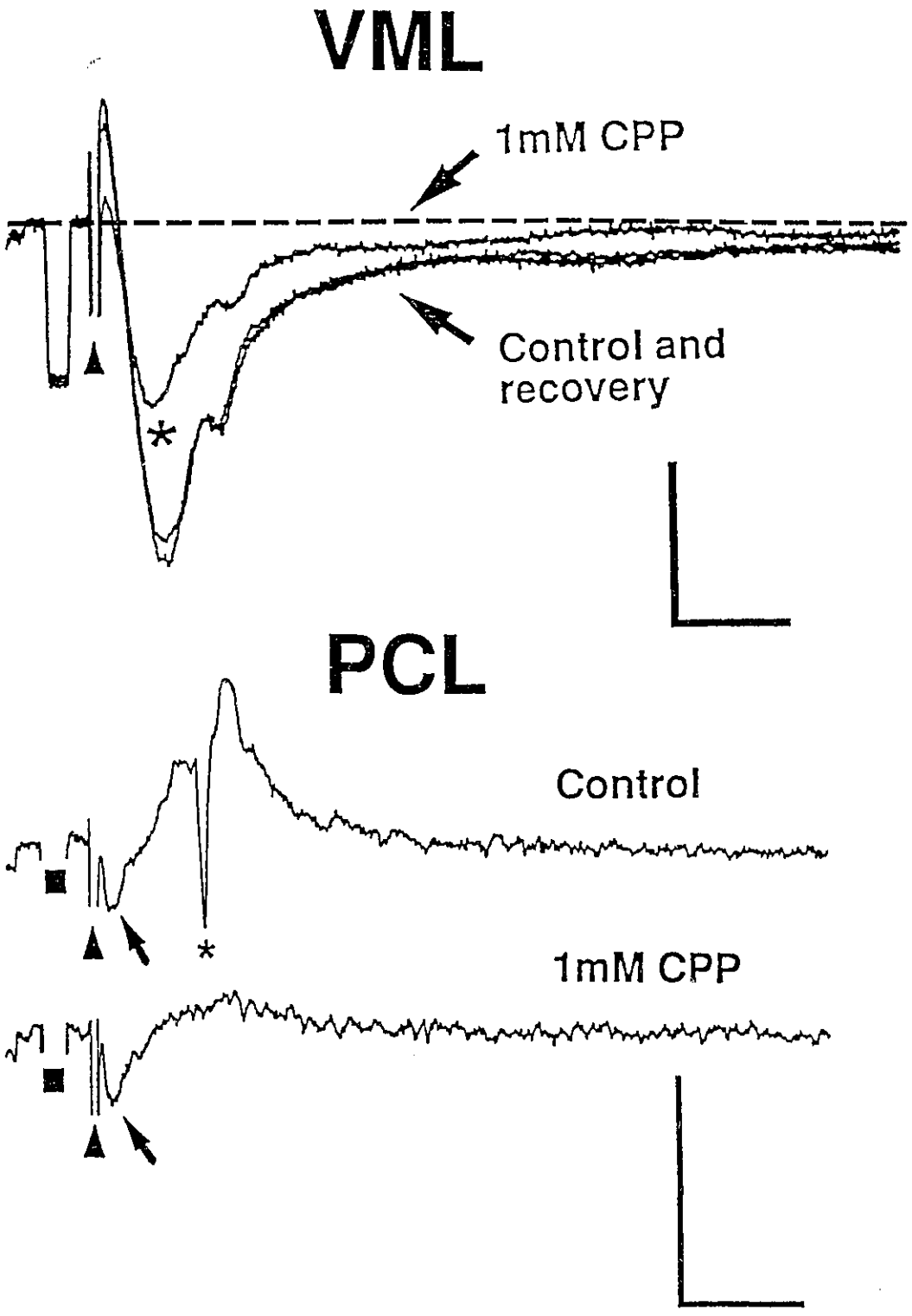
VML
1mM CPP
Control and
recovery
PCL
Control
1mM CPP

Since the mean latency to the peak of the control VML responses in these recordings was only 3.11 msec (±SD=0.40 msec), the fact that CPP application would significantly suppress the peak of the VML responses at such a short post-stimulus latency (see asterisk in figure 15, VML) was unexpected. While these results strongly suggested a significant contribution of a fast NMDA receptor-mediated process to VML synaptic transmission, further manipulations known to effect the function of NMDA receptor channels were carried out to exclude the possibility that the above results could still be an artifact of a non-specific CPP antagonism of fast non-NMDA receptor mediated transmission.

Enhancement of the VML field potential with 0-Mg^{2+} ACSF

Since current through NMDA channels exhibit a voltage dependent blockade mediated by Mg^{2+} ions (73,72,94), NMDA receptor mediated currents are enhanced when Mg^{2+} is removed from the ACSF solution while non-NMDA currents are left largely unaffected. An investigation of the effects of 0-Mg^{2+} ACSF exposure on the early negativity of the tSF-evoked VML potentials was therefore carried out in 5 experiments in an attempt to confirm the existence of fast NMDA-mediated transmission at this synapse.

After one hour exposure to 0-Mg^{2+} ACSF perfusate, tSF-evoked VML responses recorded at the mean latency of the peak of their matched control responses (3.20 msec; ±SD=0.56 msec) were significantly (t=3.803; df=4; p=0.019) enhanced to a mean of 133.28% (±SD=23.94%) of their previous control amplitude under normal ACSF perfusion (see figure 16, A). The late component of the response was also enhanced as

Figure 16. Alteration of tSF responses by 0-Mg^{2+} ACSF perfusion.
A: Enhancement of the VML response after 1 hour 0-Mg^{2+} ACSF perfusion. CPP suppressed the early and late components of the tSF-evoked VML response under control ACSF conditions (**B**), and reversed the enhancement of both the early and late components of the VML response seen with 1 hour 0-Mg^{2+} perfusion (**C**). The near equivalent antagonism of the VML response by CPP under control (**B**) and 0-Mg^{2+} conditions (**C**) strongly suggests that the growth of the response under 0-Mg^{2+} might be completely accounted for by an enhancement of NMDA receptor mediated transmission.
Calibration bars; 2mV/5msec: ▲=stimulus artifact

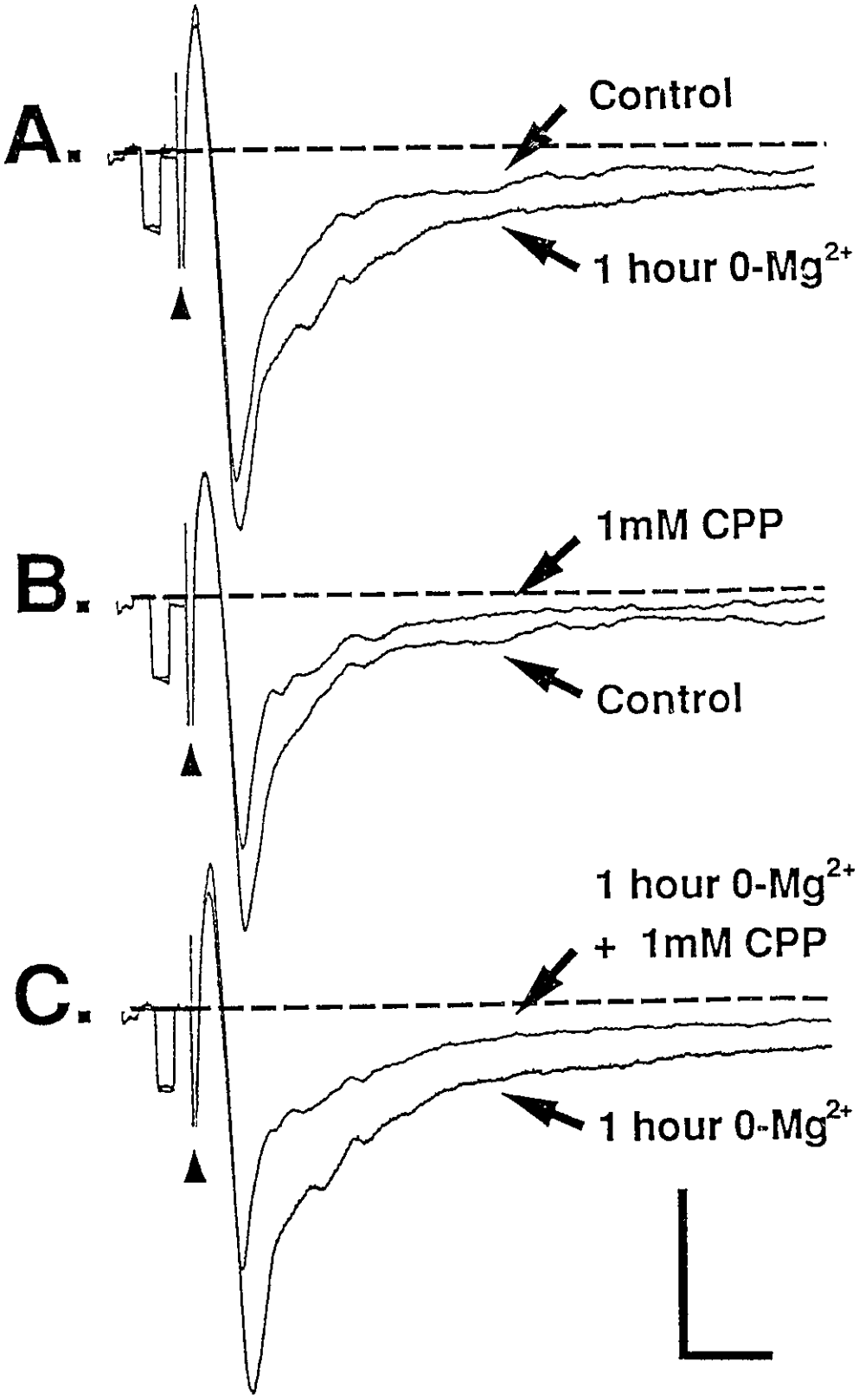
A.
Control
1 hour 0-Mg2+
B.
1mM CPP
Control
C.
1 hour 0-Mg2+
+ 1mM CPP
1 hour 0-Mg2+

reflected by the significant (t=4.103; df=4; p=0.015) increase in the mean integrated voltage under the recorded VML responses to 198.83% (±SD=64.35%) of their matched control responses. These 0-Mg^{2+} enhancements of the tSF-evoked VML responses could subsequently be reversed by re-perfusion of the slices with Mg^{2+} containing ACSF (data not shown).

In nine experiments, the effects of CPP application on 0-Mg^{2+} enhancement of the VML response was investigated. Application of CPP significantly (t=5.993; df=8; p<0.001) antagonized the augmenting effects of 0-Mg^{2+} to a mean of 43.40% (±SD=17.67%) of its previous amplitude under 0-Mg^{2+} (see figure 16, C). In addition, CPP also significantly (t=3.953; df=8; p=0.004) reduced the integrated voltages under the VML responses to a mean of 34.29% (±SD=16.67%) of their previous value under 0-Mg^{2+}. It is interesting to note that application of CPP under control and 0-Mg^{2+} ACSF conditions reduced the VML response to a similar magnitude (see figure 16, B & C), suggesting that the increase seen in the magnitude of the short latency component of the VML response under 0-Mg^{2+} might be accounted for by an enhancement of NMDA-mediated transmission.

Role of non-NMDA receptors:

Effect of CNQX on VML potential

In five experiments, the effects of antagonism of non-NMDA receptors by CNQX was investigated. Since extracellular VML field potentials are the product of tSF-evoked currents which are spatially distributed over a large area, a concentration of 1mM CNQX was used to ensure a maximal local blockade, and to allow for adequate diffusion within

the VML. Pressure ejection of CNQX into the region of the VML resulted in an almost complete blockade of the tSF-evoked VML response. The mean peak amplitude of the tSF-evoked VML field potentials was reduced to 36.67% (±SD=12.06%) of their mean peak control values (t=5.979; df=4; p=0.004), while CNQX caused a significant (t=4.77; df=4; p=0.009) reduction in the mean integrated voltage under the VML field potentials to 10.99% (±SD=3.73%) of their matched control values (see figure 17, A). This magnitude of VML response suppression by CNQX was not significantly different than that seen under Mn^{2+} blockade of synaptic transmission, (mean peak amplitude=29.90%; ±SD=15.59%, mean integrated area=18.97%; ±SD=11.14%). In light of the previously demonstrated contribution of NMDA receptors to the VML response (see above), this near complete block of the tSF-evoked VML response by CNQX was unexpected.

Effect of 0-Mg^{2+} ACSF on CNQX blockade

In a set of seven experiments, CNQX was applied under 0-Mg^{2+} ACSF perfusion to investigate the possibility that the contribution of NMDA receptors to the VML response was *dependent* on the removal of its voltage-dependent Mg^{2+} blockade by prior membrane depolarization mediated by activation of non-NMDA receptors. In contrast to the almost complete blockade of the VML potential by CNQX under control ACSF conditions, under 0-Mg^{2+} ACSF conditions CNQX reduced the mean peak amplitude of the 0-Mg^{2+}-*enhanced* VML response (see figure 17, B) to only 38.83% (±SD=21.59%) of its previous value (t=4.304; df=6; p=0.005). The mean integrated voltage evoked under the augmented 0-Mg^{2+} response was similarly reduced to only 29.51% (±SD=21.79%) of its previous value (t=3.031; df=6; p=0.023). Since exposure to 0-Mg^{2+} ACSF caused a

Figure 17. Effects of the selective non-NMDA receptor antagonist CNQX (1mM) on the tSF-evoked VML response. **A:** Unlike CPP, application of CNQX under control ACSF perfusion resulted in an almost total block of the tSF-evoked VML response. **B:** After 1 hour 0-Mg^{2+} perfusion, the enhanced VML response is significantly diminished by application of CNQX, however, a residual component is still evident which can be subsequently blocked by application of the selective NMDA receptor antagonist CPP (1mM) (C). Calibration bars; 2mV/5msec:▲=stimulus artifact

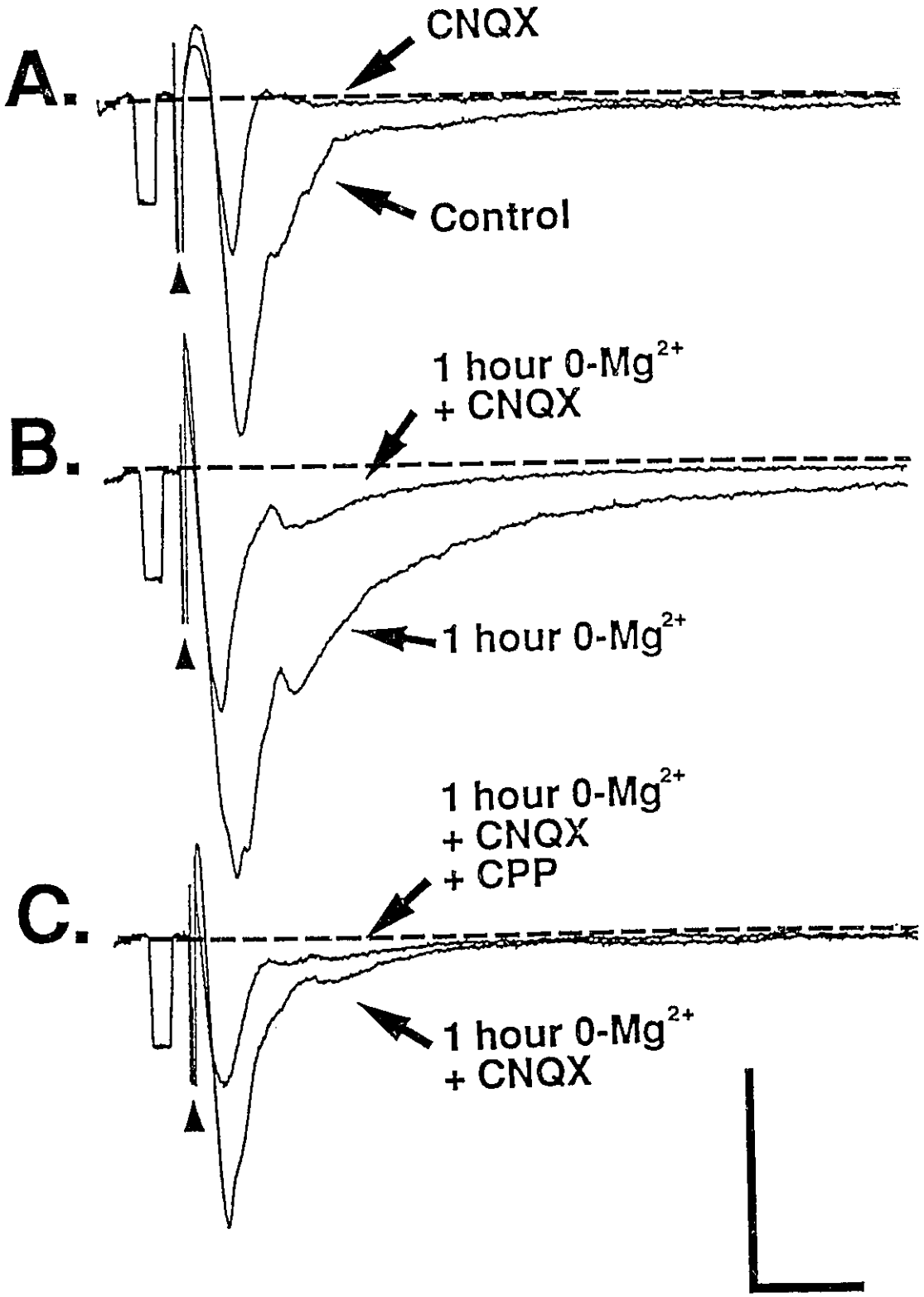
A.
CNQX
Control
B.
1 hour 0-Mg2+
+ CNQX
1 hour 0-Mg2+
C.
1 hour 0-Mg2+
+ CNQX
+ CPP
1 hour 0-Mg2+
+ CNQX

large enhancement of the peak (133.28%) and integrated (198.83%) VML response, under these conditions CNQX application still left a substantial residual synaptic component of the evoked response (see figure 17,B & C).

While the *relative* CNQX-induced reduction in the magnitude of the VML response was similar when applied under control or 0-Mg^{2+} ACSF conditions, there was a significant (t=2.544; df=6.1; p=0.044) difference in the *absolute* magnitude of the effect on the mean integrated voltages of the residual responses seen under these conditions. Application of CNQX under control ACSF perfusion resulted in a residual component of the VML response having a mean integrated voltage of 1.15 mV x msec (±SD= 0.30 mV x msec) compared to an mean integrated voltage of 5.82 mV x msec (±SD= 4.84 mV x msec) under 0-Mg^{2+} ACSF perfusion (ie CNQX in figure 17, A vs B). These results strongly suggest that 0-Mg^{2+} ACSF perfusion "un-masks" a previously hidden short latency (ie < 20 msec) CNQX resistant component of the VML response.

Effect of CPP on the CNQX-resistant component under 0-Mg^{2+}

In a subset of the above 0-Mg^{2+} experiments (n=4), CPP was subsequently applied to slices after CNQX to test whether the residual component of the VML response seen under 0-Mg^{2+}+CNQX was in fact mediated by NMDA receptors after the removal of their voltage-dependent Mg^{2+} blockade. Under 0-Mg^{2+}+CNQX, application of CPP further reduced the mean peak amplitude of the CNQX-resistant component of the VML response to 39.41% (±SD=19.05%) of its previous value. However, this effect was not statistically significant (t=2.528; df=3; p=0.086) likely due to the substantial and highly variable contribution of fiber volley to the field potentials recorded at this short latency. In

contrast, CPP significantly (t=3.537; df=3; p=0.038) reduced the temporally independent mean integrated voltage under the short latency residual CNQX-insensitive component of the VML response under 0-Mg^{2+} ACSF to 44.44% (±SD=16.97%) of its previous value (see figure 17, C). In contrast, application of CPP after CNQX under control ACSF had no effect on the residual response (data not shown).

INTRACELLULAR STUDIES

I. Control somatic and dendritic EPSPs

Using a previously published classification criteria (123), recordings were obtained from 27 somatic and 13 proximal apical dendritic impalements from a total of 28 slices. Trains of current evoked action potentials recorded from intracellular impalements classified as "somatic" were characterized by narrow action potentials (mean halfwidth= 0.37 msec;±SD=0.07 msec), followed by both fast (black arrow) and slow (open arrow) after hyperpolarizations (AHPs) (see figure 18, 2 & C). In addition, somatic spike trains occasionally exhibited a "bursting" firing response upon depolarization. This phasic firing property was mediated by action potential "doublets" with associated prolonged AHPs (see arrow in figure 18, 2), which have previously been shown to be a result of the invasion and re-firing of the soma or axon initial segment by dendritic action potentials (123).

In contrast to somatic recordings, impalements classified as "dendritic" always fired tonically during depolarizing current ejection (figure 18, 1), and had significantly (t=5.024; df=29; p< 0.001) broader action potentials with a mean halfwidth of 0.71 msec (±SD=0.28 msec). In addition, dendritic action potentials were typically only followed

Figure 18. Comparison of dendritic and somatic intracellular recordings.
1: Current ejections and their resultant effects on membrane potential for a dendritic impalement dorsal to the tSF pathway. Note the tonic firing to depolarizing current ejection, and the characteristic wide action potentials with slow AHPs. **2:** Response of a somatic impalement to current ejection. Action potentials (narrow, with fast and slow AHPs) can occur in "doublets" (arrow) producing a phasic firing pattern to depolarizing current ejection. **A:** Characteristic form of dendritic action potentials recorded from impalements above the tSF pathway, having wide spikes with only slow AHPs (open arrow), compared to a dendritic impalement just below the tSF (**B**), and a typical somatic impalement (**C**). Note the intermediate AHP characteristics of **B** which possesses wide action potentials, and both slow (open arrow) AHPs (as in **A**), and small fast (arrow) AHPs (as in the somatic recording, **C**). Calibration bars; 25mV/25msec: ▲=stimulus artifact.

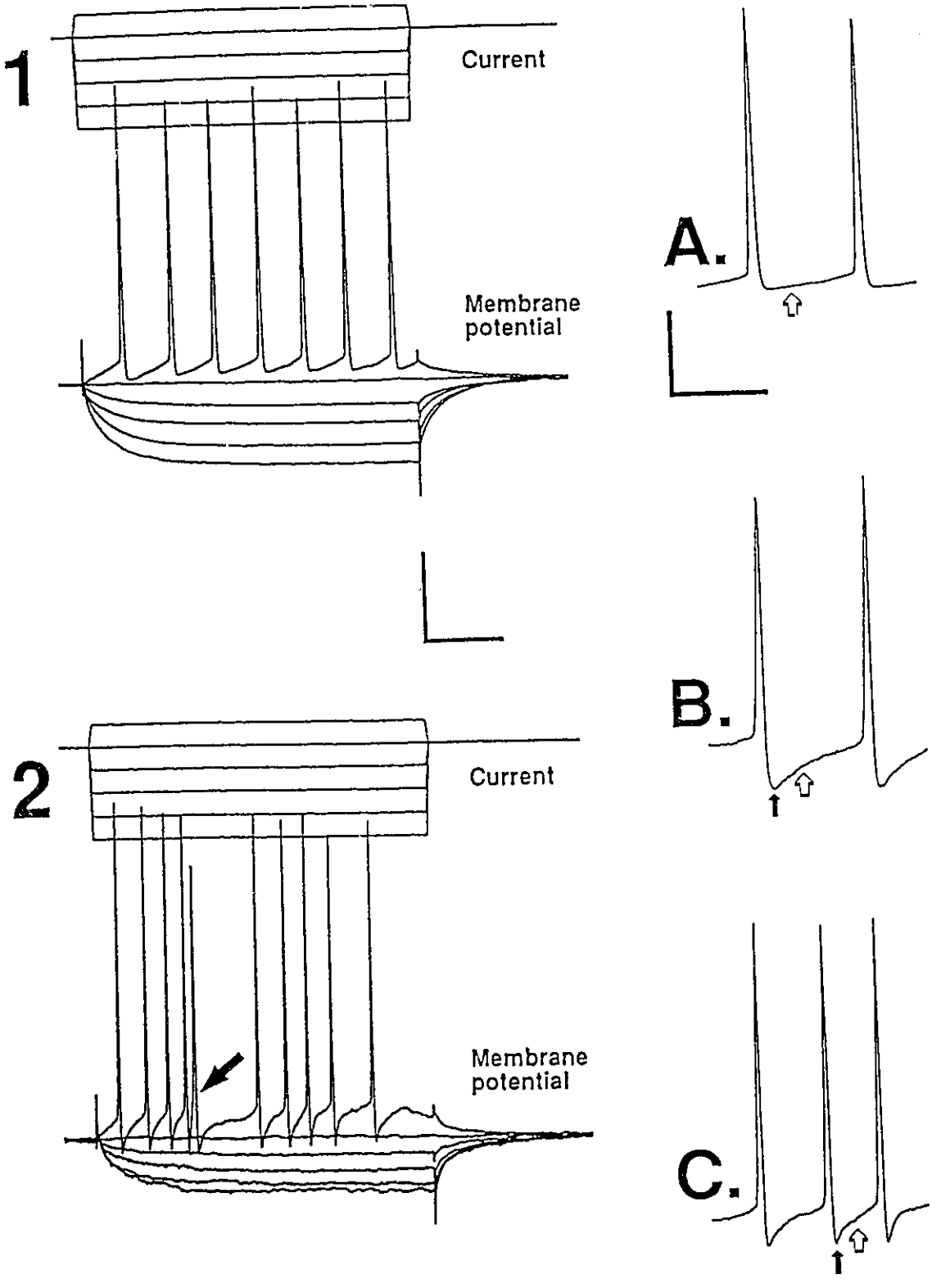
1
Current
Membrane potential
2
Current
Membrane potential
A.
B.
C.

by slow AHPs (see figure 18, I & open arrow in A). The characteristic form of dendritic action potential AHPs varied as a function of the distance of the impalement from the pyramidal cell layer, with proximal apical dendritic impalements ventral to the tSF having AHP characteristics intermediate between "somatic", and "dendritic" recordings obtained from impalements dorsal to the tSF pathway (ie figure 18, B vs A & C).

Passive Membrane Properties:

While technically difficult, the ability to obtain stable intradendritic recordings allowed for an unique opportunity to record passive membrane properties, and tSF-evoked post-synaptic EPSPs from a site both spatially and electrotonically close to the tSF synaptic input. Dendritic impalements had a mean resting membrane potential (Vm) of -72.6 mV (±SD=8.7 mV;N=13), with a mean computed input resistance (Ri) of 20.05 MΩ (±SD=8.7 MΩ;N=11). Consistent with previous results (123), these values were not significantly different from either the mean somatic resting membrane potential (-74.81 mV;±SD=7.34 mV;N=26;p=0.41), or the mean calculated somatic input resistance (21.19 MΩ;±SD=7.42 MΩ;N=19;p=0.70).

Slow Membrane Potential Oscillations

As previously reported (71,124), neurons within the ELL slice preparation can display a wide range of spontaneous (and current-evoked) fluctuations in membrane potential, the most dramatic being a synchronization of cells within an ELL segment into large slow (ie 0.3 Hz - 0.02 Hz) rhythmic oscillations or bursts. Oscillatory responses were either comprised of depolarizations terminated by large hyperpolarizing events (figure 19, A & C), or were characterized by rhythmic hyperpolarizations of the basal

Figure 19. Examples of depolarizing-hyperpolarizing form of slow membrane potential oscillations occasionally recorded in the ELL slice preparation, (typical of non-basilar pyramidal cells). **A:** Large "ultra-slow" oscillation having a period of approximately 1 minute. Oscillations with this slow of period were rarely seen (N=1).
B: Partial voltage-dependency of the slow oscillation frequency, hinting at the complex nature of the interaction between pre and postsynaptic mechanisms underlying these oscillations. **C:** A decrease in the magnitude of current evoked (-0.7 nA, 100 msec, 0.2 Hz) membrane potential hyperpolarizations at the offset of the oscillations (arrow 1 vs 2), strongly suggest that these oscillations are terminated by inhibitory processes mediated by a transient increase in membrane conductance. Calibration bars; (**A:** 1 minute), (**B:** 5 seconds), (**C:** 10mV/20 seconds).

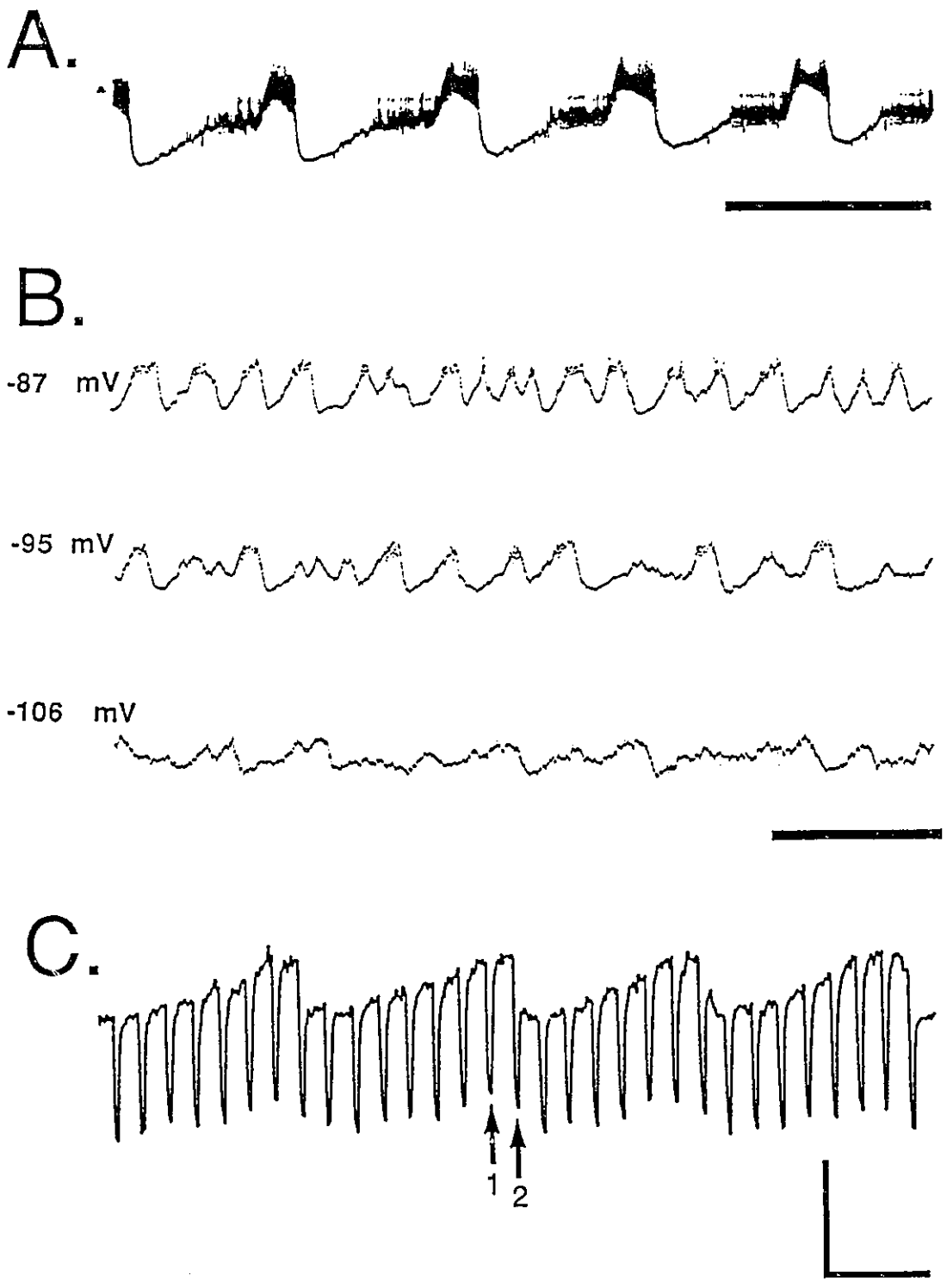
A.
B.
-87 mV
-95 mV
-106 mV
C.
1
2

membrane potential ("Giant IPSPs") without any discernible intervening depolarizing events (figure 20, A). Utilizing biocytin filling of recorded neurons, these two characteristic forms of slow membrane potential oscillations have been recently correlated with the two morphologically distinct pyramidal cell types found in the ELL. Non-basilar pyramidal cells consistently were associated with the depolarizing-hyperpolarizing form of slow oscillations, while basilar pyramidal cells only exhibited oscillatory behaviour consisting entirely of hyperpolarizing events (Turner, unpublished observation).

Slow membrane potential oscillations exhibited a partial voltage-dependency, in that depolarizing current ejection tended to enhance the underlying depolarizations of the depolarizing-hyperpolarizing form of oscillations (figure 19, B; -87 mV). Conversely, hyperpolarizing current ejection seemed to diminish certain components of these oscillation, resulting in a slowing the underlying frequency of the oscillation (figure 19, B; -106 mV). Similarly, the magnitude of the "Giant IPSPs" characteristic of the hyperpolarizing form of slow oscillations were diminished by hyperpolarizing current ejection (see figure 20). Since both forms of these prominent large slow oscillations were rather rare (occurring in less than 20% of the intracellular recordings), these events did not significantly hamper the ability to assess the post-synaptic effects of stimulation of the tSF feedback pathway.

Fast Membrane Potential Oscillations

Two forms of fast (ie 121.7 - 243.6 Hz) membrane potential oscillations were also occasionally seen during intracellular recordings. On two occasions, recurrent bursts of small fast pre-potentials (fpps) were seen which (a) tended to summate, thereby

Figure 20. Example of the hyperpolarizing form of slow membrane potential oscillations characteristic of basilar pyramidal cells. **A:** Depolarization of the membrane potential to threshold for action potential generation (-66.3 mV) enhances the magnitude of the hyperpolarizing events, without changing the basal frequency of the oscillations, or uncovering any underlying depolarizing events; action potentials (arrow) are truncated due to the low sampling rate. **B:** Hyperpolarizing events recorded at the resting potential of the cell (-70.36 mV);note that the frequency is similar to that in **A. C:** At hyperpolarizing membrane potentials (-73.68 mV), the amplitude of the hyperpolarizing events are significantly diminished, while the frequency of the oscillations are uneffected.

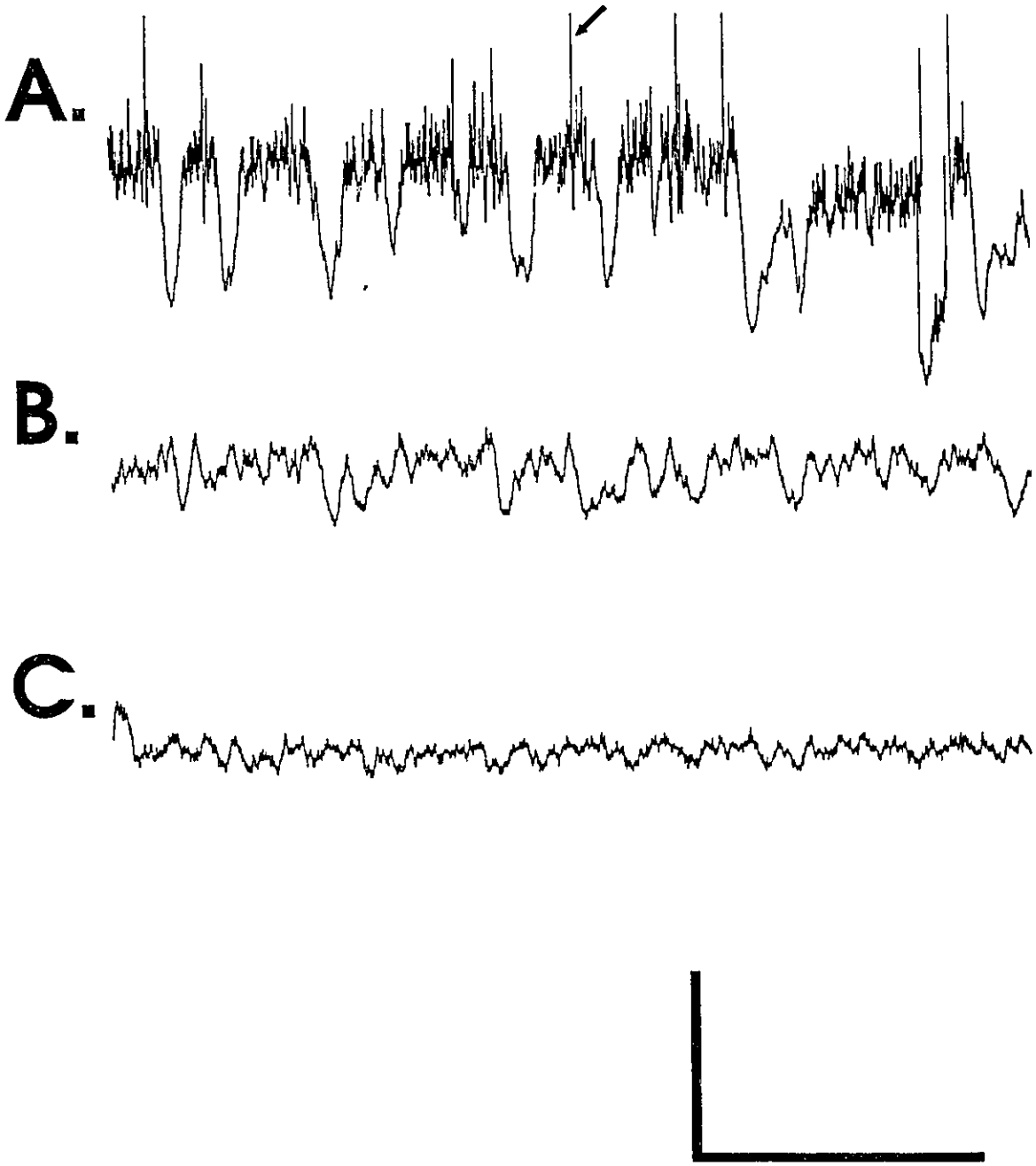
A.
B.
C.

depolarizing the membrane potential past threshold for action potential generation, and (b) whose occurrence, magnitude, and frequency were independent of the basal membrane potential of the cell (see arrow in figure 21, 1). Since these fpp bursts only occurred in the presence (and closely matched the periodicity) of the underlying depolarizing-hyperpolarizing form of slow membrane potential oscillations, these results suggest that this form of fpp reflects dynamic interactions between the intrinsic membrane characteristics of non-basilar pyramidal cells and the properties of ELL neuronal circuits mediating these slow oscillations.

The second form of fast membrane potential oscillations exhibited a strong voltage dependence, and were only observed at membrane potentials more depolarized than Vm (see figure 21, 2). As the membrane potential was depolarized, these fpps tended to drive Vm towards threshold, giving rise to bursts of action potentials. Taken together these results suggest, as previously reported (71), that this form of fpp is most likely generated by intrinsic properties of pyramidal cell excitability.

tSF-Evoked EPSPs:

Qualitative Characterization

Consistent with control extracellular VML field recordings (ie figure 8, 1), and the digitally-subtracted Mn^{2+}-sensitive component of the VML response (ie figure 9, 2), tSF-evoked dendritic and somatic EPSPs exhibited a biphasic form consisting of a fast depolarization phase (A), followed by a prolonged decay phase (B). Occasionally, a pronounced "shoulder" was seen on the rising slope of the EPSPs (ie open arrow in figure 22, 2). In three somatic recordings, tSF stimulation also resulted in a prominent small

Figure 21. Examples of two forms of fast membrane potential oscillations occasionally seen during intracellular recordings. Current ejection, and the resultant effects on membrane potential, demonstrated the existence of fast pre-potentials (fpps) that demonstrated either (1) no voltage dependence (arrow), or (2) only occurred during depolarization of the basal membrane potential (arrow). While the voltage-dependent fpps seem to be the result of intrinsic properties of membrane excitability, the voltage-independent fpps appear to be the product of dynamic circuit properties underlying the slow oscillations. Calibration bars; 25mV/25msec.

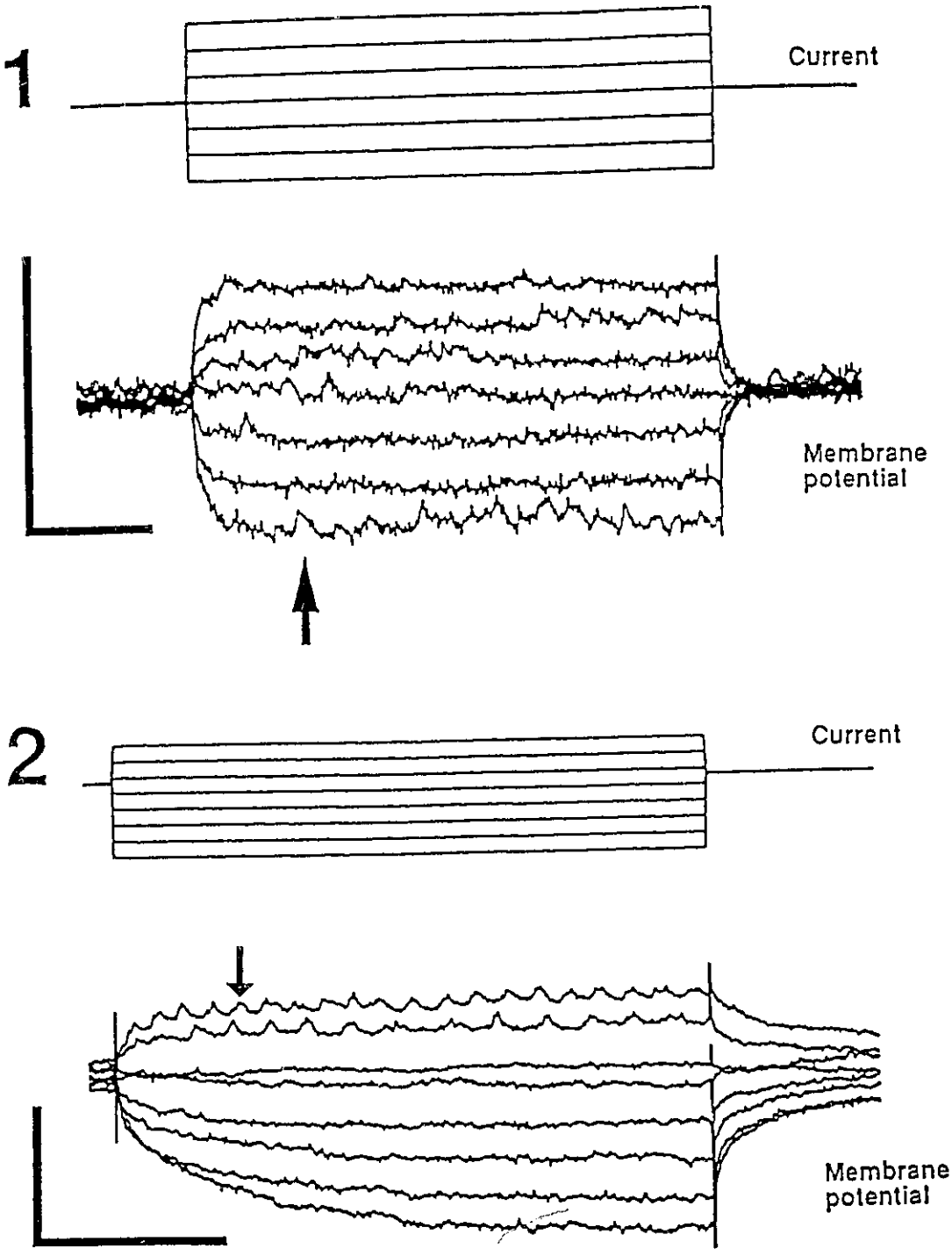
1
Current
Membrane potential
2
Current
Membrane potential

Figure 22. Comparison of intracellular recorded dendritic (1), and (average of 4 consecutive) somatic (2) tSF-evoked EPSPs. Both dendritic and somatic EPSPs generally consisted of two distinct phases; a fast depolarization phase (**A**), followed by a prolonged decay phase (**B**). Note in B that there is a shoulder or notch (open arrow) on the rising phase of the EPSP. While the general form of the tSF-evoked EPSPs, or calculated passive membrane properties did not significantly differ between somatic or dendritic impalements, the relative magnitude of EPSPs recorded in the dendrite occurred at a significantly shorter latency, and demonstrated a steeper voltage-dependence than those recorded from the soma. Calibration bars; 5mV/10msec: ▲=stimulus artifact.

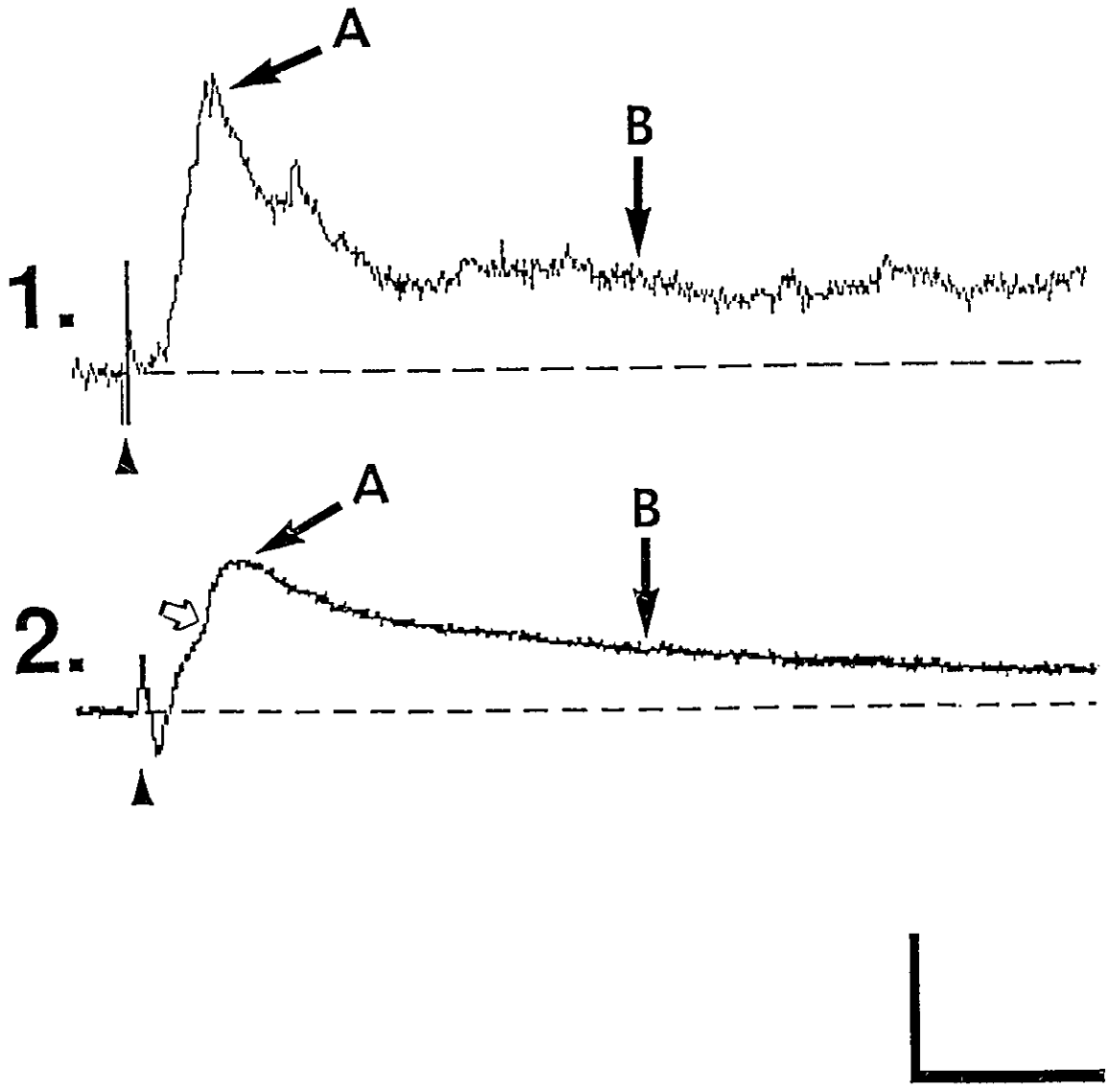
A
B
1.
A
B
2.

short latency (mean=1.34 msec;±SD=0.21 msec;n=19) rapid depolarization which preceded the normal evoked EPSP (see figure 23, B). Although these events occurred at a similar post-stimulus latency as antidromic action potentials, they could be easily distinguished by their small amplitude in comparison to the magnitude of action potentials that the neuron was capable of generating (ie figure 23, A). It is likely that these rapid evoked responses are gap junction mediated (see discussion). Given their rarity, these cases were excluded during the calculation of the mean latency and peak amplitude of the somatic EPSPs.

In two experiments, the time course of simultaneously recorded tSF-evoked VML field potentials and intracellular recorded dendritic EPSPs were compared. Antidromic dendritic action potentials (with rising phases immediately following the stimulation artifact) were temporally coincident with the earliest (Mn^{2+}-insensitive/non-synaptic) negative-going component of the VML field potential (figure 24, A and B). In contrast, the latency to peak and overall time course of orthodromic dendritic EPSPs closely paralleled that of their matched VML field potentials (figure 24, C and D).

While somatic EPSPs also displayed the characteristic biphasic form (ie figure 22, 2), the temporal overlap of competing somatic and dendritic field potentials resulted in an underestimation (when using PCL field potentials alone) of the duration and form of tSF-evoked postsynaptic events at the level of the soma (ie see figure 2, or figure 6, PCL). In the present studies the apparent discrepancy between extracellular and intracellular recorded somatic responses serves to highlight the limitations of interpreting extracellular field potentials in isolation.

Figure 23. Rapid transmission at the tSF synapse. During two somatic recordings, a fast (ie < 2 msec) depolarization of the membrane potential could be observed which was consistent with transmission via tSF gap junctions. **A:** Current ejection demonstrating the ability of the cell to produce characteristic "somatic" narrow action potentials with both fast and slow AHPs. **B:** Stimulation of the tSF evokes a complex EPSP consisting of a rapid "gap junction-like" component (solid arrow), followed by the characteristic fast (open arrow) and slow (asterisk) components. Calibration bars; (**A**:25mV/50msec), (**B**:10mV/25msec): ▲=stimulus artifact.

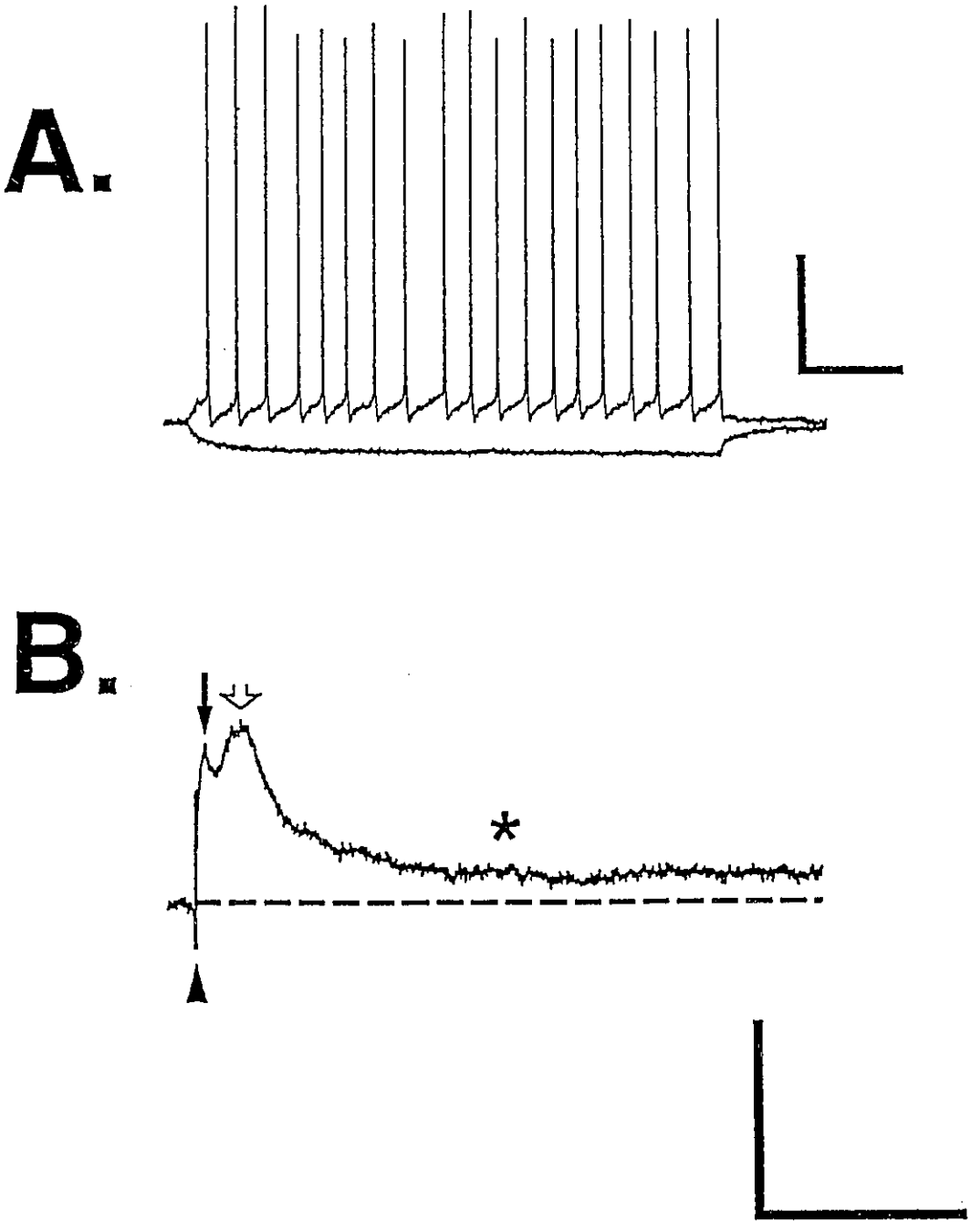
A.
B.
*

Figure 24. Correspondence of VML field potential with intradendritic recordings. **A:** Averaged (n=3) tSF-evoked VML field potential with (**B**) simultaneously recorded antidromic dendritic action potential. Antidromic action potentials temporally correlated with the earliest negative-going portion of the VML response, previously shown under Mn^{2+} perfusion to correspond to non-synaptic currents. Note the magnitude of antidromic or current evoked action potentials are easily distinguished from the rare short latency responses attributed to tSF gap junction input (ie figure 22, A2-3, & B). A small depolarizing afterpotential (open arrow) in the intracellular record (B) is an EPSP corresponding to the field EPSP in A. **C:** Single tSF-evoked VML field potential with (**D**) a simultaneously recorded dendritic EPSP, showing the temporal correspondence of the EPSP peak to the peak negativity of the VML field potential. Note the time course of the late decay phase of the VML field potential is closely matched by a slow late decay phase seen in the dendritic recording. Calibration bars; (field potentials:1mV/5msec), (intracellular:25mV): ▲=stimulus artifact.

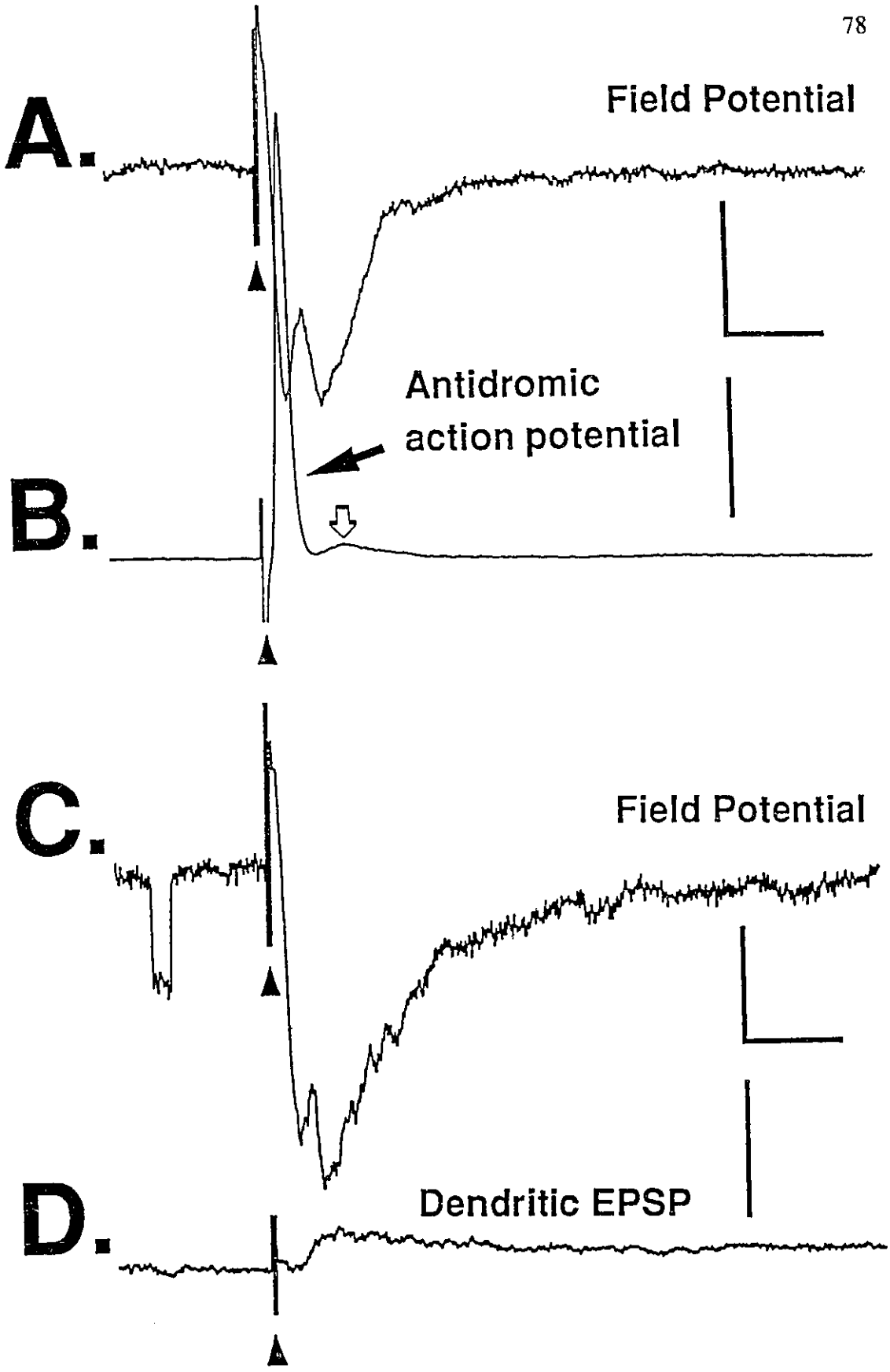
A.
Field Potential
Antidromic
action potential
B.
C.
Field Potential
D.
Dendritic EPSP

Quantitative Characterization

As previously outlined, numerous attributes of somatic and dendritic recorded tSF-evoked EPSPs were quantified and compared over a wide range of membrane potentials. When evoked at the resting membrane potential, somatic EPSPs had a mean latency to peak of 6.58 msec (±SD=1.94 msec;n=17), with a mean peak amplitude of 3.65 mV (±SD=2.27 mV;n=14). In contrast, the peak amplitude of dendritic EPSPs occurred at a significantly (t=2.67;df=22;p=0.01) shorter mean post-stimulus latency of 4.32 msec (±SD=1.71 msec;n=7), and having a mean peak amplitude (5.22 mV;±SD=2.34 mV;n=6) which was not significantly different than those seen in somatic recordings (p=0.17). The significant difference in the latency to peak for somatic and dendritic EPSPs is consistent with estimations (13b) based on resistive and capacitive membrane properties of hippocampal pyramidal neurons (see discussion). The latency to peak calculated from field potentials (4.3 msec) is in agreement with the intracellular estimate of 4.32 msec for the dendritic recordings. All other parameters measured (see Table 2.), failed to demonstrate any significant differences between somatic and dendritic recordings.

The bi-phasic nature of tSF-evoked EPSPs was further characterized in a limited number of cases by exponential fits of both the early and late phases of the EPSP decay. The decay phase of about half (6/13) of EPSPs could be best fit with two exponential curves having mean time constants of 1.5 - 3 msec and 15 - 45 msec for the fast and slow components respectively. In the remaining cases a single exponential fit was sufficient to account for the decay of the EPSP. These results suggest multiple underlying processes contributing to the post-synaptic generation of tSF-evoked depolarizations.

TABLE 2. Quantification of tSF-evoked EPSPs

Recording Position: **Somatic**		**Dendritic**	
Vm	-74.81 mV (±SD=7.34mV):n=26	-72.62 mV (±SD=8.70mV):n=13	p=0.41
Ri	21.19 MΩ (±SD=7.42MΩ):n=19	20.05 MΩ (±SD=8.70MΩ):n=11	p=0.70
APHW	0.37 ms (±SD=0.07ms):n=19	0.71 ms (±SD=0.28ms):n=12	p<0.001 ***
LAT	6.58 ms (±SD=1.94ms):n=17	4.32 ms (±SD=1.71ms):n=7	p<0.01 **
AMP	3.65 mV (±SD=2.27mV):n=14	5.22 mV (±SD=2.34mV):n=6	p=0.17
@40msec	1.06 mV (±SD=0.68mV):n=10	2.02 mV (±SD=2.11mV):n=3	p=0.21
HW	8.86 ms (±SD=4.36ms):n=12	6.61 ms (±SD=3.50ms):n=6	p=0.29
LAT10	2.76 ms (±SD=1.40ms):n=7	2.04 ms (±SD=0.75ms):n=5	p=0.32
10-90	2.14 ms (±SD=1.15ms):n=7	1.94 ms (±SD=0.94ms):n=5	p=0.75

Note: All values represent the mean ± one standard deviation: **Vm**= resting membrane potential; **Ri**= mean input resistence;**APHW**= action potential half-widths;**LAT**= latency to peak of EPSP;**AMP**= amplitude at peak of EPSP;**@40msec**= amplitude of EPSP at 40 msec post-stimulus;**HW**= EPSP half-width;**LAT10**= latency to 10% of EPSP peak amplitude;**10-90**= rise time from 10% to 90% of the peak EPSP amplitude.

Voltage-dependence of tSF-evoked EPSPs

When evoked at various hyperpolarizing or depolarizing membrane potentials, both the early and late phases of dendritic tSF-evoked EPSPs demonstrated a significant voltage dependence (N=5). In contrast, while both phases of the evoked response were typically present in somatic recordings (N=9), their voltage-dependence was often more difficult to demonstrate, possibly because of the high resistance of the recording electrode prevented passing sufficient current to significantly alter the membrane potential of the apical dendrite (about 200 μm distal to the soma).

An example of the effects of membrane potential on the magnitude and form of a voltage-dependent tSF-evoked somatic EPSP is illustrated in figure 25, A. At hyperpolarized membrane potentials, only a diminished form of the earliest component of the EPSP was evident which quickly decayed back to baseline (ie figure 25, A; -103 mV). In contrast, as the membrane potential was held at more depolarized levels, stimulation of the tSF pathway resulted in somatic EPSPs with significantly larger fast (arrow) and slow (asterisk) components. When the relative amplitude of the fast component of the somatic EPSP (at time of arrow) is plotted as a function of current injection intensity, the EPSP's voltage-dependency is clearly evident (figure 25, B; large plot). The amplitude of the late phase had a similar I/V curve (data not shown). Since calculation of the current/voltage (I/V) relationship of the pre-stimulus period results in a linear slope (figure 25, B; small plot), the diminished magnitude of the somatic EPSPs at the more hyperpolarized membrane potentials cannot be explained simply by an activation of additional ionic conductances, thereby resulting in a "shunting" of the EPSP.

Figure 25. Voltage-dependent early and late phases of tSF-evoked somatic EPSPs. **A:** When membrane potential is held at hyperpolarizing to depolarizing potentials, a pronounced voltage-dependency is seen in the early (arrow) and late (asterisk) phases of somatic EPSPs. **B:**(large plot) Peak amplitude of the early phase (at time of arrow in **A.**) plotted as a function of current injection intensity. The non-linear function reflects an enhancement of the EPSP at more depolarized potentials. **B:**(small plot) Shifts in basal membrane potential (recorded immediately before tSF stimulation), plotted as a function of current injection intensity. The resultant linear I-V curve suggests that the difference seen in the magnitude of EPSPs evoked at various potentials is not simply due to the activation of additional membrane conductances (and thereby "shunting" of the EPSPs) at more hyperpolarized potentials. Calibration bars; 10mV/50msec: ▲=stimulus artifact.

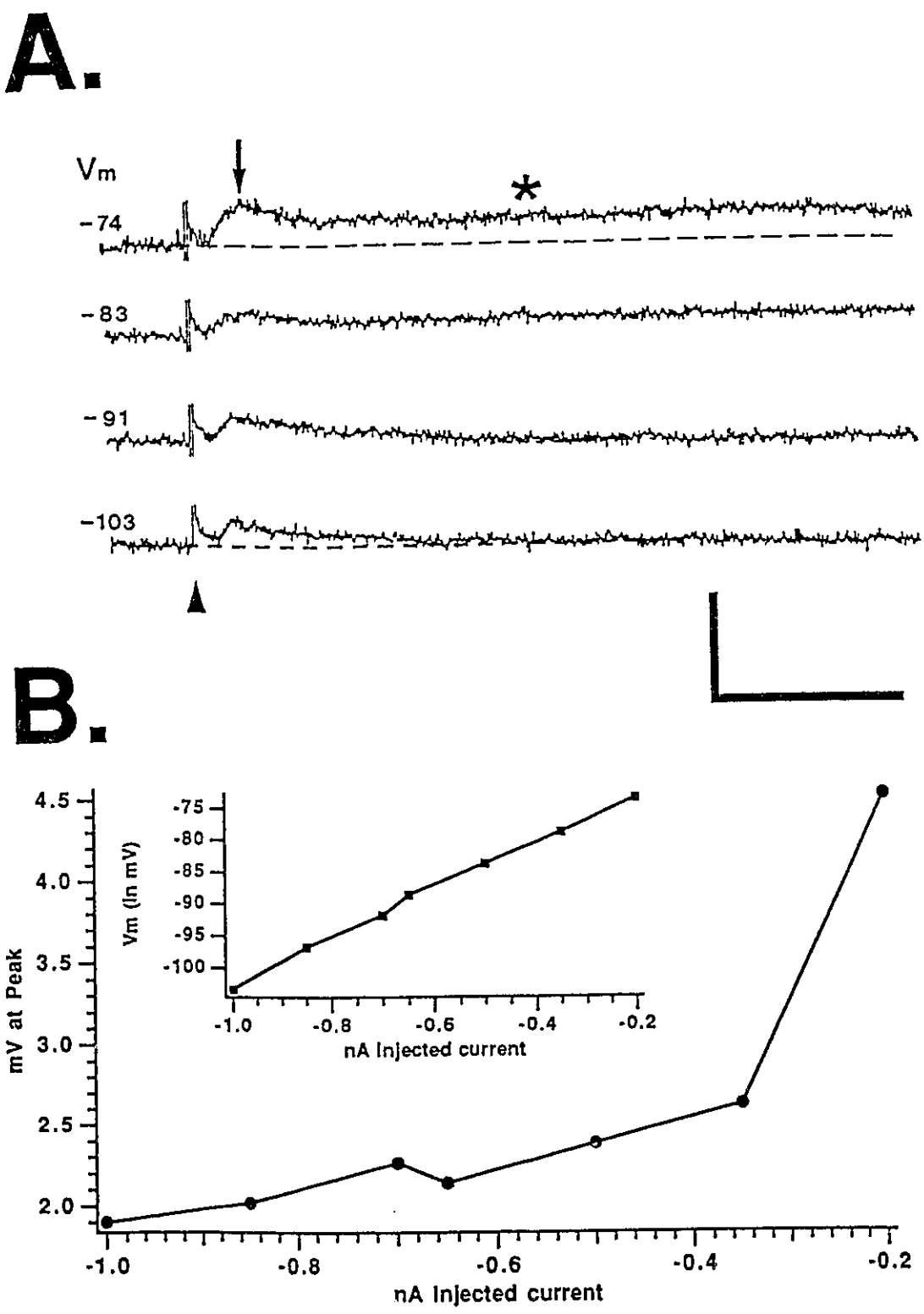
A.
Vm
-74
-83
-91
-103
B.
mV at Peak
4.5
4.0
3.5
3.0
2.5
2.0
-1.0
-0.8
-0.6
-0.4
-0.2
nA Injected current
Vm (in mV)
-75
-80
-85
-90
-95
-100
-1.0
-0.8
-0.6
-0.4
-0.2
nA Injected current

Compared to somatic EPSPs, dendritic EPSPs exhibited a qualitatively similar, but more pronounced voltage-dependency of both phases of the EPSP (figure 26, A). When the peak amplitude (relative to the pre-stimulus baseline) of the early component of the dendritic EPSP (arrow), and the amplitude (at 40 msec) of the late component, are both plotted as functions of membrane potential (figure 26, B.), the voltage-dependency of both phases of the dendritic EPSP is clearly evident. The ability to impale and record from the dendrites of neurons receiving direct synaptic input from the tSF allows for current ejection at a site both spatially and electrotonically close to the input. As a result, a clearer indication of the true voltage-dependent nature of the VML synaptic input can be gained.

Effects of NMDA receptor antagonism

Consistent with the results from extracellular studies (see above), pressure application of 1 mM CPP into the region of the VML (N=4) consistently reduced the earliest voltage-dependent component of the tSF-evoked EPSPs, while moderately reducing or having no effect on the late voltage-dependent slow component of the evoked responses (figure 27, A & B). Using digital subtraction of EPSPs evoked under control and CPP conditions (ie figure 27, A; 2), the relative insensitivity of the late voltage-dependent slow decay phase of tSF evoked EPSPs to CPP is clearly seen. These results therefore suggest that part of this late slow voltage-dependent component of tSF-evoked EPSPs is not mediated by NMDA receptors.

Figure 26. Voltage-dependency of early and late phases of tSF-evoked dendritic EPSPs. **A:** Dendritic EPSPs evoked at hyperpolarizing to depolarizing membrane potentials exhibit a pronounced voltage-dependency of both the early (arrow) and late (asterisk) phases. **B:** Plots of the peak amplitude (at arrow in A) of the early phase of the EPSP (PK), and the amplitude of the late phase of the EPSPs (at 40 msec), as a function of membrane potential. Calibration bars; 10mV/25msec: ▲=stimulus artifact.

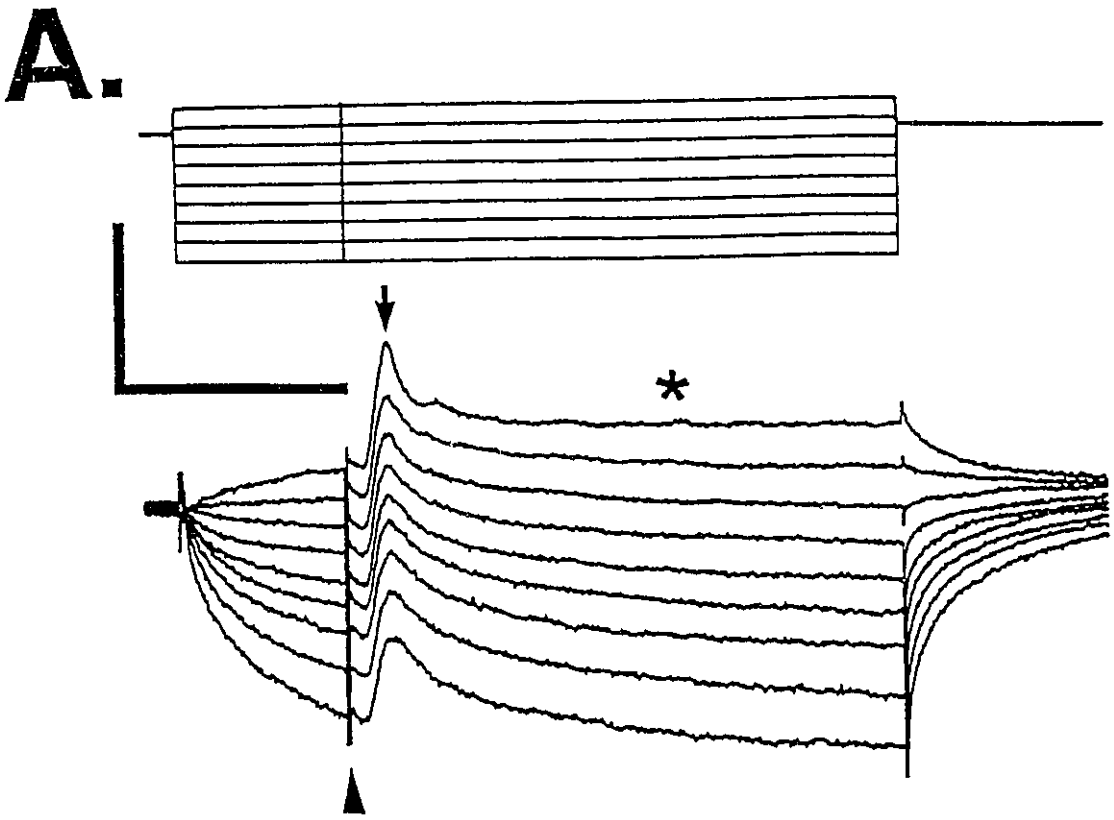
A.
*

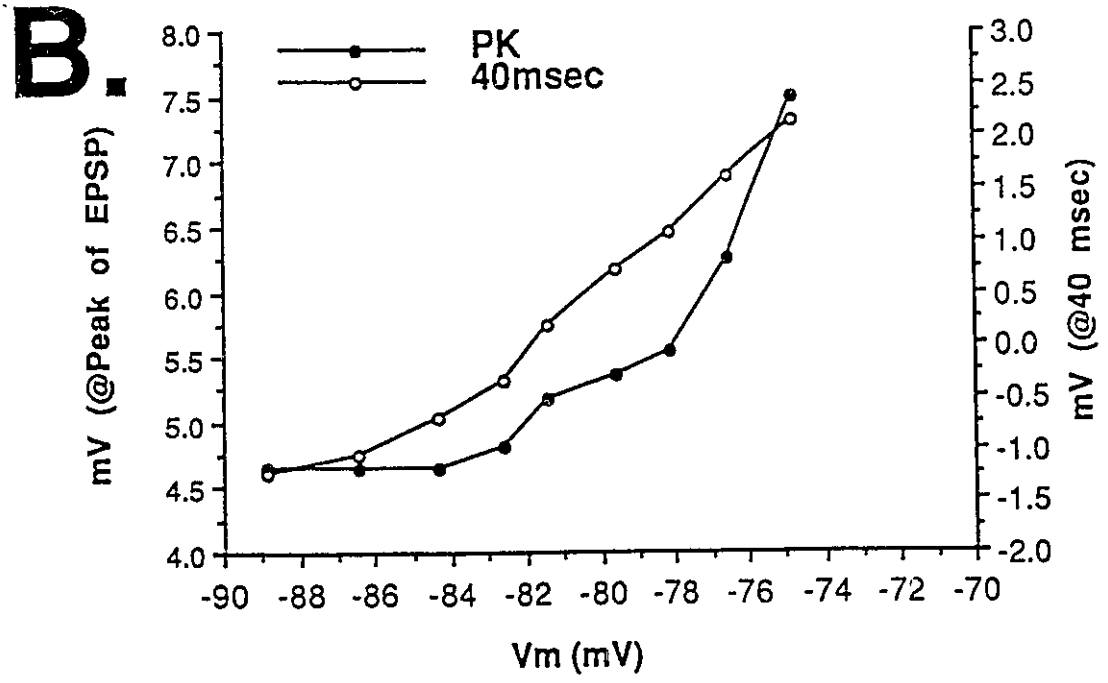
B.
PK
40msec
mV (@Peak of EPSP)
mV (@40 msec)
Vm (mV)
8.0
7.5
7.0
6.5
6.0
5.5
5.0
4.5
4.0
3.0
2.5
2.0
1.5
1.0
0.5
0.0
-0.5
-1.0
-1.5
-2.0
-90
-88
-86
-84
-82
-80
-78
-76
-74
-72
-70

Figure 27. Effects of CPP (1mM) on intracellular recorded tSF-evoked somatic EPSPs. **A(1):** Superimposition of EPSPs evoked under control and CPP conditions, showing selective suppression of the early component of the EPSP, with no discernible effect on the late phase of the EPSP (asterisk). **A(2):** Results of digital subtraction of responses shown in **A(1)**, isolating the CPP sensitive early component of the tSF-evoked EPSP. Note that the subtracted response quickly returns to zero (dashed horizontal line) demonstrating the CPP-insensitive nature of the late component of this tSF-evoked EPSP. **B(1):** Characteristic control somatic EPSP showing a small short latency "notch" in its rising phase (arrow) which corresponds to the peak of the residual component of the response seen after CPP application (2). Note that, while the late phase of the response is significantly diminished, it is still present in the response evoked under CPP. Calibration bars; (**A:** 2.5mV/25msec), (**B:** 5mV/20msec):▲=stimulus artifact.

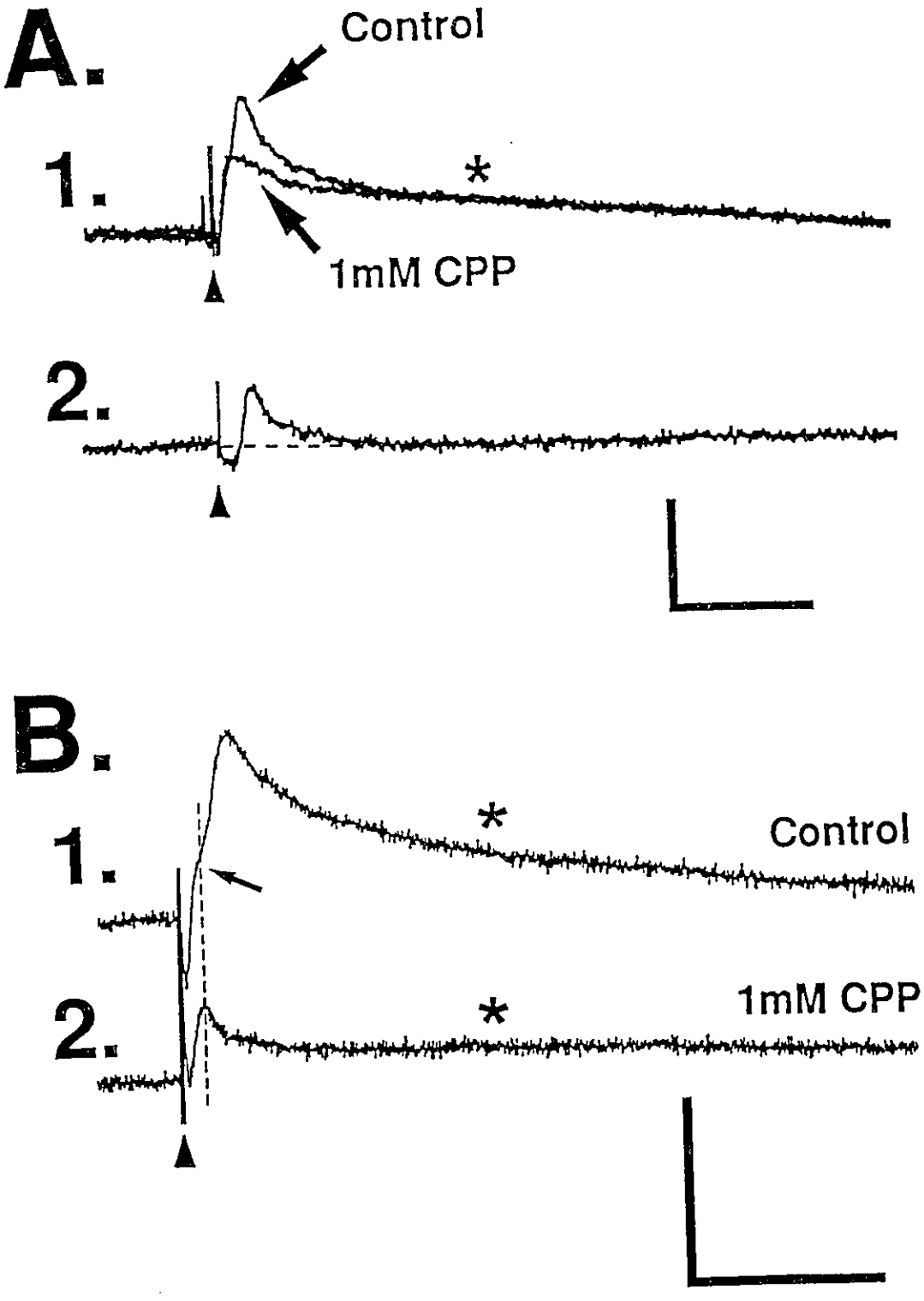
A.
Control
1.
*
1mM CPP
2.
B.
1.
*
Control
2.
*
1mM CPP

Following application of CPP, a residual fast component of the EPSP could be observed which preceded the peak of the CPP sensitive component (figure 27, B; 1 & 2). In light of the extracellular data demonstrating a significant contribution of non-NMDA receptors to the tSF-evoked VML field potential, the effects of pressure application of CNQX (1 mM) on intracellular recorded responses was assessed.

Effects of non-NMDA receptor antagonism

Similar to the results of the extracellular field potential studies, application of CNQX (N=6) resulted in a complete block of both the early and late phases of the tSF-evoked somatic EPSP (figure 28, A). Digital subtraction of EPSPs evoked under control and CNQX conditions demonstrated the complete nature of the blockade of the EPSPs by CNQX (figure 28, B). During the limited range of depolarizing current intensities which could be passed during intracellular recordings, an initial assessment of whether this complete blockade of the tSF-evoked somatic EPSPs by CNQX was due to merely a voltage dependent blockade of the early component or to a specific pharmacological blockade of this CPP sensitive component was inconclusive. As previously reported (71), upon depolarization many (presumably local) voltage-dependent processes (ie fpps) where evoked with a time course similar to that of the tSF-evoked EPSPs, and therefore precluded any estimation of a residual voltage-dependent early phase of the EPSP.

Antagonism of the slow decay phase

The slow decay phase of tSF-evoked responses consistently demonstrated significant voltage dependency (both directly with intracellular depolarization, or indirectly through extracellular field recordings), suggesting that this prolonged slow

Figure 28. Effects of CNQX (1mM) on intracellular recorded tSF-evoked somatic EPSPs. **A:** Superimposition of EPSPs evoked under control and CNQX conditions showing the total suppression of both phases of the tSF-evoked EPSP. **B:** Results of digital subtraction of responses shown in **A**, demonstrating an apparent complete blockade of the tSF-evoked EPSP by CNQX. Note that (unlike in figure 26) the late phase (asterisk) of the subtracted response does not return to zero (dashed horizontal line) again demonstrating the complete nature of CNQX blockade of the EPSP under control conditions. Calibration bars; 5mV/25msec: ▲=stimulus artifact.

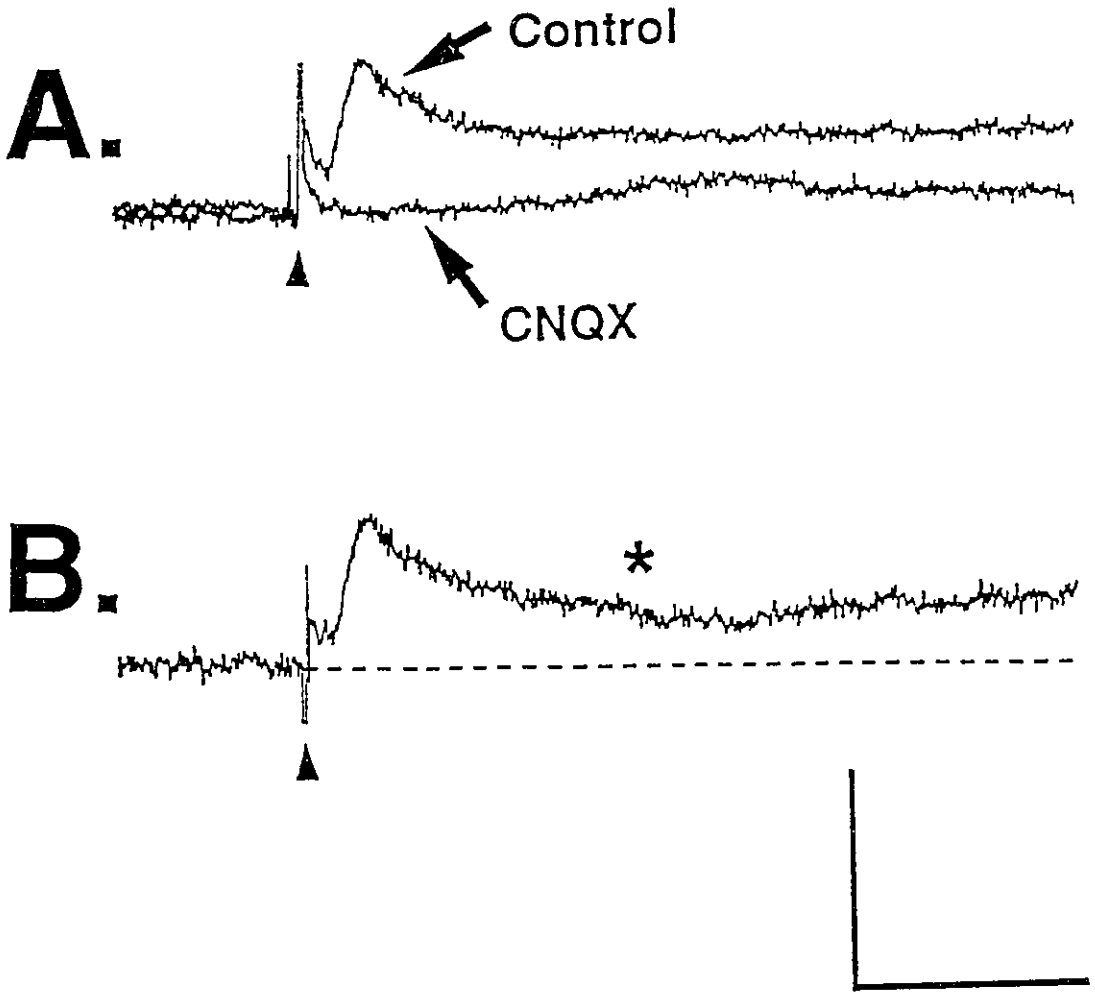
A.
Control
CNQX
B.
*

portion of tSF-evoked EPSPs response might be mediated by NMDA receptors. It was therefore surprising that this slow component of the response was only partially antagonized or effected by CPP (ie see figure 27, A & B; and figure 15), or by Kyn (ie figure 14, A). In light of the demonstrated importance of persistent Na^+ channels to the electrical activity of ELL pyramidal cells (71), an attempt was made to assess their possible contribution to the late phase of the tSF-evoked EPSPs by intracellular application of the Na^+ channel blocker QX-314.

Both at rest, and at depolarized membrane potentials, the characteristic late slow decay phase of the tSF-evoked EPSPs was conspicuously reduced or absent (N=7) when QX-314 (100 mM) was applied through the recording electrode (see figure 29, A. vs B.). Complete elimination of the late phase was obtained in some cases (ie figure 29 C), while in other cases some slow depolarization (to about 40 msec) was still present (ie figure 29 B). Further studies will be required to determine whether NMDA-mediated processes contribute to this residual component.

Due to the rapid onset of QX-314 effects, only in one recording was it possible to obtain a tSF-evoked EPSP immediately following the impalement of the cell, and in this case the EPSP possessed both an early peak and a small late decay phase. Within a few minutes, however, the amplitude of current-evoked action potentials were significantly diminished (and subsequently failed), and the previously evident late decay phase of the EPSP was completely blocked leaving only a fast EPSP component (ie figure 29, C). Taken together, these results suggest a possible role for synaptically-induced persistent Na^+ currents in the generation of the slow voltage-dependent prolonged decay

Figure 29. Effects on tSF-evoked EPSPs of intracellular antagonism of voltage-dependent Na^+ channels with QX-314 (100 mM). **A:** A typical voltage-dependent dendritic EPSP (+0.2 nA injected current) consisting of the characteristic early and late (astrisk) phases. **B:** EPSP recorded from a different intradendritic impalement with equivalent depolarization, but with QX-314 present in the recording electrode. Note that the EPSP decays to baseline in about 40 msec. **C:** Somatic EPSP recorded with QX-314 in the recording pipette. Note the absence of the late decay phase of tSF-evoked responses in **B** and **C** after the application of QX-314. These results suggest that the late phase of tSF-evoked EPSPs is mediated by voltage-dependent synaptically-mediated persistent Na^+ current. Calibration bars; (**A** & **B**: 10mV/15msec), (**C**: 5mV/25msec): ▲=stimulus artifact.

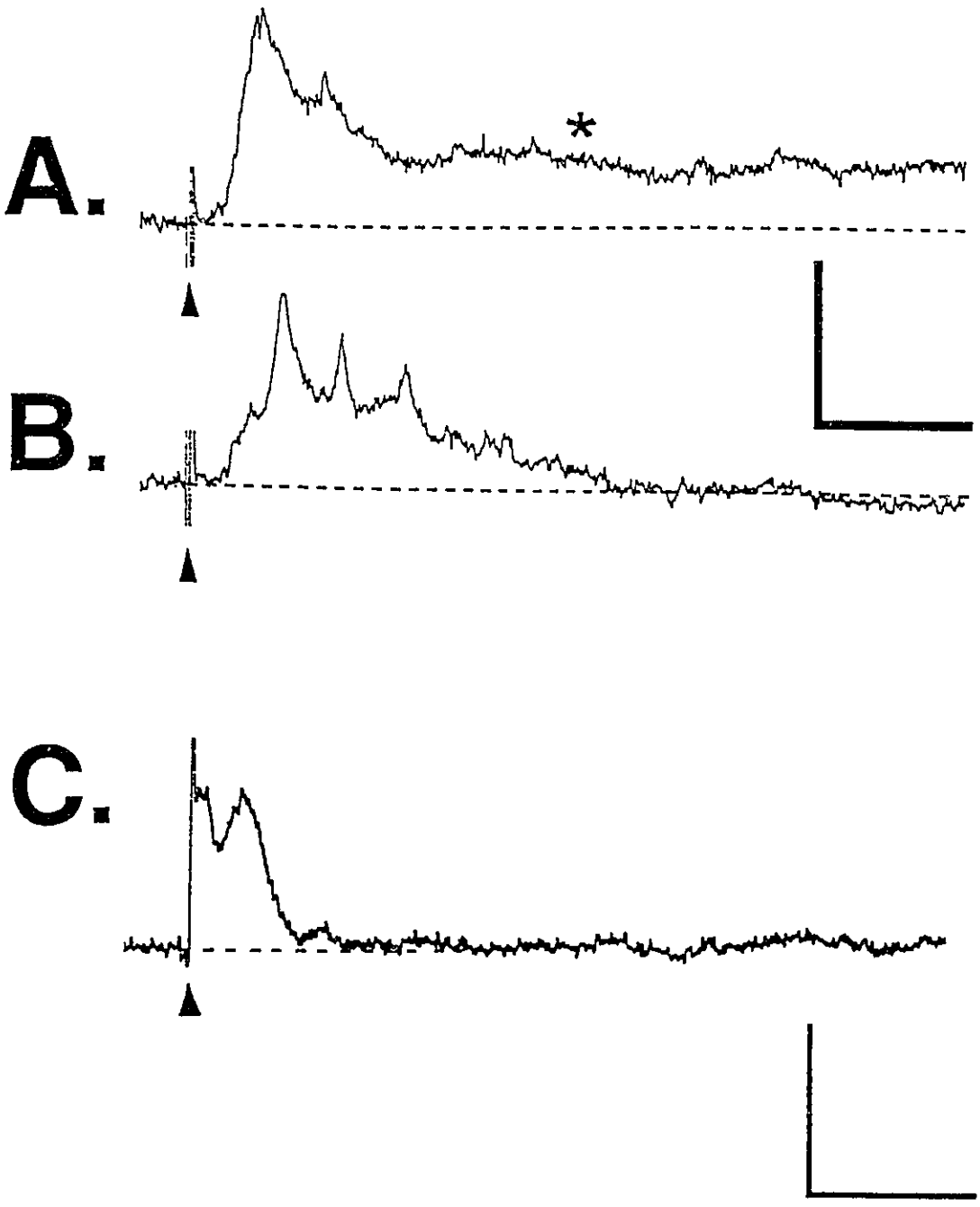
A.
B.
C.

phase of tSF-evoked EPSPs. Further studies, utilizing whole cell patch clamping and voltage clamping techniques, will be required to more clearly establish the time course and contribution this persistent Na^+ current makes to transmission at the VML synapse.

Inhibitory Post-synaptic Potentials (IPSPs)

In the present studies, selective activation of the tSF feedback projection was carried out in an attempt to experimentally isolate and characterize the functional nature of this excitatory pathway. Stimulus position and intensity were judiciously chosen to specifically avoid both antidromic activation of pyramidal cells, as well as stimulation of the recently discovered direct GABAergic Pd-ELL inhibitory feedback pathway. This inhibitory pathway is comprised of the axons of Pd bipolar cells, which run within the ventral aspect of the tSF and form synapses on the somas of pyramidal cell (67). In two experiments stimulation was delivered to the entire tSF (both the direct excitatory and inhibitory pathways) to assess their possible interaction.

Concurrent stimulation of the direct Pd-ELL excitatory and inhibitory pathways resulted in a complex post-synaptic response, comprised of a rapid EPSP followed by a prolonged IPSP (see figure 30, A; 2). The inhibitory nature of this IPSP was further confirmed by its effectiveness at significantly reducing the frequency of current evoked action potential trains (see asterisk in figure 30, A; 1). Application of CNQX to the VML resulted in a complete blockade of the early EPSP, and an apparent enhancement of the magnitude of the prolonged IPSP (figure 30, B; 1). Since application of CNQX in the VML presumably also blocked tSF-mediated responses of local inhibitory interneurons, the remaining IPSP most likely is mediated by the stimulation of the direct inhibitory

Figure 30. Effects of conjunctive stimulation of the direct excitatory and inhibitory feedback pathways. **A(2):** Stimulation of both the excitatory and inhibitory components of the tSF results in a fast EPSP followed by a prolonged IPSP. **A(1):** The inhibitory effects of the tSF-evoked IPSP can be clearly seen in its ability to depress the frequency of current evoked action potentials (asterisk). **B(1):** Comaparison of control EPSP-IPSP sequence, and a subsequent response evoked under CNQX (1 mM). Note that only the IPSP component remains after the blockade of the excitatory component of the complex tSF reponse. **B(2):** Digital subtraction of the waveforms in **B(1)** results in a reconstruction of the characteristic bi-phasic tSF-evoked EPSP which is antagonized by CNQX. Calibration bars; (A: 25mV/50msec), (B: 10mV/50msec): ▲=stimulus artifact.

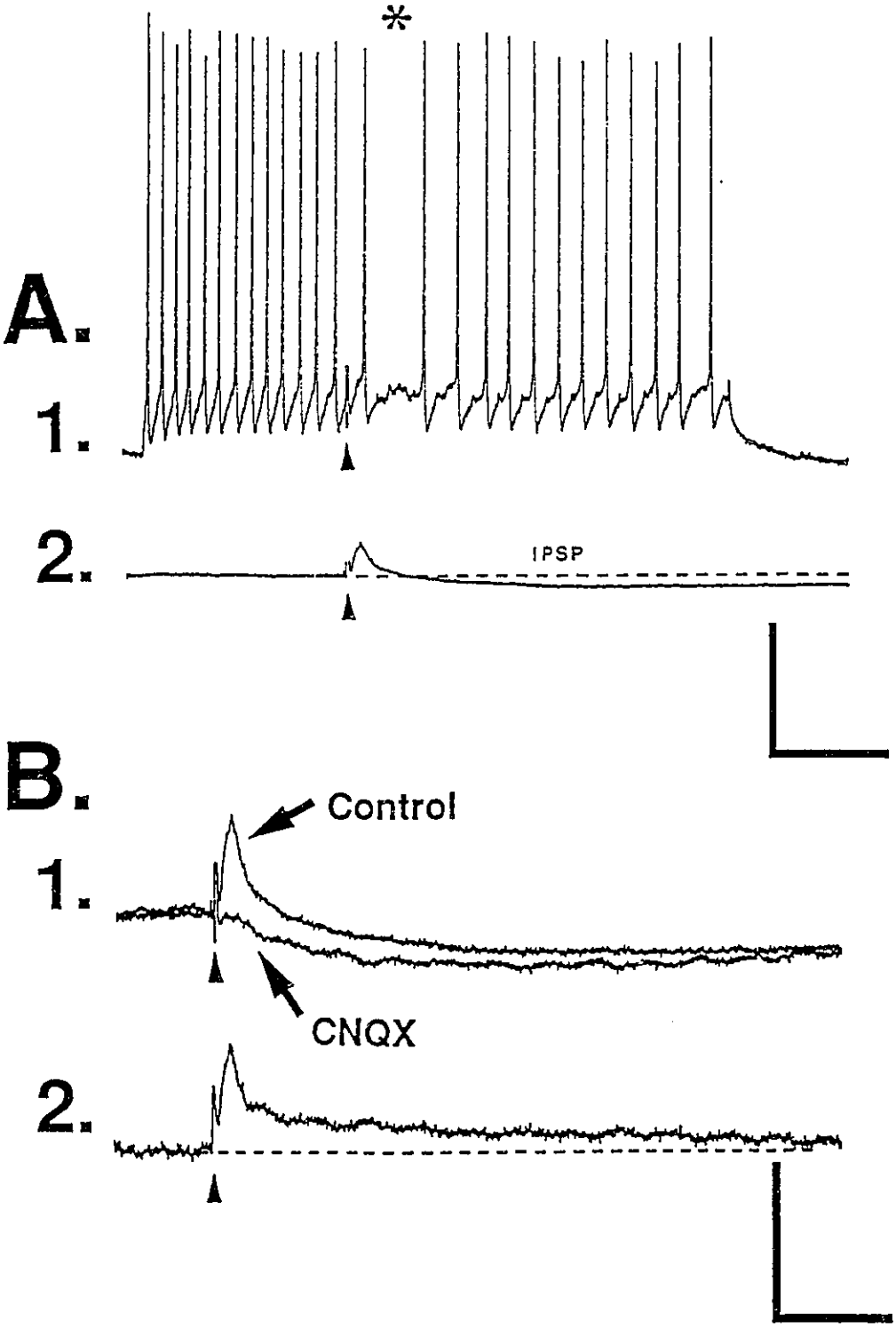
A.
1.
2.
IPSP
B.
1.
Control
CNQX
2.

pathway. Similar to the previous demonstration of a CNQX blockade of the "pure" excitatory tSF-evoked EPSPs (see above), digital subtraction of the control and CNQX responses in this case allowed for an estimation of the underlying excitatory component of this complex response in isolation from the IPSP. The resultant waveform had a form and time course closely resembling that of an excitatory tSF-mediated EPSP evoked in isolation (ie figure 28, A).

Since the late phase of the tSF-evoked EPSP temporally overlaps with, and partially antagonizes the prolonged IPSP, blockade of the EPSP with CNQX resulted in an apparent increase in the magnitude of the IPSP. Taken together, these results suggest the possible existence of complex post-synaptic interactions between these functionally opposed direct Pd-ELL feedback pathways, and demonstrates the ability to experimentally activate (*in vitro*) both pathways in isolation thereby allowing for the possible characterization of their individual effects.

Synaptic facilitation of the VML response: Paired-Pulse

In two extracellular experiments, the effects of paired-pulse stimulation of the tSF pathway was assessed. Results demonstrated a dramatic facilitation of the tSF-evoked VML field potential over the complete range of interstimulus intervals (ISIs) tested (10 - 130 msec). When expressed as a percentage of the peak amplitude of the initial response (PK1) (see figure 31, A & C), the mean relative peak amplitude of the second evoked response (PK2) ranged from 165.16% (±SD=23.93%) of the amplitude of PK1 at an ISI of 10 msec, to 122.13% (±SD=7.97%) at an ISI of 130 msec. While a post-synaptic temporal summation of the slow decay phase of the VML response might underlie this

Figure 31. Synaptic facilitation induced by paired-pulse stimulation of the tSF pathway. **A:** Stimulations over a wide range of inter-stimulus intervals (ISI) resulted in a dramatic facilitation of the tSF-evoked VML response. **B:** Even after the late phase of the VML field potential had decayed back to baseline (arrow), subsequent evoked responses still demonstrated significant enhancement (also see asterisks in **A**). **C:** When expressed as a percentage of the peak amplitude of the initial control responses (PK1), the peak amplitude of subsequent evoked responses (PK2) demonstrated significant paired-pulse facilitation over all ISIs tested (10 - 130 msec).

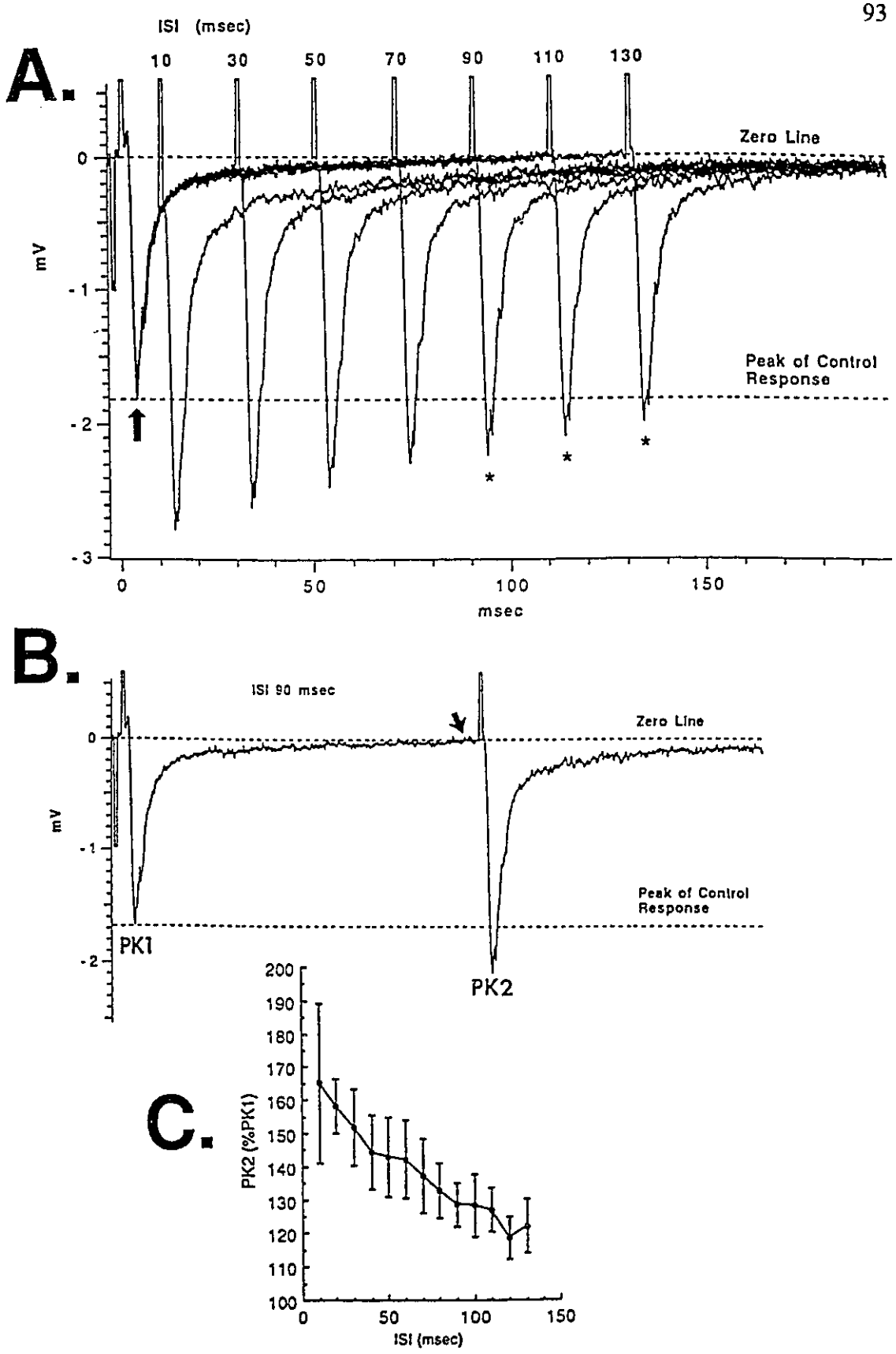
A.
ISI (msec)
10
30
50
70
90
110
130
Zero Line
Peak of Control Response
mV
0
-1
-2
-3
0
50
100
150
msec
B.
ISI 90 msec
Zero Line
Peak of Control Response
PK1
PK2
mV
0
-1
-2
C.
PK2 (%PK1)
200
190
180
170
160
150
140
130
120
110
100
0
50
100
150
ISI (msec)

observed paired-pulse facilitation, it is impossible (using field recordings) to rule out a possible significant contribution of pre-synaptic mechanisms such as increased transmitter release to account for this short-term synaptic facilitation. This problem is high-lighted by the fact that at an ISI of 90 msec or greater, while the slow late phase of the VML response appears to have decayed back to baseline (arrow in figure 31, B), the relative mean peak amplitude of PK2 still ranges from 128.67% (±SD=6.56%) to 122.13% (±SD=6.56%) of the mean peak amplitude of PK1 (see asterisks in figure 31, A).

Synaptic facilitation of the VML response: Tetanic Stimulation

Consistent with the above results from pair-pulse extracellular recordings, intracellular recordings of pair-pulse tSF-evoked EPSPs (ISI=40 msec) also demonstrated a significant facilitation. At the resting membrane potential (Vm), while initial tSF stimulation evoked an EPSP which was subthreshold for the initiation of action potentials, subsequent EPSPs (40 msec later) appeared to summate on the late decay phase of the first EPSP bringing Vm past threshold for the generation of action potentials (figure 32, A). Although these initial results are suggestive of a postsynaptic mechanism of EPSP summation, paired-pulse responses were evoked at various hyperpolarizing membrane potentials to rule out the possibility that this facilitatory effect could be accounted for by an increase in presynaptic transmitter release. Had this been the case, the second EPSP should be significantly larger than the first one regardless of Vm. Since the second EPSP was not augmented at hyperpolarized Vm, a presynaptic mechanism for paired-pulse potentiation at this synapse appears unlikely.

Figure 32. Effects of paired-pulse stimulation on intasomatic recorded EPSPs. **A:** Paired-pulse stimulation of the tSF (ISI=40 msec) results in a significant facilitation of the second EPSP, often leading to the initiation of an action potential (truncated for clarity of presentation). **B:** Results of paired-pulse stimulation carried out at hyperpolarizing to depolarized membrane potentials. Note that, at -84 mV, the magnitude of the early phase of the first and second EPSP did not significantly differ, with only slight facilitation being seen in the late phase of the second EPSP. In contrast, at more depolarized potentials the early and late (large arrow) phases of the EPSPs demonstrated a significant potentiation, summating to bring the second EPSP past threshold for the generation of both action potentials, and voltage-dependent fpps (small arrow). **C:** The late phase of tSF-evoked EPSPs significantly increases the frequency of current-evoked somatic spikes, clearly demonstrating its post-synaptic locus and underlying excitatory nature. Calibration bars; (**A**:25mV/25msec), (**B**:20mV/40msec), (**C**:50mV/100msec): ▲=stimulus artifact.

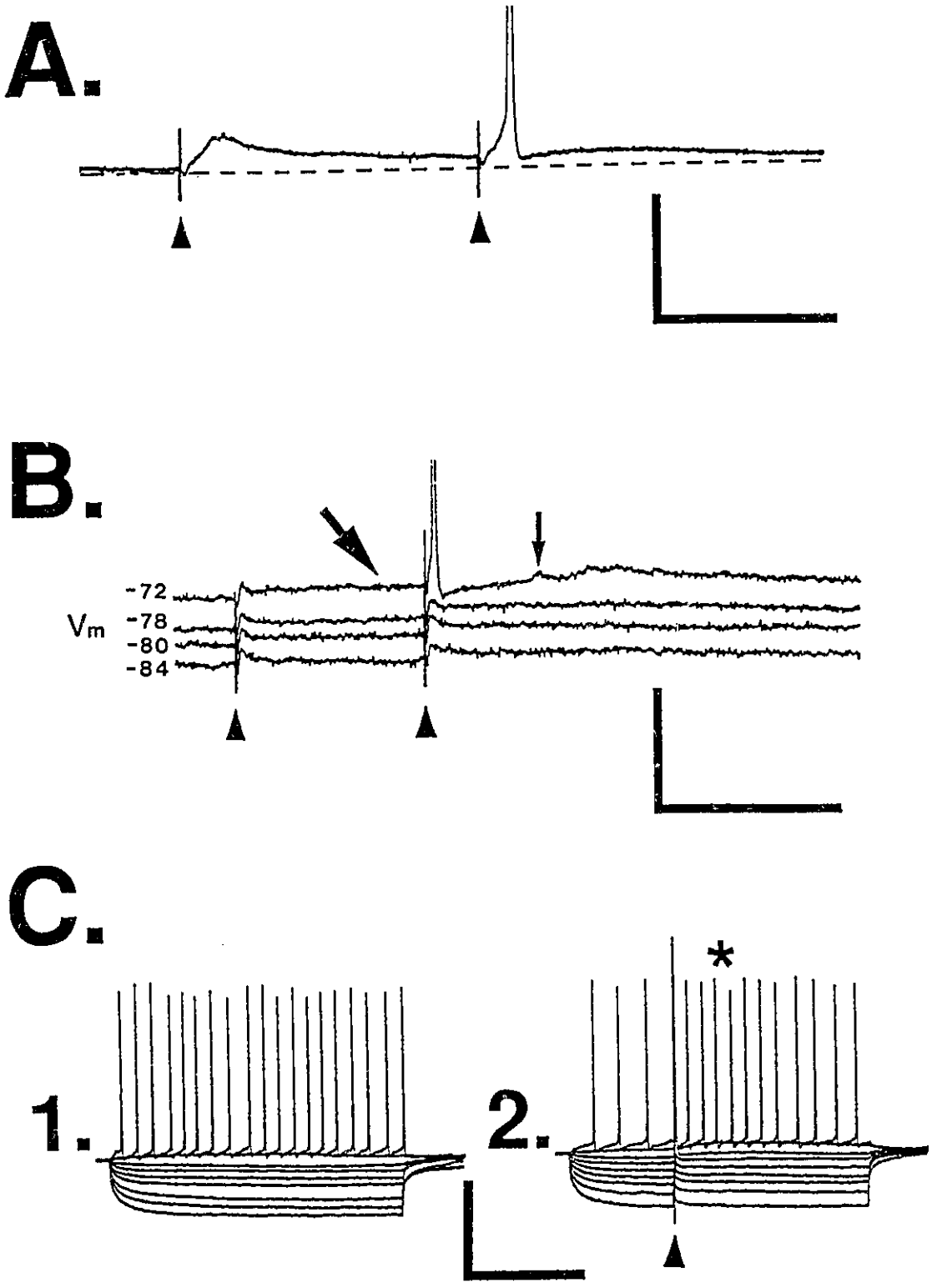
A.
B.
Vm
-72
-78
-80
-84
C.
1.
2.
*

Due to the voltage-dependence of the EPSP early and late phases, at more hyperpolarizing potentials there was only a minimal summation of the late phase of the EPSP, with no discernable increase in the magnitude of the early phase (ie -84 mV in figure 32, B.). In contrast, as the membrane potential was further depolarized, there was a gradual increase in the relative contribution of the late phase of the EPSP (see large arrow in figure 32, B; -72 mV) which summated across stimulations, eventually bringing the membrane potential past the threshold for action potential generation. The fact that this summation of the late phase of the EPSPs also resulted in the occurrence of voltage-dependent fpps (ie small arrow in figure 32, B), as well as significantly increasing the frequency of current-evoked action potentials (figure 32, C; 1 vs 2), both serve to demonstrate the significant excitatory contribution that the late phase of tSF-evoked EPSPs can make to pyramidal cell excitability.

While paired-pulse stimulation of the tSF pathway allowed for an initial identification of facilitatory processes within this feedback pathway, under more natural conditions Pd stellate cells which give rise to this projection pathway typically fire phasic high-frequency bursts of action potentials (15). A limited number (N=5) of recordings were therefore conducted with the aim of assessing the post-synaptic effects of short trains (10 pulses) of high-frequency (100 Hz) stimulation of the tSF pathway. As would be expected from the paired-pulse data, trains of stimuli resulted in a rapid and pronounced summation of the tSF-evoked EPSPs (figure 33, A). This frequency potentiation, as in the case of paired pulses, appeared to be primarily the result of a temporal summation of the prolonged late decay phase of the tSF-evoked EPSPs.

Figure 33. Temporal summation of tSF-evoked EPSPs with high-frequency stimulation. **A:** Consistent with the extracellular and intracellular paired-pulse data, activation of the tSF feedback pathway with high-frequency stimulation (10 pulses @ 100 Hz), resulted in a significant temporal summation of the EPSPs. **B:** Summation of the late decay phase resulted in a prolonged depolarization whose underlying excitatory nature was evident by its ability to initiate action potential (arrow). Calibration bars; (A:20mV/50msec), (B:20mV/75msec): ▲=stimulus artifacts.

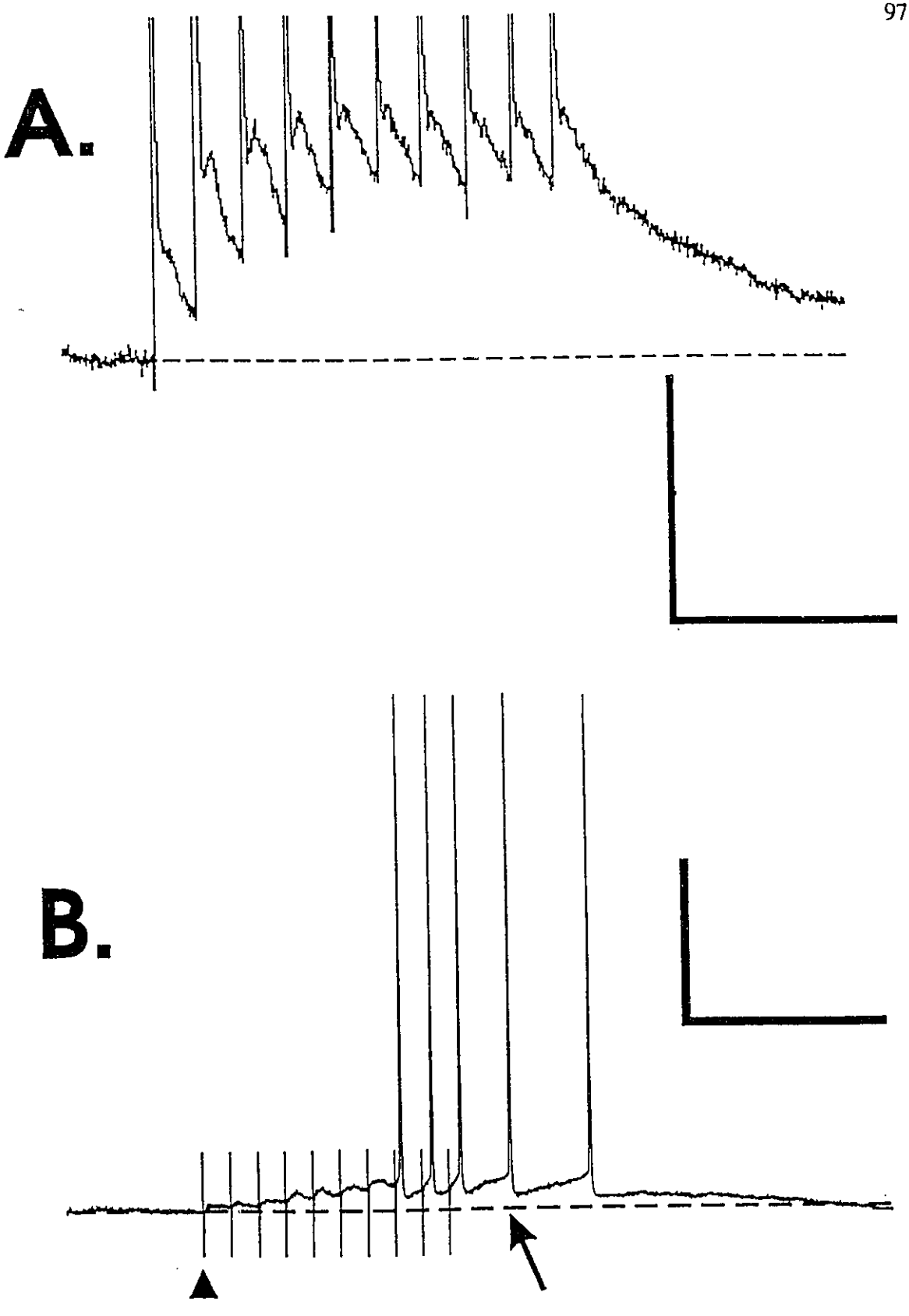
A.
B.

Following the high-frequency stimulus, summation of the late decay phase resulted in a prolonged depolarization whose underlying excitatory nature was clearly evident by the fact that it was capable of initiating action potentials (see arrow, figure 33, B.).

Application of QX-314 consistently resulted in an antagonism of the late decay phase of tSF-evoked EPSPs (ie. figure 34, A), and a subsequent block (N=3) of the prominent frequency potentiation and prolonged depolarization usually seen at this synapse (figure 34, B). Given these results it is likely that, at the frequency that the descending tSF input is known to encode electrosensory information, significant temporal summation of the late Na^+(p)-mediated phase of tSF-evoked EPSPs might occur, thereby having profound effects on naturally occurring synaptic events *in vivo*.

Application of CPP, while reducing the magnitude, failed to completely block the temporal summation of EPSPs evoked by high-frequency stimulation of the tSF (N=3), or the summation of the late decay phase (see figure 35, B). In stark contrast, intracellular application of QX-314 consistently resulted in tSF-evoked EPSPs lacking the late decay phase, and subsequently showed no frequency facilitation (ie figure 34). Taken together these results suggest that, while NMDA receptors appear to contribute to the late phase of the tSF-evoked EPSP, the major source of this depolarization is due to voltage-sensitive Na^+ currents.

Figure 34. QX-314 blockade of the temporal summation of tSF-evoked EPSPs.
A: tSF-evoked EPSP evoked after application of QX-314, lacking the late decay phase. **B:** After QX-314 application high-frequency stimulation no longer results in a temporal summation of the EPSPs, clearly indicating a crucial role for voltage-dependent Na^+ currents in the post-synaptic summation of tSF-evoked EPSPs. Calibration bars; 5mV/25msec: ▲=stimulus artifact.

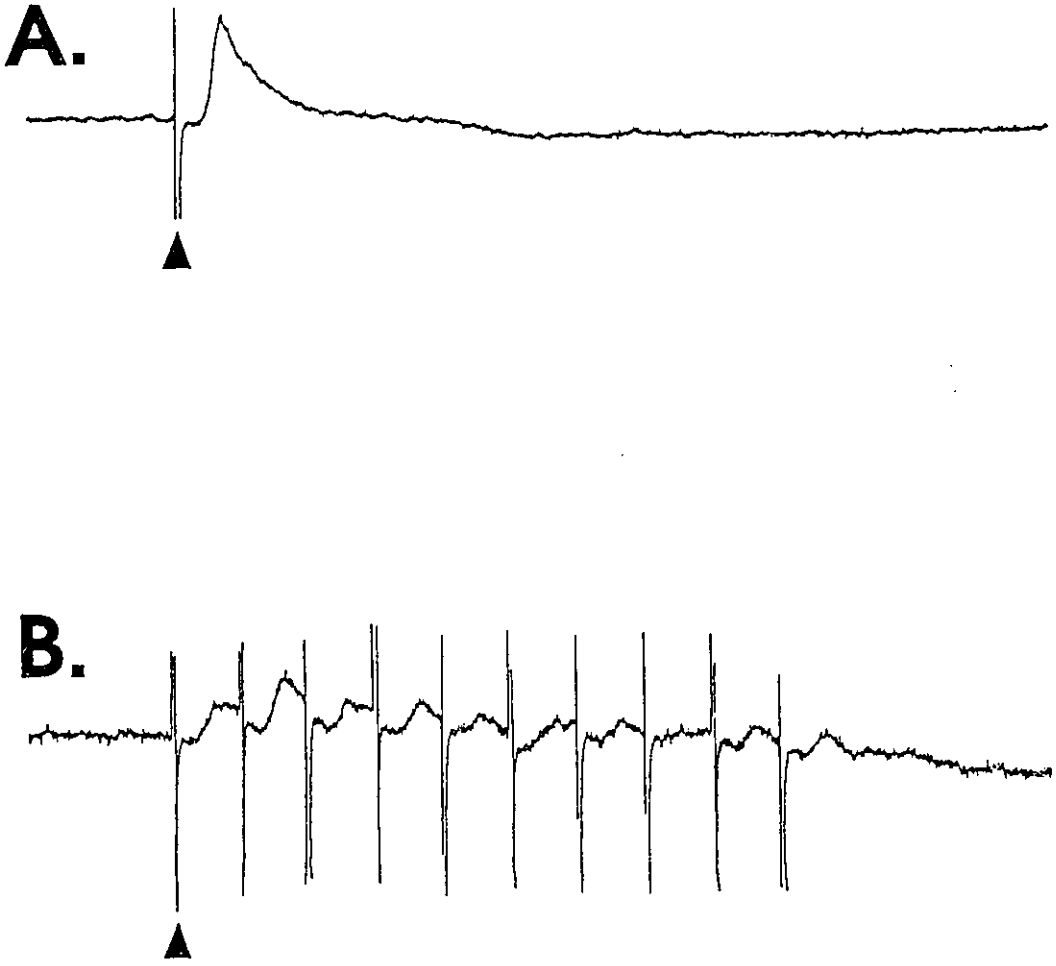
A.
B.

Figure 35. Effect of CPP on the temporal summation of tSF-evoked EPSPs.
A: Under control conditions, high-frequency stimulation results in a pronounced temporal summation of the tSF-evoked EPSPs with a prolonged late decay phase. Note that (as in figure 32, **B**) this prolonged depolarization exceeds action potential threshold. **B:** After application of CPP, the magnitude of the temporal summation (and resultant late phase) is reduced (arrow). Calibration bars; 20mV/250msec: ▲=stimulus artifacts.

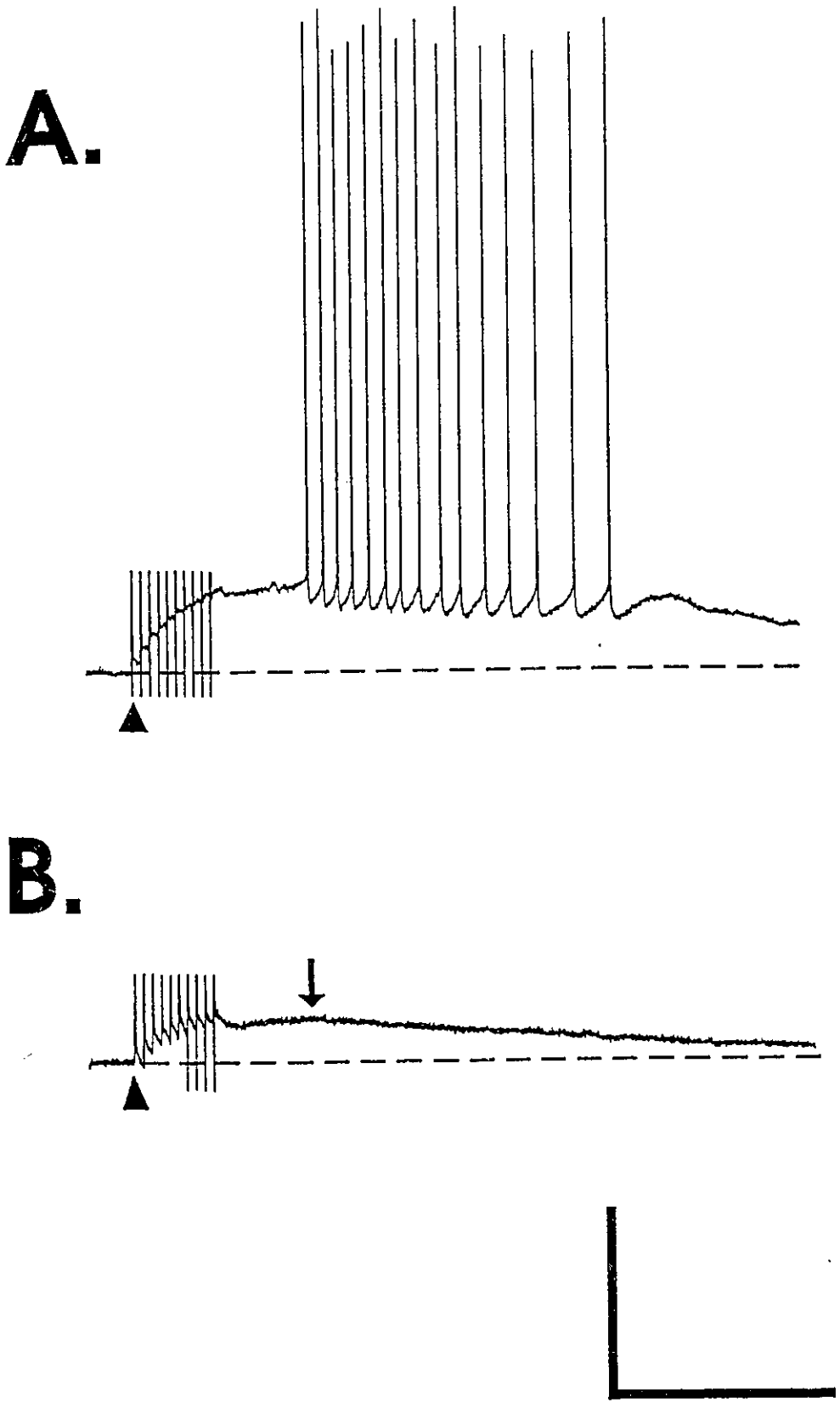
A.
B.

DISCUSSION

I. Electrophysiological Localization of the VML Synapse

In the present studies, an electrophysiological and pharmacological characterization of feedback projections were undertaken using an *in vitro* slice preparation of the electrosensory lateral line lobe (ELL) of the weakly electric fish, *Apteronotus leptorhynchus*. Direct feedback projections, running in a well-defined fiber tract (the tSF), and having a spatially restricted pattern of termination (VML), were investigated. The highly laminar structure of the ELL slice preparation, with its spatially segregated afferent pathways, allowed for an electrophysiological isolation of the excitatory components of tSF-evoked responses. This was accomplished through the careful adjustment of both stimulus intensity, and the placement of the stimulating electrode adjacent to the tSF feedback pathway. It is important to note that this was carried out without pharmacological blockade of inhibitory GABAergic local interneurons and descending input within the ELL, a manipulation which can induce large repetitive synchronous discharges or "bursts" within the ELL slice preparation (124).

Several lines of evidence suggest that this level of experimental control over the independent activation of the direct excitatory feedback pathway was indeed possible. Firstly, concurrent stimulation of both the direct excitatory and inhibitory components of the tSF feedback pathway was shown to result in evoked responses consisting of an EPSP followed by a prominent and prolonged IPSP (ie see figure 30). When the direct excitatory component of the tSF-evoked response was subsequently blocked by the application of CNQX in the VML, the inhibitory component of the response could be

seen in isolation. Secondly, the fact that minimal IPSPs were seen when stimulus position and intensity was chosen to isolate the excitatory component of the tSF-evoked response, and CNQX was subsequently applied in the VML to block the EPSP, strongly suggests that the excitatory component of the tSF-evoked response was being selectively activated. These results demonstrate the unique ability, *in vitro*, to experimentally separate and characterize these functionally and anatomically distinct components of the tSF feedback pathway. This technique might therefore be of great benefit for future studies undertaken to characterize the functional properties of the direct inhibitory component of the tSF feedback pathway in isolation.

Mapping of extracellular tSF-evoked field potentials along the dendro-somatic axis of ELL pyramidal cells revealed a large bi-phasic field potential (consisting of an early peak followed by a slow decay phase) which spatially corresponded to the previously morphologically identified zone of synaptic termination of the tSF fibers in the VML (63). Under Mn^{2+} ACSF perfusion, most of this tSF-evoked VML field potential was absent, therefore suggesting its dependence on Ca^{2+}-mediated synaptic transmission. In this case, only a short latency residual component of the VML response was evident, generated both by fiber volley within the tSF pathway itself, and (as demonstrated with simultaneous intradendritic and extracellular VML field recordings) by antidromic activation of a small number of pyramidal cells via stimulation of their axons in the underlying plexiform layer.

A spatially restricted current sink, (characteristic of excitatory postsynaptic potentials), was subsequently localized at the level of the VML using one-dimensional current source density analysis. This current sink corresponded both spatially and temporally with the peak of the VML field potential, thereby supporting the interpretation that the Mn^{2+}-sensitive portion of the bi-phasic VML field potential truly reflects local tSF-evoked excitatory post-synaptic currents. Furthermore, the peak negativity and subsequent slow decay phase of the VML field potential was shown to be in precise temporal register with the peak and slow decay phase of intracellularly recorded EPSPs.

II. EAA transmission in the Dorsal and Ventral molecular layers of the ELL.

Effects of EAA Agonists and Antagonists in the DML

Both the biochemically defined distribution of amino acids within the lamina of the ELL (86), as well as the spatial distribution of NMDA and non-NMDA EAA ligand binding (65), have previously been interpreted as suggesting an important role for EAAs as neurotransmitters within the molecular layer of the ELL. Certain neurons within the ELL, such as pyramidal cells and various inhibitory interneurons, possess apical dendrites which extend dorsally to form the overlying molecular layer of the ELL. The molecular layer is further divided, on the basis of the synaptic termination patterns of the direct and indirect feedback pathways, into the ventral (VML) and dorsal (DML) molecular layers respectively. As the pyramidal cell's dendrites ascend through the VML they receive synaptic input from tSF fibers, and then continue to ascend into the DML where they receive synaptic input from parallel fibers originating from the overlying EGp. While the ultrastructure of VML synapses are typical of excitatory synapses (70), only recently has

extensive physiological and pharmacological studies been undertaken to directly assess the roles of EAAs in transmission within this region of the ELL molecular layer.

Application of both NMDA and non-NMDA EAA agonists within the DML *in vivo* has previously been shown to result in a significant increase in the firing rate of ELL pyramidal cells when the pressure pipette is located in the region of the recorded cell's apical dendrite (9). In contrast, ejection of EAA agonists lateral in the DML, (relative to the position of the recorded pyramidal cell's apical dendrites), results in a substantial decrease in the cell's firing rate. This inhibition has been interpreted, on the basis of the known anatomical and physiological organization of ELL circuitry, as being mediated by the activation of adjacent inhibitory interneurons which functionally contribute to the recorded pyramidal cell's inhibitory surround. Based on the above results, it was concluded that functional EAA receptor-gated channels are localized both on the apical dendrites of ELL pyramidal cells, and on the apical dendrites of at least a subset of inhibitory interneurons within the ELL. However, due to the potential spread or diffusion of applied EAA agonists from the DML ejection site into the region of the VML, the precise spatial location within the molecular layer of the EAA receptors responsible for the above effects is unclear.

Further results, however, conclusively demonstrated that EAAs play a direct, and significant functional role in synaptic transmission within the DML. *In vivo* application of the non-NMDA receptor antagonist DNQX within the DML results in a notable alteration in the response properties of pyramidal cells to electrosensory input. Firstly, the transient reduction in firing frequency which normally accompanies the cessation of

an electrosensory stimuli is significantly enhanced immediately following the application of DNQX. This enhanced inhibition is subsequently followed by a gradual increase in the overall excitatory response of the pyramidal cell to EOD modulations. In contrast to the effects of non-NMDA receptor antagonism by DNQX, although pyramidal cells were previously shown to be responsive to application of NMDA in the DML, application of the NMDA receptor antagonist APV in the DML has no discernable effect on pyramidal cell responsiveness to electrosensory input. Based on the diffusional estimates of Bastian (9), it is unlikely that APV ejections in the DML would diffuse to the VML at a high enough concentration to effect NMDA transmission at these synapses.

Effects of EAA Agonists and Antagonists in the VML

Recently glutamate has been immunohistochemically localized in the pre-synaptic terminals of tSF fibers forming synapses on the apical dendrites of pyramidal cells in the VML (126), strongly suggesting an important role for EAAs as neurotransmitters at the VML synapse. However, both the potential spread of applied EAA antagonists across the VML-DML boundary, and the difficulty *in vivo* of independently activating the direct or indirect feedback pathways, have made it difficult to assess in isolation the possible contribution of EAA receptors to synaptic transmission at the VML synapse. Many of these limitations were overcome in the present studies with the use of the true transverse *in vitro* slice preparation of the ELL.

Similar to the results of the above *in vivo* studies in the DML, the present *in vitro* studies demonstrated that pressure ejection of AMPA within the VML, directly dorsal to a recorded cell in the PCL, resulted in a significant (and immediate) increase in the cell's

spontaneous firing rate (ie. figure 12, A). This excitatory response was then followed shortly after by a transient reduction in the cell's spontaneous firing rate. In contrast, when the pressure ejection pipette was initially positioned in the VML lateral to the soma of the recorded pyramidal cell, pressure ejection of AMPA resulted in an initial decrease in the cell's firing rate, which was subsequently followed by a transient increase in the spontaneous firing rate of the cell. These bi-phasic effects of AMPA application (like those seen with changes in the position of the ejection pipette *in vivo*) are presumably mediated in the first case by an initial direct activation of the apical dendrite of the recorded cell, followed by a subsequent diffusion to (and excitation of) the dendrites of adjacent inhibitory interneurons. In contrast, when AMPA is applied lateral to the recorded cell's apical dendrite in the VML, the initial activation of inhibitory interneurons contributing to the pyramidal cell's inhibitory surround results in a transient inhibition of the pyramidal cell's firing rate. This inhibition is then followed by a subsequent diffusion of AMPA to the apical dendrite of the recorded pyramidal cell, resulting in its direct excitation. NMDA applied within the VML directly dorsal to the recording site, was also found to strongly excited pyramidal cells. This dramatic correspondence between *in vivo* and *in vitro* data demonstrating the excitatory actions of AMPA and NMDA, and the presence of inhibitory surrounds within the ELL molecular layer, highlights the experimental utility of the transverse ELL slice preparation and the potential for future convergent lines of investigation using these two experimental preparations.

In addition to being in agreement with previous *in vivo* data suggesting a post-synaptic localization of EAA receptors on pyramidal and inhibitory interneurons, the

present *in vitro* results are also similarly confounded by the potential spread of applied EAA agonists across the subdivisions of the ELL molecular layer. Therefore, the ability to determine the spatial location of the EAA receptors underlying the observed responses is likewise limited. However, utilization of the *in vitro* ELL slice preparation did allow for the selective activation of the tSF pathway (as described above), and the precise placement of pressure ejection pipettes within the VML. The effects of EAA receptor antagonism on transmission at the VML synapse could therefore be *directly* assessed.

In the present studies, the ability of CNQX and CPP to selectively block the excitatory effects of their respective agonists was demonstrated, and was comparable to their demonstrated specificity both in other species (46,97), and similar in effectiveness to DNQX and APV in *in vivo* preparations of the same species (9). This specificity of the NMDA and non-NMDA EAA receptor antagonists therefore allowed for a direct assessment of the effects of selective EAA receptor antagonism on the magnitude, shape, and overall time course of tSF-evoked postsynaptic responses. In this way, a preliminary characterization of the relative contribution of both NMDA and non-NMDA receptors to synaptic transmission at the VML synapse was possible.

Contribution of "fast" NMDA receptors to sensory transmission.

Extracellular field potentials recorded at the level of the VML suggested a complex, multi-phasic postsynaptic response to stimulation of the direct excitatory component of the tSF feedback pathway. Both the bi-phasic form and excitatory nature of tSF-evoked postsynaptic responses were subsequently confirmed with intrasomatic and intradendritic recordings. Intracellular recordings also demonstrated the presence of a

very early depolarizing component of the tSF evoked response, with a latency comparable to that of an antidromically evoked action potential. The early onset of this potential suggests that it is not mediated via chemical synaptic transmission, but rather is due to electrotonic transmission. Consistent with this hypothesis, morphological studies have demonstrated that pyramidal cell dendritic shafts within the VML do receive a small number of gap junctional contacts (70). These putative electronic EPSPs were rarely seen (N=3), but it is not clear whether this is due to the scarcity of gap junctional contacts as reported in Maler et al.(70), or because these potentials were difficult to discern due to the presence of the stimulus artifact. The rarity of these events, however, precluded direct proof of their mediation by gap junctional contacts.

Stimulation of the tSF pathway *in vitro* always resulted in a fast EPSP, with a mean post-stimulus latency to peak of 4.32 msec in dendritic recordings. This latency was significantly shorter than the latency to the peak of somatic EPSPs (6.58 msec), consistent with the closer proximity of the dendritic impalements to the tSF synaptic input. While at first this latency difference for the peaks of somatic and dendritic EPSPs appears unusually long (considering the recording site are separated by only 200 μm), similar latency differences have been estimated based on computer simulations of hippocampal pyramidal cells (13b). In simulations of somatic EPSPs evoked by synaptic input to the soma or half way up the apical dendrite, latencies difference of up to 6 msec were observed purely as a result of the dendritic membrane resistence and capacitance. Since the latency differences observed for somatic and dendritic EPSPs in the present studies are similar, future simulation studies based on known ELL pyramidal cell and

VML feedback properties will be of great benefit in addressing the question of how passive membrane properties shape the integrative characterisitic of pyramidal cells to VML input. Attempts to fit tSF-evoked responses with exponential curves revealed that the peaks of somatic and dendritic EPSPs were typically followed by both a rapid, and a prolonged decay phase with different underlying time courses. Similar multi-phasic EPSPs have been reported to exist at a number of central synapses, and their generation has typically been attributed to the post-synaptic interaction of various receptor-mediated currents possessing distinct kinetics. For example, in the ventrobasal nucleus (vb) of the rat thalamus, responses evoked by stimulation of vibrissa follicle sensory afferents are comprised of two distinct temporal phases, an "early" phase mediated by non-NMDA receptors, and a "late" phase mediated by NMDA receptors (104,105). It is interesting to note that the relative contribution of NMDA and non-NMDA receptor subtypes to the overall form and time course of sensory-evoked vb responses was directly related to the duration of the sensory stimuli itself, suggesting a division of *functional* roles for these two classes of EAA receptors.

Several lines of evidence in the present *in vitro* studies suggest that a significant portion of the early tSF-evoked response, with a latency of under 10 msec, is actually being mediated by "fast" NMDA receptors. Firstly, CPP significantly diminished the amplitude of both the early peak of VML field potentials (often reducing the size of matched PCL field potentials below threshold for the generation of orthodromic "pop-spikes"), as well as the peak amplitude of intracellular recorded tSF-evoked EPSPs. Secondly, upon removal of the intrinsic Mg^{2+}-mediated blockade of NMDA channels by

perfusion of the slice preparations with 0-Mg^{2+} ACSF, the short latency negativity within the tSF-evoked field potential was significantly enhanced. Since this 0-Mg^{2+} enhancement of the VML response was subsequently antagonized by CPP, it is unlikely that this effect was due to non-specific mechanisms, such as a reduction in surface charge screening, and a subsequent increase in presynaptic transmitter release. Finally, intracellular recordings allowed for a direct demonstration of the voltage-dependence of both the early and late components of tSF-evoked EPSPs, a classic criterion for the identification of NMDA receptor-mediated postsynaptic responses. In combination, these three convergent lines of evidence (CPP, Mg^{2+}, and voltage sensitivity) strongly suggest that, in contrast to the "classical" description of its slower kinetics, "fast" NMDA receptor-mediated currents appear to contribute substantially to short-latency transmission at the VML synapse. It is notable that the "fast" NMDA component of the EPSPs occurred at resting membrane potentials, and with single stimulations of the tSF. As such, it appears that activation of these NMDA receptors do not require tetanic stimulation with prominent membrane depolarization (ie < -60 mV). It is therefore very likely that NMDA receptors contribute significantly to regular synaptic transmission within the VML during the processing of electrosensory input.

Careful reassessment of previously published data suggests that the present finding of a "fast" NMDA EPSP component is not as unusual as one might first expect. While sensory-evoked EPSPs in the vb thalamus were qualitatively described by the authors as being comprised of both an "early" non-NMDA and a "late" NMDA component, (thereby maintaining the "classical" kinetic distinction of these receptor subtypes), examination of

their published figures clearly indicates that the duration of the whole excitatory component of the response (including both the "early" and "late" components) is in the range of 10 to 15 msec (105). Similarly, in a study of the role of NMDA and non-NMDA receptors in synaptic transmission within the rat SI barrel cortex (3), or in the rat visual cortex (93), it was concluded that NMDA receptors only contribute to "longer" latency synaptic transmission. The definition of "longer latency" components, however, was arbitrarily defined as being at post-stimulus latencies of between 10-100 msec. In fact, as in the above study, careful examination of their published figures indicate that the majority of sensory-evoked responses for layer-II neurons, (which were blocked by the NMDA receptor antagonist AP5), were actually at post-stimulus latencies of under 20 msec. Therefore, this qualitative and arbitrary classification or description of EPSP components as being either "early" or "late", without explicitly stating their relative post-stimulus latencies, tends only to obscures the fact that (in many cases), NMDA receptors are contributing significantly to many synaptic responses having post-stimulus latencies of under 20 msec.

In addition to the present demonstration of a "fast" NMDA-mediated component in tSF-evoked EPSPs, several recent studies have directly reported the existence of similar "fast" NMDA-mediated currents contributing to short-latency depolarizations and EPSPs at a number of synapses. Intracellularly recorded lateral geniculate EPSPs evoked by stimulation of the retinogeniculate pathway in the ferret demonstrated that NMDA currents contribute significantly to EPSPs at latencies of under 10 msec (35). In addition, *in vitro* analysis of synaptic potentials of layer II/III neurons in the cat's visual cortex

evoked by stimulation of the underlying white matter clearly indicated that the NMDA receptor antagonist APV (2-amino-5-phosphonovalerate) significantly reduced the rising slope of EPSPs in 60% of the cells tested (112). Digital subtraction of the APV-sensitive component from the overall EPSP revealed that this NMDA-mediated component had an onset latency which was roughly equal to that of the non-NMDA component.

Both of the above observations, however, are complicated by the many factors, (such as the multiplicity and distance of the synaptic inputs from the recording site), which makes the characterization of the underlying kinetics of NMDA channel-mediated whole-cell currents difficult. A very elegant solution to this problem was employed by D'Angelo et al (26). Similar to the bi-phasic form of many EPSPs (ie in vb neurons), these authors demonstrated, (using high-resolution whole-cell *in vitro* recording techniques), that synaptic currents generated by the spontaneous quantal release of neurotransmitter from mossy fiber presynaptic terminals onto the proximal dendrites of rat cerebellar granule cells were comprised of both a fast and slow component. However, both components of these currents were found to be mediated exclusively by the activation of NMDA receptors. In light of these recent reports, and the results of the present studies, the traditional view that NMDA receptors only are activated under conditions of high-frequency stimulation (41), or that they possess slower kinetics which relegate them only to temporally slower functional roles such as integration (28) or synaptic plasticity (22), must now be seriously reconsidered.

III. Role of ligand-gated Na^+ currents at the VML synapse.

In the present studies, both non-NMDA and NMDA receptors were shown to contribute to the early phase of the tSF-evoked EPSP. Initially, the pronounced overall voltage-dependence of these EPSPs suggested a substantial contribution of NMDA receptors throughout the complete time course of the evoked responses. However, while CPP consistently reduced the early component of the tSF-evoked response, the late voltage-dependent component was relatively resistant to CPP. In some cases CPP appeared to have no effect on the late decay phase, although in most experiments it caused a small to moderate reduction. In contrast to the effects of CPP, the late decay phase of tSF-evoked EPSPs was consistently antagonized by QX-314, and in most cases complete block was achieved. The voltage-dependence and QX-314 sensitivity of the late decay phase suggests that the majority of this component of tSF-evoked EPSPs is primarily mediated by a voltage-dependent persistent Na^+ current, and to a lesser degree, by a slow NMDA receptor mediated current.

Several lines of evidence have previously demonstrated that persistent Na^+ currents can be mediated by ligand-gated channels, or by the activation of their associated signalling pathways in neurons. For example, cultured buccal (B19) neurons from the snail *Helisoma trivolvis* exhibit a c-AMP-dependent Na^+ current which can be evoked by the application of serotonin, or various substances which increase intracellular c-AMP levels (ie. 8-bromo-CAMP, forskolin, or phosphodiesterase inhibitors) (99). Similar c-AMP-mediated (1), and a vassoactive intestinal polypeptide (VIP) activated inward persistent Na^+ [$Na^+(p)$] current (125) have also been demonstrated in vertebrate neurons,

suggesting an important and widespread role for this type of ligand-gated current in the regulation of neuronal excitability.

In addition to currents evoked by the application of exogenous ligands, synaptically-mediated, voltage-dependent Na^+ currents (similar to those seen in the present study) have been demonstrated to exist at a number of vertebrate central synapses (2,37,44,47,58,100,117). While the prolonged temporal characteristics of $Na^+(p)$ are such that it is well suited to contribute to long-lasting increases in neuronal excitability, its kinetics are such that single EPSPs are often sufficient to activate this current (117). As such, the presence of this type of current might have significant implications on the integrative properties of cells to synaptic input. Such an effect was clearly demonstrated by Deisz et al. (29) in that synaptically-evoked EPSPs in rat neocortical neurons exhibit both a significant voltage-dependent, and paired-pulse enhancement. While these authors directly demonstrated that the voltage-dependent "boosting" of EPSPs was mediated by a QX-314 sensitive persistent Na^+ current, the effects of QX-314 application on paired-pulse facilitation was not directly assessed.

A QX-314-sensitive EPSP late decay phase, similar to the one reported in the present studies, has been previously observed in *in vitro* slice preparations of the visual cortex of the cat (44). Stimulation of white matter underlying the visual cortex evokes EPSPs in layer IV neurons exhibiting a prolonged late decay phase. While application of NMDA antagonists have no effect on this late component of these EPSPs, intracellular application of QX-314 significantly reduces this phase of the EPSPs. However, unlike the present study, these responses were only evoked at the resting membrane potential of

the recorded cells, leaving the possible voltage-dependence of this QX-314 sensitive synaptically-mediated persistent Na^+ current undetermined.

Due to the fact that persistent sodium currents can be activated at membrane potentials close to the resting membrane potentials of neurons (ie. approximately -70 mV) (37), $Na^+(p)$ is well suited to significantly effect neuronal processes such as temporal integration (ie figures 32, 33, and 34) and repetitive firing (47). Previous findings have demonstrated important roles for voltage-dependent Na^+ channels in contributing to both ELL pyramidal cell excitability (71), as well as in the generation of active dendritic conductances which interact with somatic currents to modulate the phasic or "bursting" firing behaviour of pyramidal cells (123). The existence of such active ionic conductances in dendrites has the potential to significantly influence neuronal processes of synaptic integration and information processing in the nervous system (111,116,121,123). Therefore, the present demonstration of synaptically-mediated voltage-dependent currents within the tSF feedback pathway offers a unique opportunity to investigate the role of such conductances in sensory processing.

The nature and localization of the Na^+ channels contributing to the late phase of the tSF-evoked EPSP is still unclear. Both Mathieson and Maler (71), and Turner et al (123) demonstrated the presence of a persistent sodium current in ELL pyramidal cells. In addition, immunocytochemistry has demonstrated that Na^+ channels are present on the somata and proximal apical dendrites of ELL pyramidal cells (123). This same study reported that persistent Na^+ currents were more prominent in somatic, rather than apical dendritic recordings, with Na^+ channels in the apical dendrites producing current-evoked

action potentials. Therefore, it is not certain (in the present studies) where the slow Na^+ current contributing to the late decay phase of the tSF-evoked EPSP originates. The fact that the late decay phase was more prominent, and more readily modulated by changes in membrane potential in dendritic recordings, however, suggests that this phase of the tSF-evoked EPSP might originate in the apical dendrite near the site of the VML synaptic input. This conclusion is apparently contradictory to the earlier findings of Turner et al. (123) which suggested a somatic location for persistent Na^+ currents. Further work will therefore be required to resolve this question.

It is also not certain whether the persistent Na^+ current which contributes to the late decay phase is activated simply by depolarization, or whether it also requires glutaminergic transmission. However, injection of depolarizing current into pyramidal cell somata does not induce depolarizations which outlasts the current injection (71, Turner et al, personal observation), suggesting that ligand binding is a prerequisite for the activation of this late Na^+-dependent current. A further possibility is, however, that somatic current ejection does not adequately mimic the current density obtained in the apical dendrites by synaptic activation.

While synaptic activation of slow voltage-sensitive dendritic currents has been observed in a number of cell types (see above), the linkage between ligand binding and these currents is often difficult to elucidated. For example, the expression of this late decay phase of tSF-mediated EPSPs might be due to the unmasking of a $Na^+(p)$ current which is normally offset by standing outward currents (such as K^+), or it might be mediated by a process such as a switch between Na^+ channel gating modes (2). Given

the present findings, and the experimental utility of the ELL slice preparation, the tSF synaptic input in the VML might prove to be a very useful system in which to address this complex and important question.

The *in vivo* role of the tSF-evoked EPSP's late phase (both Na^+ and NMDA components) is also unclear. Anatomical studies (66,67) suggest that, when Pd stellate cells are activated, they will in turn activate Pd bipolar cells which project densely onto the somata of pyramidal cells through the direct inhibitory feedback pathway. As illustrated in figure 30, activation of this inhibitory pathway results in a large IPSP with a time course similar to that of the late decay phase of the tSF-evoked EPSP. It is therefore possible that, when the direct excitatory feedback system is activated *in vivo*, the late decay phase of the EPSP is shunted out by powerful concurrent inhibition mediated by the direct inhibitory pathway. In contrast to the abundant presence of inhibitory inputs onto the somata of ELL pyramidal cells, inhibitory boutons are relatively sparse on the apical dendritic tree (67). It is therefore possible that, even in the presence of somatic inhibition, the prolonged phase of the tSF-evoked EPSP might act to depolarize the apical dendritic tree, and therefore might only be directly affecting dendritic processing of subsequence feedback input (ie in the VML and DML). However, if the direct excitatory feedback pathway (tSF) could be selectively activated during specific forms of sensori-motor activity, it would allow for the regulated expression of the powerful and long-acting late phase of the EPSP at the level of the somata, effectively summating with and augmenting electrosensory afferent input. Further *in vivo* studies of this direct Pd-ELL (bipolar cell) inhibitory feedback projection are clearly needed to

answer these questions.

IV. Summary of currents contributing to transmission at the VML synapse

EPSPs evoked by tSF stimulation therefore consist of at least one voltage-independent (non-NMDA), and two voltage-dependent (NMDA and $Na^+(p)$) currents which interact to produce complex post-synaptic responses to synaptic input. In addition, a small gap junction-mediated component of this complex EPSP may also be present. Figure 36 serves to illustrate these various EPSP components, and their relative contribution (at various membrane potentials) to the form and time course of tSF-evoked EPSPs. At the resting membrane potential of the cell (figure 36, 2), stimulation of the tSF evokes a response mediated by non-NMDA EAA receptors, which subsequently depolarizes the postsynaptic membrane to the point where Mg^{2+}-mediated blockade of NMDA channels is sufficiently removed for the "fast" NMDA-mediated currents to contribute to the evoked response. In addition, at the resting membrane potential there also exists a moderate contribution of the voltage-dependent $Na^+(p)$ current to the evoked response.

Due to their inherent voltage-dependence, at hyperpolarized membrane potentials (figure 36, 3), both the "fast" (and possible slow) NMDA, as well as the $Na^+(p)$ currents contribute very little to the form or magnitude of the evoked responses. In contrast, depolarization of the postsynaptic membrane (figure 36, 1) increases both the voltage-dependent NMDA and $Na^+(p)$ currents, resulting in a significant enhancement of both the early and late components of the EPSPs. In this way, variations in membrane potential can significantly modify the time course of tSF-mediated EPSPs, and therefore the

Figure 36. Summary illustration depicting the various components of the tSF-evoked EPSPs. **1:** Upon post-synaptic depolarization, tSF-evoked responses are comprised of a significantly enhanced voltage-dependent fast NMDA (and variable slow NMDA component), as well as a prolonged slow Na^+ conductance which significantly alter the temporal integrative properties of the post-synaptic membrane. **2:** At rest, stimulation of the tSF feedback pathway results in EPSPs comprised of a significant non-NMDA-mediated fast component (dark shading) which depolarizes the membrane potential to the point where (A) the voltage-dependent blockade of NMDA channels is partially removed allowing for a contribution by NMDA channels (light shading), as well as (B) partial activation of a voltage-dependent persistent Na^+ conductance (clear). **3:** Upon hyperpolarization, the vast majority of the response is mediated by fast non-NMDA receptors. Note:the small and variable putative gap junction-mediated component occasionally seen at this synapse is not illustrated: ▲=stimulus artifact.

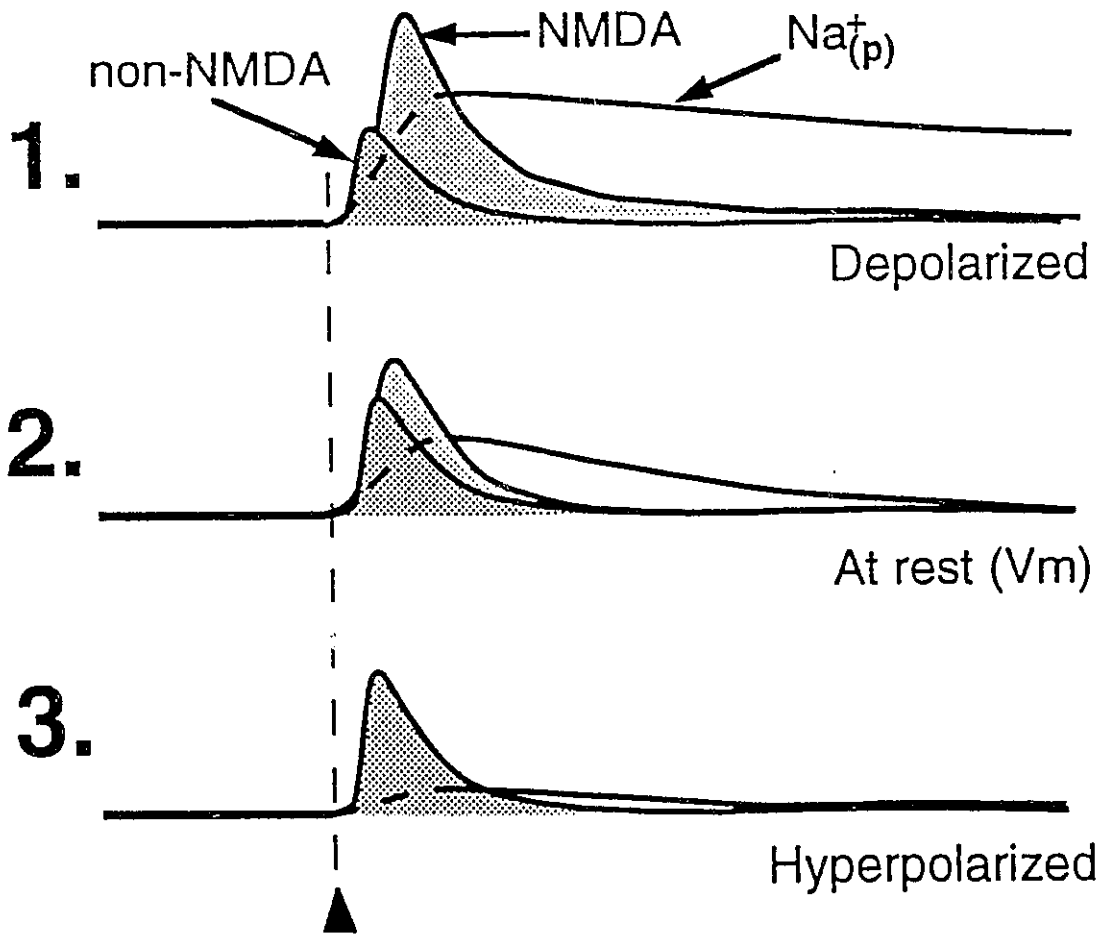
NMDA
$Na^{+}_{(p)}$
non-NMDA
1.
Depolarized
2.
At rest (Vm)
3.
Hyperpolarized

integrative properties of the postsynaptic cells to both descending and ascending electrosensory input.

It is not yet certain whether ionotropic EAA receptors and voltage-gated Na^+ channels can completely account for the tSF-evoked EPSP. Kynurenic acid failed to completely block this EPSP; an effect that may either be due to the low potency of this drug, or to the presence of additional EAA receptors (metabotropic?) at the VML synapse.

V. Potential roles of the VML synapse in electrosensory processing

Functional consequences of tSF feedback system organization

Several lines of evidence suggest that Pd stellate cells are specifically involved in the electrosensory task of detecting moving objects. Lannoo and Lannoo (56) have reported that, when hunting for food, *Apteronotus leptorhynchus* initiates a behaviour which scans its environment with rostro-caudal movements of 10-15 cm/s. Bastian (10) has shown that, at this velocity, objects will generate EOD amplitude modulations (AMs) of under 10 Hz. Higher frequencies of AMs (ie 50-100 Hz) can be generated by certain intraspecific electrical communication signals, such as "chirps" (128), or by beat frequencies produced by the interaction of the fish's EOD with that of a conspecific (e.g. if the two fish have respective frequencies of 700 and 800 Hz, a beat frequency of 100 Hz will be generated).

In support of their presumed role, Bratton and Bastian demonstrated that Pd stellate cells functionally act as low-pass temporal filters tuned to frequencies of approximately 5 Hz, with AMs of frequencies greater than 16 Hz being actively inhibited (15). In addition, Pd stellate cells are as sensitive as ELL pyramidal cells to the detection

of moving objects at various distances from the body, and in fact demonstrate a higher gain to electrosensory input than do ELL pyramidal cells. Furthermore, Pd stellate cells adapt very rapidly to electrosensory input, a response property suggesting that they are only transiently activated during behaviours such as the active scanning movements made by the fish itself. Thus, as already pointed out by Bratton and Bastian, Pd stellate cells are functionally well suited to reject signals caused by conspecifics, and respond preferentially to low frequency AMs such as those generated by moving objects.

Results from the present studies concerning the conduction velocity of tSF fibers, as well as on the dynamic properties of the VML synapse, are both supportive of the above arguments suggesting a role for Pd stellate cells (and their tSF projections) in the detection of moving objects. Bratton and Bastian (15) have previously noted that Pd stellate cells respond with a relatively long latency (in comparison to ELL pyramidal cells and Pd multipolar cells) to modulations of EOD amplitude. While Pd stellate cells respond to step changes in EOD amplitude with a mean latency of 8.2 or 13.8 msec ("E" vs "I" stellate cells; mean latency= 11 msec), ELL pyramidal cells respond with latencies of 3.6 and 6.8 msec (mean= 5.2 msec) respectively. In contrast, Pd multipolar cells (which project to the EGp) respond with a mean latency of 5.7 msec. Therefore, the relatively long delay in the response of Pd stellate cells following activation of ELL pyramidal cells (mean delay= 5.8 msec) is greater than that which would be expected based purely on the conduction velocity of the lateral lemniscal fibers. Bastian and Courtright (12) proposed that this delay is due to the thin calibre of the lateral lemniscal fiber collaterals which project to the Pd stellate cells (multipolar cells receive input from

different ELL pyramidal cells, deep basilar pyramidal cells, which have thicker axons).

Stratum fibrosum fibers are much thinner in diameter than those of the lateral lemniscus (70), and in the present study it was estimated that they have a mean conduction velocity of 0.31 m/s. Using the atlas of the *Apteronotus* brain (68), I have estimated that the tSF pathway (*in vivo*) is approximately 3500 µm in length (from mid Pd to mid ELL). Therefore, based on the present data it can be calculated that there will be an estimated delay of 11.3 msec for activity to be conducted along the tSF pathway, with conduction and synaptic delays in the ELL contributing a further 7 msec delay. This implies that, as an object increases input to a given pyramidal cell, there will be a total delay of approximately 29.3 msec (11+11.3+7) before any Pd stellate cell feedback can reach that pyramidal cell. Such a delay would, it appears, constrain the functional roles which might be attributed to this sensory feedback pathway.

Using moving objects, Bastian has mapped the receptive fields of both ELL pyramidal cells, as well as Pd stellate cells (10). ELL pyramidal cells have receptive field centres which are approximately circular in shape (Bastian, personal communication), and the area bounded by a contour at which the pyramidal cell's response is 50% of its peak response to moving objects (its 50% response contour), is approximately 96 mm^2. In comparison, the average (50% contour) receptive field area of Pd stellate cells is 255 mm^2. As a Pd stellate cell's activation is determined by pyramidal cell input, this greater size of the Pd stellate cell's receptive field can presumably be attributed to a convergence of ELL pyramidal cell inputs through numerous lateral lemniscal fibers within the Pd. As such, while the estimated diameter of pyramidal cell receptive fields has been

calculated as being 11 mm, those of Pd stellate cells are approximately 18 mm in diameter.

Since pyramidal and Pd stellate cells are both topographically organized and reciprocally connected (69,106), pyramidal cells will receive input from Pd stellate cells with receptive fields concentric and surrounding their own (see figure 37, A). This concentric organization of receptive fields also implies that a given Pd stellate cell's receptive field will extend approximately 3.5 mm beyond that of its concentrically matched pyramidal cell's receptive field. This "extra" 3.5 mm overlap of the stellate cell's receptive field will therefore be driven by adjacent pyramidal cells with partially overlapping receptive fields. I assume that an object will excite a stellate cell when it lies over at least the edge of its receptive field, that is, when it is at least over 1 mm of the 3.5 mm "overhang" area. As such, when a moving object reaches the perimeter of a Pd stellate cell's receptive field (ie figure 37 A, & 1), the change in electroreceptor activity will take approximately 29.3 msec to feedback to the reciprocally connected pyramidal cells (figure 37, 3). If actively scanning its environment at a velocity of 10-15 cm/s (56), a fish will have traversed 2.5 mm within 17-25 msec, and within this period of time the object will have entered the receptive field of the next pyramidal cell. This cell will then activate with a mean delay of 5.2 msec. It can therefore be concluded that, because of the spatial organization of pyramidal and Pd stellate cell receptive fields, and the delays inherent in their input and output fiber pathways, moving objects will tend to excite ELL pyramidal cells simultaneously via primary afferent input and direct feedback projections from Pd stellate cells (figure 37, 3 vs 4).

Figure 37. Predicted functional consequences of receptive field size and conduction delays within the tSF feedback pathway. **A:** Partial overlap of pyramidal cell receptive fields (a & b) contribute to the formation of a larger Pd stellate cell receptive field (c). Conduction delays in the ascending (LL) and descending (tSF) pathways (black arrows), in combination with the partial spatial overlap (3.5 mm) of a Pd stellate cell's receptive field (c) with that of its concentrically matched pyramidal cell (b:shaded receptive field), combine to ensure temporal and spatial convergence of both primary afferent and tSF input. **B:** Graphic illustration of the temporal convergence of tSF and primary afferent input.

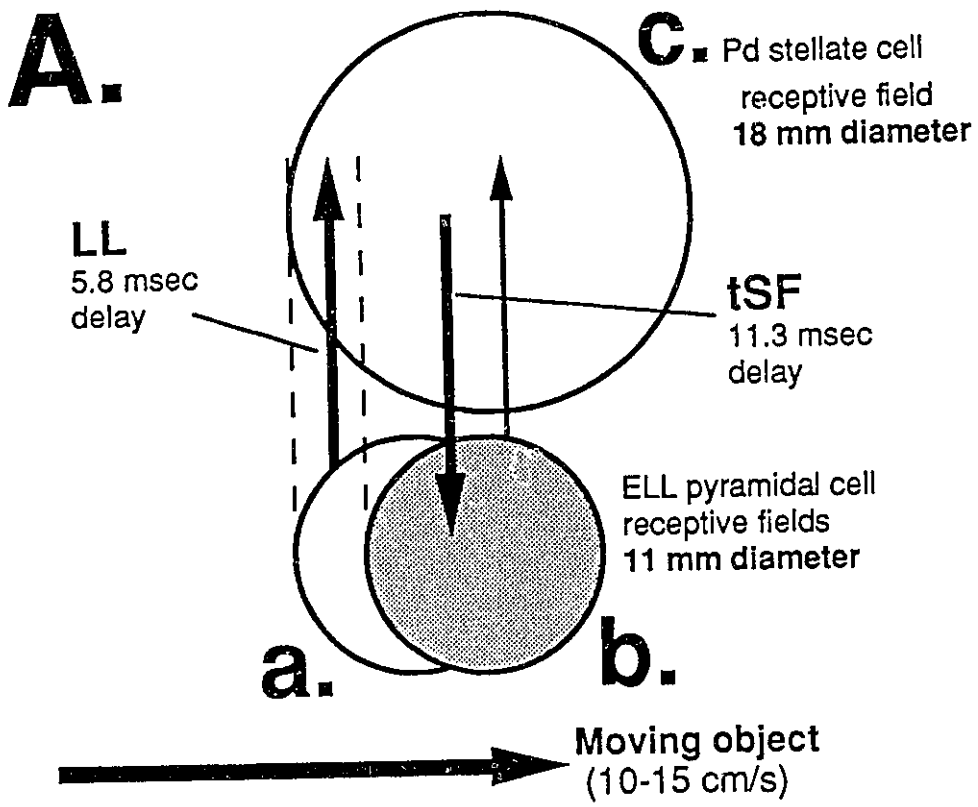
A.
C. Pd stellate cell
receptive field
18 mm diameter
LL
5.8 msec
delay
tSF
11.3 msec
delay
ELL pyramidal cell
receptive fields
11 mm diameter
a.
b.
Moving object
(10-15 cm/s)

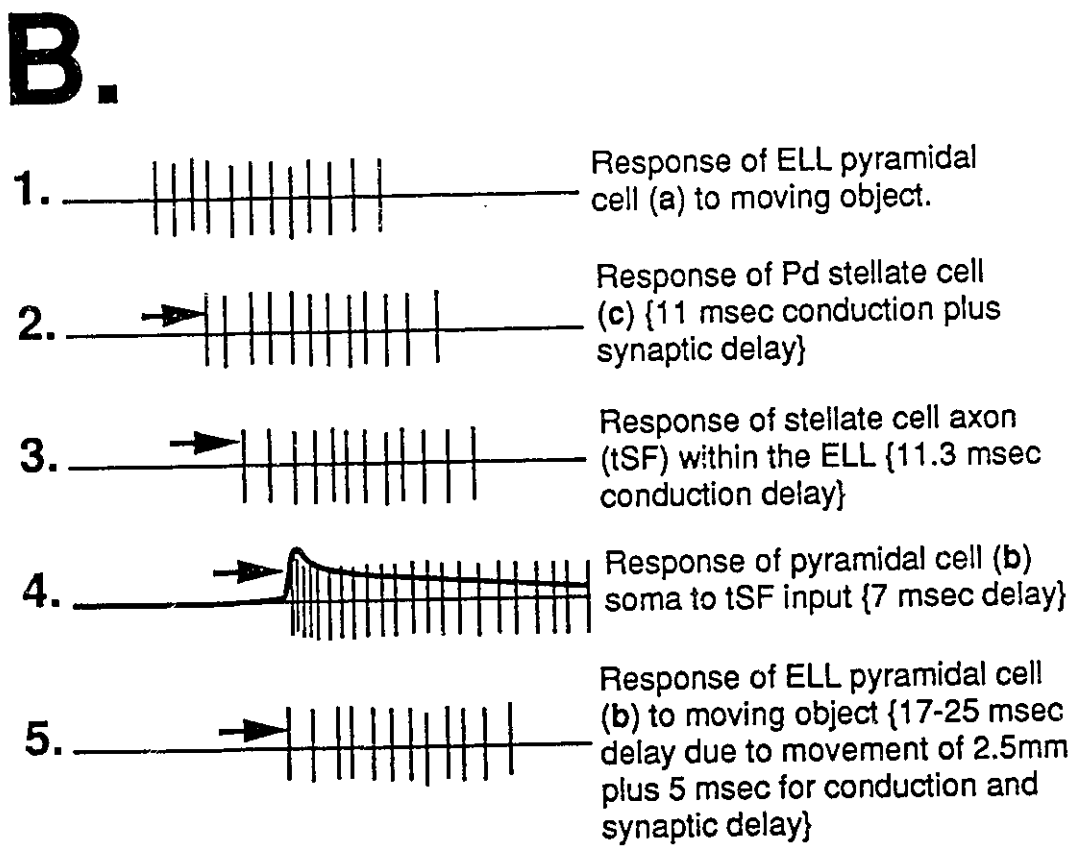
B.
1.
Response of ELL pyramidal cell (a) to moving object.
2.
Response of Pd stellate cell (c) {11 msec conduction plus synaptic delay}
3.
Response of stellate cell axon (tSF) within the ELL {11.3 msec conduction delay}
4.
Response of pyramidal cell (b) soma to tSF input {7 msec delay}
5.
Response of ELL pyramidal cell (b) to moving object {17-25 msec delay due to movement of 2.5mm plus 5 msec for conduction and synaptic delay}

Since Pd stellate cells respond in a very phasic manner to electrosensory input (with an average time constant of adaptation of about 20 msec), a stellate cell will tend to only give a strong response to electrosensory input for approximately 50 msec. During this period of time an object will traverse approximately 5-7.5 mm (given a scan rate of 10-15 cm/s). As a result, an object will have moved to, or just beyond the edge of the pyramidal cell's receptive field (11 mm), and therefore presumably into the perimeter of an adjacent pyramidal cell's receptive field. Thus, both the temporal characteristics of a Pd stellate cell's response onset and offset are optimized so that they exactly overlap the response properties of its reciprocally connected pyramidal cell to primary afferent input.

Functional consequences of the non-linear response characteristics of the VML synapse

The dynamic properties of the VML synapse also appear to be optimized to ensure a powerful effect of this feedback projection on an ELL pyramidal cell's response to moving objects. When primary afferent input depolarizes a pyramidal cell, concurrent tSF-mediated EPSPs will be maximized due to the strong voltage-dependence of both their early NMDA component, as well as their late voltage-sensitive $Na^+(p)$ component. As a consequence, given the high frequency at which Pd stellate cells fire (15), and the strong frequency potentiation of EPSPs demonstrated at the VML synapse (ie see figure 33), maximal EPSPs possessing large slow $Na^+(p)$ and NMDA currents will likely result as an object traverses the centre of the pyramidal cell's receptive field. Thus, the VML synapse appears to be well suited to profoundly effect the activity of ELL pyramidal cells, through modulating their responsiveness to primary afferent and subsequent feedback

input.

The topographic reciprocal excitatory connections between ELL pyramidal cells and Pd stellate cells, together with the response characteristics of stellate cells to AMs and moving objects (see above), led Bratton and Bastian to suggest that the positive feedback of the Pd stellate cell to the ELL might act as an attentional "searchlight" mechanism to enhance the response of pyramidal cells to "important" electrosensory input. These authors pointed out that such a "searchlight" mechanism was similar to that proposed by Crick (25) for the cortical-thalamic projections. Crick listed three properties which he considered essential for the operation of such a feedback "searchlight" mechanism; (1) reciprocal topographic excitatory connections; (2) parallel inhibitory feedback connections which are diffusely organized (non-topographic) and can therefore reduce excitation in regions mediating the detection of sensory input not of immediate interest (the GABAergic thalamic reticular nucleus in mammals was proposed as a substrate for this inhibition), and (3) a non-linearity in the topographic excitatory feedback projection resulting in a "thresholding" behaviour which increases the contrast between excited and inhibited neurons. Crick proposed a hyperpolarization activated Ca^{2+} current in thalamic relay neurons as the biophysical substrate of such a non-linearity.

Both the anatomical and functional organization of the ELL appears to satisfy many of the above requirements. Maler and Mugnaini (66,67) have recently described a parallel inhibitory feedback pathway from Pd bipolar cells (GABAergic) to ELL pyramidal cells. The diffuse organization of this direct inhibitory projection led these authors to suggest that Pd bipolar cells might be functionally equivalent to thalamic

reticular neurons, and therefore might produce the background inhibition which is an essential component for the operation of an attentional "searchlight" mechanism as proposed by Crick.

On the basis of the present data demonstrating the voltage-sensitive NMDA and $Na^+(p)$ components of tSF-mediated EPSPs, I propose that the VML synapse might provide the necessary non-linear component required to perform "thresholding" operations within the context of such a "searchlight" mechanism. Because of these voltage sensitive conductances, tSF activation would only tend to produce substantial EPSPs in ELL pyramidal cells which have already been depolarized by appropriate direct electrosensory input, or by indirect feedback from the EGp (ie DML input). In these cells, the added excitation from the now functional voltage-dependent tSF feedback projections might greatly enhance their response to primary afferent input, thereby acting functionally as an attentional "searchlight". As described above, both the spatial and temporal matching of stellate cell and pyramidal cell activity would tend to make this attentional "searchlight" mechanism very focused, since the activation of topographical excitatory and diffuse inhibitory connections would result in an enhanced responsiveness of a spatially restricted subset of pyramidal cells (corresponding to a spatially restricted position in electrosensory space), to primary afferent input.

While it is relatively easy to conceptualize how the tSF feedback pathway might function to enhance the responsiveness of ELL pyramidal cells to primary afferent input, it is important to note that there are conditions under which this feedback projection system would be rendered functionally ineffective. Such would be the case if there were

a significant spatial or temporal mismatches within the Pd-ELL feedback loop. For example, a Pd stellate cell might continue to discharge after the electrosensory input to its reciprocally connected pyramidal cell has ceased (as in the case of higher velocity scan rates). In this case, without primary afferent input the pyramidal cell will tend to be hyperpolarized by input from the diffuse Pd bipolar cell inhibitory feedback projections (as well as local ELL interneurons related to surround inhibition; 66,67). Because of their inherent voltage-dependence, any VML synaptic connections between Pd stellate cells and these hyperpolarized pyramidal cells will therefore be ineffective at contributing to their further excitation.

The demonstrated voltage-dependence of VML synapses might also play an important role in contributing to the functional specificity of the tSF feedback pathway itself. As previously mentioned, there are two major morphological classes of ELL pyramidal cells: basilar and non-basilar pyramidal cells (63,70). Physiologically, basilar pyramidal cells correspond to "E" type cells which are excited by increases in EOD amplitude. In contrast, non-basilar pyramidal cells correspond functionally to "I" type cells which are inhibited by increases in EOD amplitude, and are conversely excited by decreases in EOD amplitude (108). Similarly, Pd stellate cells are also classified on the basis of their electrophysiological response to changes in electrosensory input as being either an "E" or "I"-type stellate cell (15). However, it is not presently known whether the descending Pd stellate cell projections to ELL pyramidal cells (the tSF) maintains this strict functional specificity; that is whether an "E"-type stellate cell makes exclusive synaptic connections with only "E" type pyramidal cells, or "I"-type stellate cells project

only to "I"-type pyramidal cells within the ELL.

Shumway and Maler (115) have shown that when the GABAergic antagonist bicuculline is applied to the ELL pyramidal cell layer *in vivo*, the strict functional specificity of "E" and "I"-type pyramidal cells appears to break down. These authors have therefore suggested that functionally non-specific synapses between Pd stellate cells and ELL pyramidal cells might be responsible for this effect. If this is the case, the functional specificity of tSF projections might normally be maintained by the inherent voltage-dependence of the VML synapses, elegantly balanced by a background of diffuse inhibitory input. For example, if an increase in EOD amplitude caused an "E"-type pyramidal cell to discharge, its reciprocally connected "E"-type stellate cell in the Pd would also fire, and therefore its descending tSF projections would effectively stimulate the depolarized "E"-type pyramidal cell through its voltage-dependent synaptic connections. Conversely, if the EOD amplitude was decreased, the "E"-type pyramidal cell would become hyperpolarized and nearby "I"-type pyramidal cells would be excited. In this case, projections from "I"-type stellate cells in the Pd would be activated, and even if these "I"-type stellate cells were to form synapses on the apical dendrites of "E"-type pyramidal cells in the ELL, these VML synapses would be functionally ineffective since the hyperpolarized state of the "E"-type pyramidal cells would not permit the expression of the voltage-sensitive components of the tSF-mediated EPSPs. Such a mechanism might be of great value if it were not possible to developmentally specify the precise anatomical, and functionally appropriate connections within the tSF projections. In this case, the voltage-dependence of the VML synapses might permit adequate functional

specificity of their synaptic connections despite the absence of precise anatomical specificity.

Potential for the modulation of the Pd-ELL feedback projections.

There are several sites at which the effectiveness of the putative tSF "searchlight" mechanism might be functionally modified. In addition to the direct projections to the Pd, pyramidal cells of the ELL also project to the midbrain *torus semicircularis* (TS), which in turn is responsible for further electrosensory projections to structures mediating diverse functions such as motor control (optic tectum), or electrocommunication (nucleus electrosensorius). In addition, the TS also contributes a major feedback projection back to the Pd. In light of the delayed response of Pd stellate cells to electrosensory input, this TS feedback might be able to interact directly with the ELL input at the level of the Pd, thereby further shaping the response of Pd stellate cells to electrosensory input (15). Based on this anatomical relation, Maler and Mugnaini (66) proposed that "novelty" detecting neurons in the TS may be involved in choosing the electrosensory input on which the "searchlight" mechanism is to be focused.

Inhibition is also likely to play an important role in modulating the response of Pd stellate cells to ascending electrosensory input, since Maler and Mugnaini (67) have shown these cells to be surrounded by GABAergic boutons. Future studies aimed at determining the origin and functional consequences of these inhibitory connections will be essential before a clear understanding of the role of descending Pd projections can be obtained. In addition, other sites at which the putative "searchlight" mechanism might be modulated include at the level of the Pd bipolar cells, at the VML synapse itself, or

at the inhibitory synapses of the bipolar cells within the PCL of the ELL. Further studies investigation the potential of these synapses (or interacting systems) to demonstrate long-term plasticity will be essential to fully understand what functional contributions the direct excitatory and inhibitory feedback pathways might make to electrosensory processing.

SUMMARY AND CONCLUSIONS

This discussion has emphasized the early components of the tSF-evoked EPSP, in which "fast" NMDA currents appear to make a significant contribution to synaptic transmission. The late decay phase of these EPSPs is also substantial, and can last for greater than 100 msec. In this time a fish would typically traverse 1 cm (at 10 cm/s) during active scanning behaviour. Therefore, temporal summation of the late phase of tSF-mediated EPSPs could contribute to a significant enhancement in the response of an ELL pyramidal cell to objects moving along the fish's body, an enhancement which would tend to amplify input over great distances. As discussed above, it is not certain whether the late phase of the tSF-evoked EPSP contributes significantly to somatic depolarization, or is shunted out by simultaneous IPSPs from Pd bipolar cells. This question of interplay between excitatory and inhibitory inputs is of key importance in elucidating the functional role of the entire (ie. excitatory plus inhibitory) direct Pd feedback projection systems to the ELL.

While generalizations to *in vivo* conditions must be made with caution (101), the present studies served to demonstrated both the experimental utility of the ELL slice preparation for characterizing EAA synapses, and highlight the potential for future convergent *in vivo* and *in vitro* lines of enquiry into the functional organization and role

of descending projections in the modulation of electrosensory processing within the ELL. Given the ubiquity of feedback projections and EAA transmission in vertebrate sensory systems, this preparation may contribute more generally to the understanding of the role of feedback projections in sensory processing.

References

1. Adachi, S., Oka, J-I., Nagao, T. and Fukuda, H. (1992): Cyclic AMP analog activates Na^+-dependent inward currents in dissociated frog motoneurons. Brain Res. 573:349-352.

2. Alzheimer, C., Schwindt, P.C. and Crill, W.E. (1993): Modal Gating of Na^+ Channels as a Mechanism of Persistent Na^+ Current in Pyramidal Neurons from Rat and Cat Sensorimotot Cortex. J. Neurosci. 13:660-673.

3. Armstrong-James, M., Welker, E., and Callahan, C.A. (1993): The contribution of NMDA and non-NMDA receptors to fast and slow transmission of sensory information in the rat S1 barrel cortex. J. Neurosci. 13:2149-2160.

4. Artola, A., and Singer, W. (1987): Long-term potentiation and NMDA receptors in rat visual cortex. Nature 330:649-652.

5. Artola, A., Brocher, S., and Singer, W. (1990): Different voltage-dependent thresholds for inducing long-term depression and long-term potentiation in slices of rat visual cortex. Nature 347:69-72.

6. Barbaresi, P., Fabri, M., Conti, F. and Manzoni, T. (1987): D-[^{3}H] Aspartate retrograde labelling of callosal and association neurons of somatosensory areas I and II of Cats. J. Comp. Neurol. 263:159-178.

7. Bastian, J. (1986a): Gain control in the electrosensory system mediated by descending inputs to the electrosensory lateral line lobe. J. Neurosci. 6:553-562.

8. Bastian, J. (1986b): Gain control in the electrosensory system: a role for the descending projections to the electrosensory lateral line lobe. J. Comp. Physiol. A. 158:505-515.

9. Bastian, J. (1993): The role of amino acid neurotransmitters in the descending control of electroreception. J. Comp. Physiol. A. 172:409-423.

10. Bastian, J. (1981): Electroreception II: The effects of moving objects and other electrical stimulation on the activity of two categories of posterior lateral line cells in *Apteronotus albifrons*. J. Comp. Physiol. 144:481-499.

11. Bastian, J. and Bratton, B. (1990): Descending control of electroreception. I. Properties of nucleus praeeminentialis neurons projecting indirectly to the electrosensory lateral line lobe. J. Neurosci. 10:1226-1240.

12. Bastian, J. and Courtright, J. (1991): Morphological correlates of pyramidal cell adaptation rate in the electrosensory lateral line lobe of weakly electric fish. J. Comp. Physiol. A 168:393-407.

13a. Benveniste, M. and Mayer, M.L. (1991): Kinetic analysis of Agonist Action at N-Methyl-D-Aspartate Receptors: Two Binding Sites Each for Glutamate and Glycine. Biophys. J. 59:560-573.

13b. Bernander, O., Douglas, R.J., Martin, K.A.C. and Koch, C. (1991): Synaptic background activity influences spatiotemporal integration in single pyramidal cells. Proc. Natl. Acad. Sci. U.S.A. 88:1156-1153.

14. Bode-Greuel, K.M., Singer, W. and Aldenhoff, J.B. (1987): A current source density analysis of field potentials evoked in slices of visual cortex. Exp. Brain Res. 69:213-219.

15. Bratton, B., and Bastian, J. (1990): Descending control of electroreception II: Properties of nucleus praeminentialis neurons projecting directly to the electrosensory lateral line lobe. J. Neurosci. 10:1241-1253.

16. Burnashev, N., Moyer, H., Seeburg, P.H. and Sakmann, B. (1992): Divalent ion permeability of AMPA receptor channels is dominated by the edited form of a single subunit. Neuron 8:189-198.

17. Burnashev, N., Schoepfer, R., Monyer, H., Ruppersberg, J.P., Gunther, W., Seeburg, P.H. and Sakmann, B. (1992): Control by asparagine residues of calcium permeability and magnesium blockade in the NMDA receptor. Science 257:1415-1419.

18. Carmignoti, G., and Vicini, S. (1992): Activity-dependent decrease in NMDA receptor responses during development of the visual cortex. Science 258:1007-1011.

19. Charpak, S., Gahwiler, B.H., KQ, D. and Knopfel, T. (1990): Potassium conductances in hippocampal neurons blocked by excitatory amino-acid transmitters. Nature 347:765-767.

20. Christine, C.W. and Choi, D.W. (1990): Effect of Zinc on NMDA Receptor-Mediated Channel Currents in Cortical Neurons. J. Neurosci. 10:108-116.

21. Collingridge, G.L., Kehl, S.J. and McLennan, H. (1983): Excitatory Amino Acids in Synaptic Transmission in the Schaffer-Collateral Commissural Pathway of the Rat Hippocampus. J. Physiol. (Lond) 334:33-46.

22. Collingridge, G.L., and Bliss, T.V.P. (1987): NMDA receptors: their role in long-term potentiation. Trends in Neurosci. 10:288-293.

23. Connors, B.W. and Prince D.A. (1981): Effects of Local Anesthetic QX-314 on the Membrane Properties of Hippocampal Pyramidal Neurons. J. Pharmacol. Exp. Ther. 220:476-481.

24. Conti, F., Fabri, M. and Manzoni, T. (1988): Glutamate-positive corticocortical neurons in the somatosensory areas I and II of cats. J. Neurochem. 12:339-342.

25. Crick, F. (1984): Function of the thalamic reticular complex: the searchlight hypothesis. Proc. Natl. Acad. Sci. 81:4586-4590.

26. D'Angelo, E., Rossi, P., and Garthwaite, J. (1990): Dual-component NMDA receptor currents at a single central synapse. Nature 346:467-470.

27. Davies, J., Miller, A.J. and Sheardown, M.J. (1986): amino acid receptor mediated excitatory synaptic transmission in the cat red nucleus. J. Physiol. 376:13-29.

28. Daw, N., Stein, P.S.G., and Fox, K. (1993): The role of NMDA receptors in information processing. Ann. Rev. Neurosci. 16:207-222.

29. Deisz, R.A., Fortin, G. and Zieglgansberger, W. (1991): Voltage Dependence of Excitatory Postsynaptic Potentials of Rat Neocortical Neurons. J. Neurophysiol. 65:371-382.

30. Deschenes, M. and Hu, B. (1990): Electrophysiology and pharmacology of the corticothalamic input in to lateral thalamic nuclei: An intracellular study in the cat. Eur. J. Neurosci. 2:140-152.

31. Dingledine, R. (1991): New wave of non-NMDA excitatory amino acid receptors. TIPS 12:360-362.

32. Dori, I., Petrou, M. and Parnavelas, J.G. (1989): Excitatory transmitter amino acid-containing neurons in the rat visual cortex: A light and electron microscopic immunocytochemical study. J. Comp. Neurol. 290:169-184.

33. Dudek, S. and Bear, M. (1992): Homosynaptic long-term depression in area CA1 of the hippocampus and effects of N-methyl-D-aspartate receptor blockade. PNAS 89:4363-4367.

34. Durand, G., Gregor, P., Zheng, X., Bennett, M.V.L., Uhl, G., and Zukin, R.S. (1992): Cloning of an apparent splice variant of the rat N-methyl-D-aspartate receptor NMDAR1 with altered sensitivity to polyamines and activators of protein kinase C. Proc. Natl. Acad. Sci. 89:9359-9363.

35. Esguerra, M., Kwon, Y.H., and Sur, M. (1992): Retinogeniculate EPSPs recorded intracellularly in the ferret lateral geniculate nucleus *in vitro*: Role of NMDA receptors. Vis. Neurosci. 8:545-555.

36. Fleck, M.W., Henze, D.A., Barrionuevo, G. and Palmer, A.M. (1993): Aspartate and Glutamate Mediate Excitatory Synaptic Transmission in Area CA1 of the Hippocampus. J. Neurosci. 13:3944-3955.

37. French, C.R., Sah, P., Buckett, K.J. and Gage, P.W. (1990): A Voltage-dependent Persistent Sodium Current in Mammalian Hippocampal Neurons. J. Gen. Physiol. 95:1139-1157.

38. Gasic, G.P and Heinemann, S. (1991): Receptors coupled to ionic channels: the glutamate receptor family. Curr. Opin. Neurobiol. 1:20-26.

39. Heggelund, P. and Harveit, E. (1990): Neurotransmitter receptors mediating excitatory input to cells in the cat lateral geniculate nucleus. 1. Lagged cells. J. Neurophysiol. 63:1347-1360.

40. Herb, A., Burnashev, N., Werner, P., Sakmann, B., Wisden, W. and Seeburg, P.H. (1992): The KA-2 subunit of excitatory amino acid receptors shows widespread expression in the brain and forms ion channels with distantly related subunits. Neuron 8:775-85.

41. Herron, C., Lester, R., Coan, E. and Collingridge, G. (1986): Frequency-dependent involvement of NMDA receptors in the hippocampus: a novel synaptic mechanism. Nature 322:265-268.

42. Hestrin, S. (1992): Developmental regulation of NMDA receptor-mediated synaptic currents at a central synapse. Nature 357:686-689.

43. Hickmott, P.W. and Constantine-Paton, M. (1993): The Contribution of NMDA, Non-NMDA, and GABA Receptors to Postsynaptic Responses in Neurons of the Optic Tectum. J. Neurosci. 13:4339-4363.

44. Hirsch, J. and Gilbert, C. (1991): Synaptic physiology of horizontal connections in the cat's visual cortex. J. Neurosci. 11:1800-1809.

45. Hollmann, M., O'Shea-Greenfield, Rogers, S.W. and Heinemann, S. (1989): Cloning by functional expression of a member of the glutamate receptor family. Nature 342:643-648.

46. Honore, T., Davies, S.N., Drejer, J., Fletcher, E.J., Jacobsen, P., Lodge, D. and Nielsen, F.E. (1988): Quinoxalinediones:potent competitive non-NMDA glutamate receptor antagonists. Science 241:701-703.

47. Huguenard, J.R., Hamill, O.P. and Prince, D.A. (1989): Sodium channels in dendrites of rat cortical pyramidal neurons. Proc. Natl. Acad. Sci. USA 86:2473-2477.

48. Ikeda, K., Nagasawa, M., Mori, H., Araki, K., Sakimura, K., Watanabe, M., Inoue, Y. and Mishina, M. (1992): Cloning and expression of the ε4 subunit of the NMDA receptor channel. FEBS 313:34-38.

49. Issaacson, J.S. and Nicoll, R.A. (1991): Aniracetam Reduces Glutamate Receptor Desensitization and Slows the Decay of Fast Excitatory Synaptic Currents in the Hippocampus. Proc. Natl. Acad. Sci. USA 88:10936-10940.

50. Ishii, T., Moriyoshi, K., Sugihara, H., Sakurada, K., Kadotani, H., Yokoi, M., Akazawa, C., Shigemoto, R., Mizuno, N., Masu, M. and Nakanshi, S. (1993): Molecular characterization of the family of the N-Methyl-D-aspartate receptor subunits. J. Biol. Chem. 268:2836-2843.

51. Jahr, C.E. and Lester, R.A.J. (1992): Synaptic excitation mediated by glutamate-gated ion channels. Curr. Opin. Neurobiol. 2:270-274.

52. Jones, K. and Baughman, R. (1988): NMDA and non-NMDA-receptor components of excitatory synaptic potentials recorded from layer V of rat visual cortex. J. Neurosci. 8:3522-3534.

53. Kelso, S.R., Ganong, A.H. and Brown, T.H. (1986): Hebbian synapses in hippocampus. Proc. Natl. Acad. Sci. USA 83:5326-5330.

54. Kutswada, T., Kashiwabuchi, N., Mori, H., Sakimura, K., Kushiya, E., Araki, K., Meguro, H., Masaki, H., Kumanishi, T., Arakawa, M. and Mishini, M. (1992): Molecular diversity of the NMDA receptor channel. Nature 358:36-41.

55. Kwon, Y., Esguerra, M. and Sur, M. (1991): NMDA and non-NMDA receptors mediate visual responses of neurons in the cat's lateral geniculate nucleus. J. Neurophysiol. 66:414-428.

56. Lannoo, M.J. and Lannoo, S.J. (1992): Why do electric fish swim backwards? An hypothesis based on gymnotiform foraging behavior, interpreted through sensory constraints. Environ. Biol. Fish 36:157-165.

57. Lannoo, M., Maler, L. and Tinner, B. (1989): Ganglion cell arrangement and axonal trajectories in the anterior lateral line nerve of the weakly electric fish *Apteronotus leptorhynchus*. J. Comp. Neurol. 289:331-342.

58. Lasser-Ross, N. and Ross, W.N. (1992): Imaging voltage and synaptically activated sodium transients in cerebellar Purkinje cells. Proc. R. Soc. Lond. B. 247:35-39.

59. Lester, R.A., Clements, J., Westbrook, G. and Jahr, C. (1990): Channel kinetics determine the time course of NMDA receptor-mediated synaptic currents. Nature 346:565-567.

60. Liu, S-J., Matute, G.C. and Streit, P. (1989): Glutamate-like immunoreactivity revealed in rat olfactory bulb, hippocampus and cerebellum by monoclonal antibody and sensitive staining method. Histochem. 90:427-445.

61. MacDermott, A. and Dale, N. (1987): Receptors, ion channels and synaptic potentials underlying the integrative actions of excitatory amino acids. TINS 10:280-284.

62. MacDonald, J.F. (1984): Measurments of transmitter action: the problem of voltage dependence. Can. J. Physiol. Pharmacol. 63:825-830.

63. Maler, L. (1979): The posterior lateral line lobe of certain gymnotiod fish: Quantitative light microscopy. J. Comp. Neurol. 183:323-363.

64. Maler, L. (1989): The role of feedback pathways in the modulation of receptive fields: an example from the electrosensory system. In Erber, J., Menzel, R., Pfluger, H-J. and Todt, D., eds. Neural Mechanisms of Behavior. Stuttgart, Georg Thieme Verlag, 111-115.

65. Maler, L. and Monaghan, D. (1991): The distribution of excitatory amino acid binding sites in the brain of an electric fish, *Apteronotus leptorhynchus*. J. Chem. Neuroanat. 4:36-91.

66. Maler, L. and Mugnaini, E. (1993): Organization and function of feedback to the electrosensory lateral line lobe of gymnotiform fish, with emphasis on a searchlight mechanism. J. Comp. Physiol. A. (In press).

67. Maler, L. and Mugnaini, E. (in press): Correlating GABAergic circuits and sensory function in the electrosensory lateral line lobe of a gymnotiform fish. J. Comp. Neurol.

68. Maler, L., Sas, E., Johnston, S. and Ellis, W. (1991): An atlas of the brain of the electric fish *Apteronotus leptorhynchus*. J. Chem. Neuroanat. 4:1-38.

69. Maler, L., Sas, E., Carr, C. and Matsubara, J. (1982): Efferent Projections of the posterior lateral line lobe in Gymnotiform fish. J. Comp. Neurol. 211:154-164.

70. Maler, L., Sas, E.K.B. and Rogers, J. (1981): The cytology of the posterior lateral line lobe of high-frequency weakly electric fish (Gymnotidae): Dendritic differentiation and synaptic specificity in a simple cortex. J. Comp. Neurol. 195:87-139.

71. Mathieson, W.B. and Maler, L. (1988): Morphological and electrophysiological properties of a novel in vitro preparation: the electrosensory lateral line lobe slice. J. Comp. Physiol. A. 163:489-506.

72. Mayer, M.L. and Westbrook, G. (1987): The physiology of excitatory amino acids in the vertebrate central nervous system. Prog. Neurobiol. 28:197-276.

73. Mayer, M.L., Westbrook, G.L. and Guthrie, P.B. (1984): Voltage-dependent block by Mg^{2+} of NMDA responses in spinal cord neurons. Nature 309: 259-263.

74. Meguro, H., Mori, H., Araki, K., Kushiya, E., Kutsuwada, T., Yamazaki, M., Kumanishi, T., Arakawa, M., Sakimura, K. and Mishina, M. (1992): Functional characterization of a heteromeric NMDA receptor channel expressed from cloned cDNAs. Nature 357:70-74.

75. Meldrum, B. and Garthwaite, J. (1990): Excitatory Amino Acid Neurotoxicity and Neurodegenerative Desease. Trends Pharmacol. Sci. 11:379-387.

76. Metzner, W. and Heiligenberg, W. (1992): The coding of signals in the gymnotiform fish *Eigenmannia*: From electroreceptors to neurons in the torus semicircularis of the midbrain. J. Comp. Physiol. A. 169:135-150.

77. Miller, R.J. (1991): The revenge of the kainate receptor. TINS 14:477-479.

78. Miller, K.D., Chapman, B. and Stryker, M. (1989): Visual responses in adult cat visual cortex depend on N-methyl-D-aspartate receptors. Proc. Natl. Acad. Sci. 86:5183-5187.

79. Monyer, H., Seeburg, P.H. and Wisden, W. (1991): Glutamate-Operated Channels: Developmentally Early and Mature Forms Arise by Alternative Splicing. Neuron 6:799-810.

80. Monyer, H., Sprengel, R., Schoepfer, R., Herb, A., Lomeli, H., Burnashev, N., Sakman, B. and Seeburg, P. (1992): Heteromeric NMDA receptors: Molecular and functional distinction of subtypes. Science 256:1217-1221.

81. Mooney, R., Madison, C. and Shatz, C. (1993): Synaptic enhancement of transmission at the developing retinogeniculate synapse. Neuron 10:815-825.

82. Mori, H., Masaki, H., Yamakura, T. and Mishina, M. (1992): Identificantion by mutagenesis of a Mg^{2+}-block site of the NMDA receptor channel. Nature 358:673-675.

83. Morrisett, R., Mott, D., Lewis, D., Swartzwelder, S. and Wilson, W. (1991): GABA-B receptor-mediated inhibition of the N-methyl-D-aspartate component of synaptic transmission in the rat hippocampus. J. Neurosci. 11:203-209.

84. Moriyoshi, K., Masu, M., Ishii, T., Shigemoto, R., Mizuno, N. and Nakanishi, S. (1991): Molecular cloning and characterization of the rat NMDA receptor. Nature 354:31-37.

85. Mulkey, R. and Malenka, R. (1992): Mechanisms underlying induction of homosynaptic long-term depression in area CA1 of the hippocampus. Neuron 9:967-975.

86. Nadi, S. and Maler, L. (1987): The laminar distribution of amino acids in the caudal cerebellum and electrosensory lateral line lobe of weakly electric fish (*Gymnotidae*). Brain Res. 425:218-224.

87. Nakanishi, N., Schneider, N.A. and Axel, R. (1990): A family of Glutamate Receptor Genes: Evidence for the Formation of Heteromultimeric Receptors with Distinct Channel Properties. Neuron 5:569-581.

88. Nakanishi, N., Axel, R. and Schneider, N. (1992): Alternative splicing generates functionally distinct N-methyl-D-aspartate receptors. Proc. Natl. Acad. Sci. 89:8552-8556.

89. Lasser-Ross, N. and Ross, W.N. (1992): Imaging voltage and synaptically activated sodium transients in cerebellar Purkinje cells. Proc. R. Soc. Lond. B. 247:35-39.

90. Neher, E. and Steinbach, J.H. (1978): Local anaesthetics transiently block currents through single acetylcholine-receptor channels. J. Physiol. 277:153-176.

91. Nelson, S. and Sur, M. (1992): NMDA receptors in sensory information processing. Curr. Opin. Neurobiol. 2:484-488.

92. Nicholson, C. and Freeman, J.A. (1975): Theory of current source density analysis and determination of conductivity tensor for Anuran cerebellum. J. Neurophysiol. 38:356-368.

93. Nishigori, A., Tsumoto, T. and Kimura, F. (1990): Contributions of quisqualate/kainate and NMDA receptors to excitatory synaptic transmission in the rat's visual cortex. Vis. Neurosci. 5:591-604.

94. Nowak, L., Bregestovski, P., Ascher, P., Herbet, A. and Prochiantz, A. (1984): Magnesium gates glutamate-activated channels in mouse central neurones. Nature 307:462-465.

95. Orrego, F. and Villanueva, S. (1993): The chemical nature of the main central excitatory transmitter: A critical appraisal based upon release studies and synaptic vesicle localization. J. Neurosci. 56:539-555.

96. Ottersen, O.P. and Storm-Mathisen, J. (1985): Different neuronal localization of aspartate-like and glutamate-like immunoreactivities in the hippocampus of rat, guinea-pig and senegalese baboon (papio papio), with a note on the distribution of γ-aminobutyrate. Neurosci. 16:589-606.

97. Olverman, H.T., Monaghan, D.T., Cotman, C.W. and Watkins, J.C. (1986): [^{3}H]CPP, a new competitive ligand for NMDA receptors. Eur. J. Pharmacol. 131:161-162.

98. Patneau, D.K. and Mayer, M.L. (1990): Structure-Activity Relationships for Amino Acid Transmitter Candidates Acting at N-Methyl-D-Aspartate and Quisqualate Receptors. J. Neurosci. 10:2385-2399.

99. Prince, C.J. and Goldberg, J.I. (1993): Serotonin Activation of a Cyclic AMP-Dependent Sodium Current in an Identified Neuron from *Helisoma trivolvis*. J. Neurosci. 13:4979-4987.

100. Raggenbass, M., Goumaz, M., Sermasi, E., Tribollet, E. and Dreifuss, J.J. (1991): Vasopressin Generates a Persistent Voltage-dependent Sodium Current in a Mammalian Motoneuron. J. Neurosci. 11:1609-1616.

101. Reid, K.H., Edmonds Jr., H.L., Schurr, A., Tseng, M.T. and West, C.A. (1988): Pitfalls in the use of brain slices. Prog. Neurobiol. 31:1-18.

102. Richardson, T.L., Turner, R.W. and Miller, J.J. (1987): Action-Potential Discharge in the Hippocampal CA1 Pryamidal Neurons: Current Source-Density Analysis. J. Neurophysiol. 58:981-996.

103. Sahara, Y. and Westbrook, G.L (1993): Modulation of Calcium Currents by a Metabotropic Glutamate Receptor Involves Fast and Slow Kinetic Components in Cultured Hippocampal Neurons. J. Neurosci. 13:3041-3050.

104. Salt, T. (1987): Excitatory amino acid receptors and synaptic transmission in the rat ventrobasal thalamus. J. Physiol. 391:499-510.

105. Salt, T. and Eaton, S. (1991): Sensory excitatory postsynaptic potentials mediated by NMDA and non-NMDA receptors in the thalamus *in vivo*. Eur. J. Neurosci. 3:296-300.

106. Sas, E. and Maler, L. (1983): The nucleus praeeminentialis: A golgi study of a feedback center in the electrosensory system of gymnotid fish. J. Comp. Neurobiol. 221:127-144.

107. Sas, E. and Maler, L. (1987): The organization of afferent input to the caudal lobe of the cerebellum of the gymnotid fish *Apteronotus leptorhynchus*. Anat. Embryol. 177:55-79.

108. Saunders, J. and Bastian, J. (1984): The physiology and morphology of two types of electrosensory neurons in the weakly electric fish *Apteronotus leptorhynchus*. J. Comp. Physiol. 154:199-209.

109. Scharfman, H., Lu, S., Guido, W., Adams, P. and Sherman, S. (1990): N-methyl-D-aspartate receptors contribute to excitatory postsynaptic potentials of cat lateral geniculate neurons recorded in thalamic slices. Proc. Natl. Acad. Sci. 87:4548-4552.

110. Seeburg, P. (1993): The molecular biology of the mammalian glutamate receptor channels. Trends Neurosci. 16:359-365.

111. Shepherd, G.M. and Brayton, R.K. (1987): Logic operations are properties of computer-simulated interactions between excitable dendritic spines. Neurosci. 21:151-165.

112. Shirokawa, T., Nishigori, A., Kimura, F. and Tsumoto, T. (1989): Actions of excitatory amino acid antagonists on synaptic potentials of layer II/III neurons of the cat's visual cortex. Exp. Brain Res. 78:489-500.

113. Shumway, C. (1989): Multiple electrosensory maps in the medulla of weakly electric gymnotiform fish. I. Physiological differences. J. Neurosci. 9:4388-4399.

114. Shumway, C. (1989): Multiple electrosensory maps in the medulla of weakly electric gymnotiform fish. II. Anatomical differences. J. Neurosci. 9:4400-4415.

115. Shumway, C.A. and Maler, L. (1989): GABAergic inhibition shapes temporal and spatial response properties of pyramidal cells in the electrosensory lateral line lobe of gymnotiform fish. J. Comp. Physiol. A. 164:391-407.

116. Softky, W.R. and Koch, C. (1993): The Highly Irregular Firing of Cortical Cells Is Inconsistent with Temporal Integration of Random EPSPs. J. Neurosci. 13:334-350.

117. Stafstrom, C.E., Schwindt, P.C., Chubb, M.C. and Crill, W.E. (1985): Properties of Persistent Sodium Conductance and Calcium Conductance of Layer V Neurons From Cat Sensorimotor Cortex In Vitro. J. Neurophysiol. 53:153-170.

118. Sugihara, H., Moriyoshi, K., Ishii, T., Masu, M. and Nakanishi, S. (1992): Structures and properties of seven isoforms of the NMDA receptor generated by alternative splicing. Biochem. Biophys. Res. Comm. 185:826-832.

119. Sutor, B. and Hablitz, J. (1989): EPSPs in rat neocortical neurons *in vitro*. II. Involvement of N-methyl-D-aspartate receptors in the generation of EPSPs. J. Neurophysiol. 61:621-634.

120. Taube, J.S. and Schwartzkroin, P.A. (1988): Mechanisms of Long-Term Potentiation: A Current-Source Density Analysis. J. Neurosci. 8:1645-1655.

121. Traub, R.D. and Llinas, R. (1979): Hippocampal Pyramidal Cells: Significance of Dendritic Ionic Conductances for Neuronal Function and Epileptogenesis. J. Neurophysiol. 42:476-496.

122. Trussell, L.O. and Fischbach, G.D. (1989): Glutamate Receptor Desensitization and its Role in Synaptic Transmission. Neuron 3:209-218.

123. Turner, R.W., Maler, L., Deerinck, T., Levinson, S.R. and Ellisman, M.H. (in press): TTX-sensitive sodium channels underlie oscillatory discharge in a vertebrate sensory neuron. J. Neurosci.

124. Turner, R.W., Plant, J.R. and Maler, L. (1991): Conditional Oscillatory Discharges in Topographic Maps of the Electrosensory Lateral Line Lobe (ELL). Soci. Neurosci. Abstr. 17.

125. Wang, Y.-Y. and Aghajanian, G.K. (1989): Excitation of locus coeruleus neurons by vasoactive intestinal peptide:evidence for a G-protein-mediated inward current. Brain Res. 500:107-118.

126. Wang, D. and Maler, L. (1994): The Immunocytochemical Localization of Glutamate in the Electrosensory System of the Gymnotiform Fish, *Apteronotus leptorhynchus*. Brain Res. 653:215-222.

127. Yamazaki, M., Mori, H., Araki, K., Mori, K.J. and Mishina, M. (1992): Cloning, expression and modulation of a mouse NMDA receptor subunit. FEBS 300:39-45.

128. Zupanc, G.K.H. and Maler, L. (in press): Evoked chirping in the weakly electric fish Apteronotus leptorhynchus: A quantitative biophysical analysis. Can. J. Zool.